Developing Advanced Polymer Colloids via Thiol-ene Click Chemistry

by

Lamyaa Alsuhaymi

A thesis submitted in partial fulfilment of the requirements of the degree of Doctor of Philosophy in Chemistry

Deapartment of Chemistry, University of Warwick

March 2019

Contents

Table of Figures

Table of Tables

Table of Schemes

Acknowledgements

Many thanks to Professor David Haddleton for giving me the chance to run this project under his supervision and for his support and advice. Considerable thanks to Dr Alan Wemyss for his generous help during lab work and in writing the thesis. Thanks also to Professor Neil Cameron for his collaboration throughout the PolyHIPEs synthesis, and to all members of the Haddleton group both past and present for all their help, the team of Electron microscopy Research Technology Platform, the Spectroscopy Research Technology Platform and Thermal Analysis. Special thanks to Professor Martin Wills for being such a great supporter since I started my PhD

Last but not least, I gratefully acknowledge the financial support of the government of Saudi Arabia.

To my parents, my husband and my son; there are no words that could express my gratitude to you.

Declaration

This thesis is submitted to the University of Warwick in support of my application for the degree of Doctor of Philosophy. It has been composed by myself and has not been submitted in any previous application for any degree

The work presented (including data generated and data analysis) was carried out by the author.

Abbreviations and Symbols

AIBN	Azobisisobutyronitrile
ATRP	Atom Transfer Radical Polymerisation
COSY	correlation spectrum
CuAAC	Copper catalysed alkyne-azide cycloaddition
DCE	1,2- dichloroethane
DCM	Dichloromethane
DEAEA	2 (Diethylamino)ethyl acrylate
DEE	Diethyl Ether
DNA	Deoxyribonucleic acid
DNTB	5.5′-Dithiobis(2-nitrobenzebenzoic acid)
DP	Degree of polymerisation
DPEHA	Dipentaerythritol penta/hexa-acrylate
DSC	Differential Scanning Calorimetry
DVB	Divinylbenzene
ESI-MS	Electrospray Ionisation-Mass Spectrometry
HA	Hexa-allyl
FT-IR	Fourier Transform Infrared Spectroscopy
HDT	1,6-Hexanedithiol
HEA	2-Hydroxyethyl acrylate
HIPEs	high internal phase emulsions
MA	Methyl acrylate
MeOH	Methanol
NMR	Nuclear magnetic resonance
O/W	Oil in water
PDI	Polydispersity

EGMEA	Ethylene glycol methyl ether acrylate
PETMP	pentaerythritol tetrakis(3-mercaptopropionate) particles
ppm	parts per million
RBF	round-bottomed flask
ROMP	Ring opening metathesis polymerisation
rpm	Revolution per minute
SEM	scanning electron microscopy
SDS	Sodium dodecyl sulfate
TAP	Thiol Allyl Particle
TEGDT	2,2′-(Ethylenedioxy) diethanethiol
T_g	Glass transition temperatures
UV-light	Ultraviolet-light
UV-Vis	Ultraviolet-Visible
W/O	Water-in-oil
MHz	Megahertz
hν	Radiation
µm	Micrometer
nm	Nanometers
λ	Wavelength
δ	Chemical shift

Abstract

Thiol-allyl cross-linked microstructure polymer particles were prepared via a high shear suspension polymerisation technique using the thiol-ene click reaction of hexa-allyl (HA) with pentaerythritol tetrakis(3-mercaptopropionate) (tetrathiol, 4T), trimethylolpropane tris(3-mercaptopropionate) (trithiol, 3T), 2,2′-(ethylenedioxy) diethanethiol (dithiol, 2T, TEGDT) and 1,6-hexanedithiol (dithiol, 2T, HDT). HA was made as the result of a one-step reaction by combining the epoxy ring opening reaction with the Michael addition reaction reagent. ^{1}H NMR, ^{13}CNMR, ^{1}H COSY NMR FT-IR and mass specrometry were used for characterisation. Various acrylate monomers of 2-hydroxyethyl acrylate (HEA), methyl acrylate (MA), ethylene glycol methyl ether acrylate (EGMEA) and 2 (diethylamino)ethyl acrylate (DEAEA) were introduced into the residual thiol functional groups on the surface of tetrathiol-HA microsphere polymer particles via the thiol-ene Michael addition reaction. The chemical structure and composition of these particles was studied using FT-IR, Raman spectroscopy and energy dispersive X-ray spectroscopy (EDX), and illustrated that producing particles with the residual of the thiol functional group achieved excellent structure and functionality before and after the post polymerisation functionalization. The investigation using EDX mapping confirms that C, N, O and S and are uniformly spread over particles before and after post polymerisation functionalization**.** We explore the role of parameters such as the molar ratio of the thiol monomer, homogenizer speed, crosslinking density, photo polymerization time and thermal curing method in terms of the glass transition temperatures (T_g) and the surface morphology of the cross-linked microsphere thiol-allyl particles, before and after post-

polymerization functionalization, as well as different types and volumes of the solvents used in the functionalization process. The T_g and the morphology of these particles was analysed by Differential Scanning Calorimetry (DSC) and using scanning electron microscopy (SEM). Water-in-oil (W/O) high internal phase emulsions (HIPEs) containing trimethylolpropane tris(3-mercaptopropionate) (trithiol) and dipentaerythritol penta/hexaacrylate (oil phase) were emulsified via the use of three different pieces of equipment - an overhead stirrer (300 rpm), a vortex mixer (30 Hertz), and a homogenizer (up to 8000 rpm). A porous polymeric foam with an interconnected pore structure was produced by polymerisation of the continuous phase of the HIPEs. It was characterised by SEM.

1 Introduction

1.1 General introduction

Polymeric materials take the form of enormously large molecules that are crucial for our subsistence.[1] They are a main component of our food, our clothes, our houses and our bodies.[1] Owing to recent rapid advances, the biomedical application of polymers to drug delivery, gene therapy, and tissue engineering has grown significantly.[2] This chapter provides an overview of polymer science, heterogeneous polymerisation systems, thiol-ene click chemistry, and their application in polymeric colloid materials.

1.2 BASIC REVIEW

A polymer is a large molecule built up from several smaller molecules.[3] There are different types of polymer including linear, branched or highly interconnected polymers in the form of structures that develop into large three-dimensional networks.[3] Monomers are identified as small molecules which are used as basic building blocks for forming the polymers (large molecules).[3] Both the number of repeat units of the molecule, the degree of polymerisation (DP) and its mass are considered as a measure of the size of the polymer.[3] The relative molar mass of the polymer is therefore the result of the relative molar mass of the repeat units and the DP. The chemical properties of polymers match those of analogues small molecules.[1] There is no clear separation between polymer chemistry and all other forms of chemistry. As a very rough guide, molecules of a relative molar mass of at least 1000, or a DP of at least 100, relate to the field of polymer chemistry.[3] The great majority of commercially available polymers are of an organic nature, that is they are based on the covalent compounds of carbon.[3] Hydrogen, oxygen, chlorine, fluorine, phosphorus, silicon and sulphur are the most commonly found elements involved in polymer science. These

are elements which are able to form covalent bonds, even with some polarity, with carbon.[3]

1.3 Heterogeneous polymerisation system

Heterogeneous polymerisation processes are often referred to as a phases system (two or more) where the starting monomer and/or the resulting polymer are in the form of fine dispersion in an immiscible liquid.[4, 5] The initiator may be soluble in the organic monomer or the liquid. In addition to the monomer, the initiator and polymerisation medium (the liquid phase) in the form of an emulsifier is added to the polymerisation mixture to stabilize the monomer droplets.[5] The classical categorization of heterogeneous polymerisation includes suspension emulsion, dispersion and precipitation.[5, 6]

1.3.1 Suspension polymerisation

As mentioned previously, suspension in the case of heterogeneous systems consist of two phases.[7] The external phase is also called the continuous phase. The dispersion medium is usually liquid or is sometimes semi-solid (in the form of a gel).[7] The internal phase or dispersed phase is insoluble in the external, continuous phase. Given that the physical classification that considers the suspension as solid/liquids dispersion doesn't apply in the case of heterogeneous polymerisation, the discussion in this section is limited to suspension polymerisations that start with liquid/liquid mixture initially, and end up as solid/liquid dispersion.[4]

The typical oil in water technique includes the suspension of an immiscible, oil-soluble monomer in water (O/W).[8] As shown in Figure 1.2 the suspension is polymerised with the help of stirring to directly produce polymer particles.[6, 8] That is

to say, the suspension polymerisation starts when the monomer droplet is dispersed in the continuous phase. A surfactant is added to prevent droplet breaking/coalescence (see Figure 1.2).[4, 6, 8]

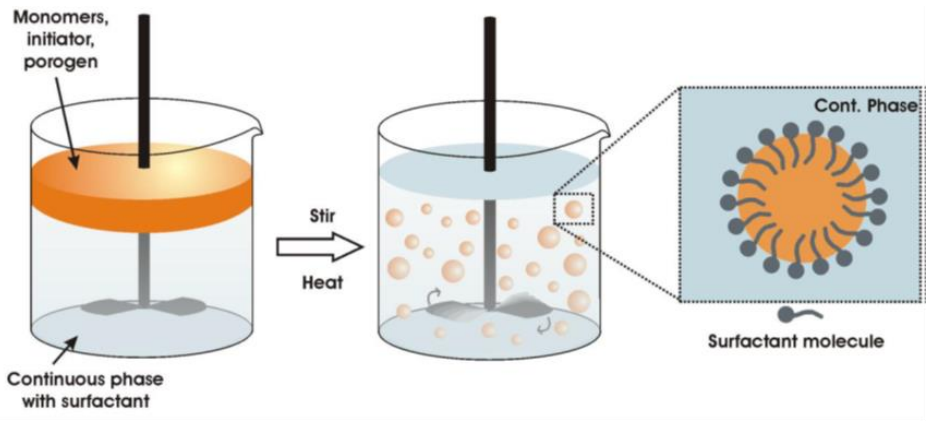

Figure 1. 1. General description of the suspension polymerization procedure.[4]

In suspension polymerisation the initiator being well soluble in the dispersed phase this is different from emulsion polymerisation where a continuous soluble initiator is used. For this reason the mechanism is completely changed.[4, 8, 9] Eduardo and co-workers (1997) provides a review of in-depth phenomena including mixing, rheological, surface, breaking and coalescence as well as the polymerisation effect, and show their influence on particle size distribution in suspension polymerisation.[6]

1.3.2 Emulsion polymerisation

These are two/multi-phase liquid systems that also refer to several common procedures such as conventional emulsion polymerisation, inverse emulsion polymerisation, mini-emulsion polymerisation, and micro-emulsion polymerisation.[4, 10] In its common variants, the monomers are dispersed in the aqueous phase to provide particles with a size of 50-1000 nm.[10, 11] In the case of emulsion polymerisation, the initiator is preferably soluble in the continuous phase.[8] Even so, monomers are usually

organic–soluble. In some cases, however, it is possible to copolymerize water-soluble monomers.[8]

1.3.3 Dispersion polymerisation

Unlike emulsions both monomers and initiators are dissolved in an organic solvent of the dispersion polymerisation resulting in insoluble monodisperse particles that are in the size range of 1-10 µm.[5, 8, 11] The polymerisation initiated in the reaction creates a mixture that is initially homogenous.[5, 8] The resulting primary particles during the early stage of phase separation, are swollen by the polymerisation medium or monomer.[5]

1.3.4 Precipitation polymerisation

Similar to dispersion polymerisation, the initial state of the reaction mixture is homogenous.[8] Both the monomer and the initiator of the precipitation polymerisation are soluble in the continuous phase.[8] In fact, the primary particles don't swell in the medium, and this leads to continuous nucleation during the formation of the polymer. This precipitates the formation of larger and larger particles, mostly in the form of undefined, agglomerated powder.[8]

1.4 Polymer colloids

The terms polymeric colloid usually refers to micron and sub-micron polymer particles, polymer beads in the size range 10-1000 µ. These were developed by using one of the notable heterogeneous polymerisation methods which is that of suspension polymerisation (beads or pearl polymerisation).[6, 8, 9, 11, 12] Over the last century there has been a challenge in the area of colloid science regarding the production of monodispersed spherical colloids.[13] Colloids and particles are beneficial for the preparation of various artificial materials.[11] Important innovative techniques have

been developed to produce non-spherical or chemically-patterned particles, thereby opening up new applications with regard to colloidal products.[11]

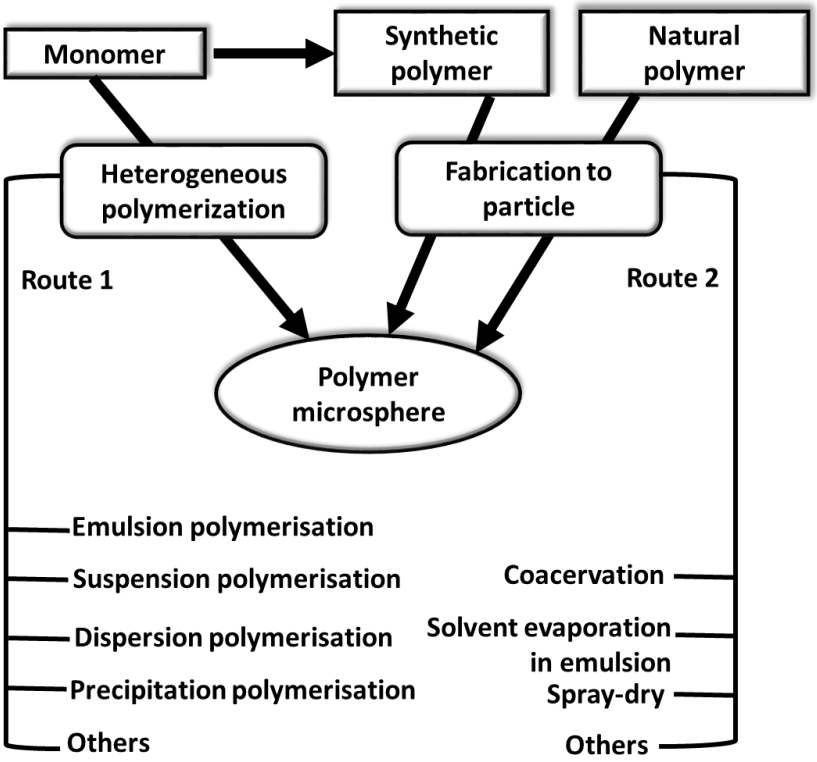

Figure 1. 2. General preparation route for polymer particles.[12]

1.5 Functional polymer particles

Recently, the development of novel materials with active functional groups on their surface or as part of their bulk has gained significant interest, particularly in biomedical fields such as drug delivery.[14] There exist several approaches to the preparation of functional microspheres.[15] The modification of particles with functional polymers is a creative method to synthesise alternative polymer composites. The importance of this system is connected to its multi-functionality, given that the same macromolecule has functional groups with nano/micro-particles available for further chemical reactions.[8, 16] In this sense, the synthetic procedure can involve surface functionality. However, the optimisation of the synthetic procedure is crucial for each

functional monomer. A higher ratio would be essential to obtain a greater percentage of active groups on the surface. Alternatively, the modification of the existing particles addresses new surface functionalities. Post-polymerisation functionalization and the preparation of other complex polymer materials under mild conditions in highly efficient and selective ways are allowed by using both click chemistry and heterogeneous polymerisation system.[9, 17]

1.6 Click chemistry

In 2001, Sharpless and his co-workers proposed the concept of click chemistry.[18] The inspiration behind the synthetic philosophy of click chemistry came from the simplicity and efficiency of nature.[19] In fact, highly complex biological system rely on a modest library of monomers that are linked together by a few but efficient organic reactions. Likewise, the purpose of click chemistry would be establish an ideal set of straightforward and highly selective reactions in synthetic chemistry.[19] Click chemistry refers to a mechanism that is insensitive to ambient conditions, proceeds in solvent-free conditions, and rapidly proceeds to high degrees of conversion with no by-products.[20-24] Since the discovery of the copper catalysed cycloaddition reaction between azide and alkyne (CuAAC), the additional highly orthogonal and efficient reactions that can be conducted under mild conditions have also been explored.[25] Examples of the click reactions which are widely explored are thiol-ene/yne reactions, nucleophilic ring opening reactions as well as Diels–Alder/Hetero Diels-Alder ligation.[25] The thiol-click reaction has been widely spared in use due to the fact that large amounts of commercially-available thiol monomers exist, together with the possible multiple reaction pathways, including thiol-ene thiol epoxy and thiol acrylate etc.[20] Comprehensive studies of the thiol-ene reaction and the Thiol-Michael Addition reaction has been investigated previously.[26]

1.6.1 Thiol-ene click chemistry

Because of the relatively weak sulphur-hydrogen bond, thiols can take part in a large number of chemical reactions. These reactions can be initiated by a variety of methods under mild conditions.[21] Posner first discovered the thiol-ene addition, and the thiol-ene reaction mechanism. Monomer reactivities and polymerization kinetics have since been extensively explored.[27] In the early 1900s, the highly efficient reactions of thiols with reactive carbon-carbon double bonds and the general concept of reactions between thiols and ene, was well known.[21] For over 100 years, two thiol reactions of specific note appeared (as described in Scheme 1.1): thiol-ene free-radical additions to electron-rich/electron-poor carbon-carbon double bonds, and the catalysed Thiol-Michael Addition to electron-deficient carbon-double bonds.[21]

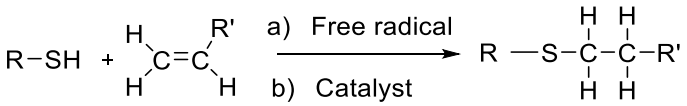

Scheme 1.1. Typical thiol-ene coupling by a) Free radical and b) Thiol-Michael Addition reactions. There is a single thiol that reacts with a single ene to yield the product in these two common reactions.[21]

Specific examples of these two reaction is shown in Schemes 1.2. and 1.3. Typically, the reaction of peracetylated allyl b-D-glucopyranoside with these thiols was carried out in hot dioxane (75 °C) in the presence of α-azobisisobutyronitrile (AIBN) as a radical initiator (scheme 1.2).[28] As shown in Scheme 1.3, the photoinduced reactions at λ_{max} 365 nm of per acetylated lactose thiol with *N*-protected allyl and vinyl glycinates. proceeded readily in the presence of catalytic DPAP.[28]

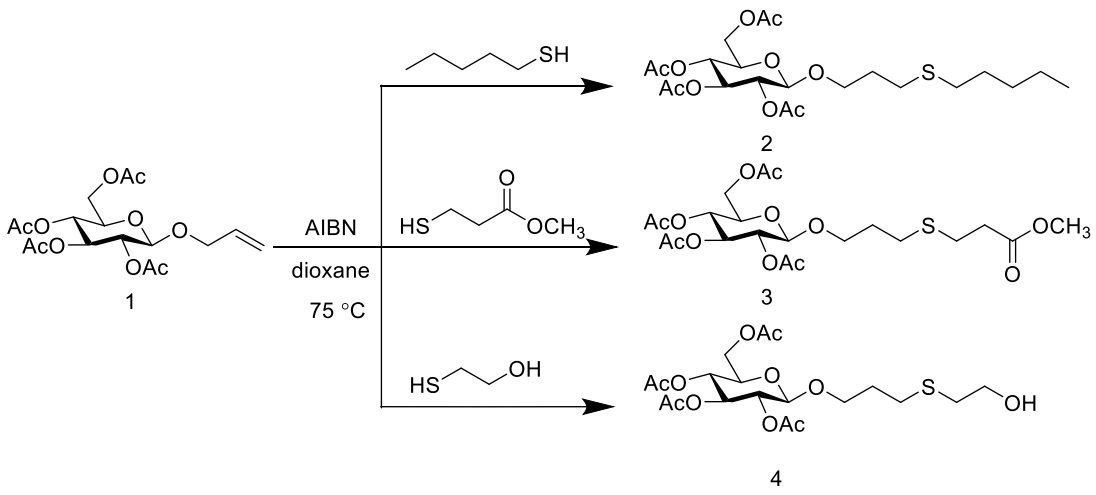

Scheme 1.2. Typical thiol–ene coupling between an allyl glycoside and various thiols.[28]

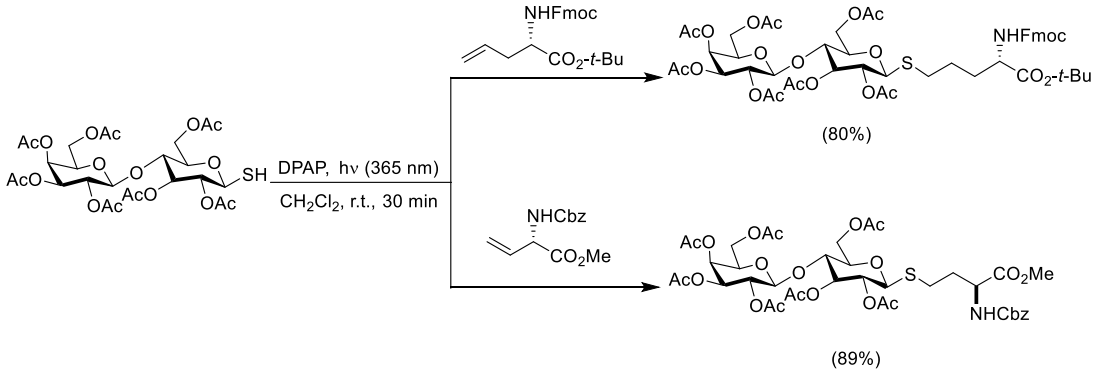

Scheme 1.3. Synthesis of alkyl-tethered S-lactosyl glycinates.[28]

There are several features associated with the thiol-ene reaction which make it an especially attractive, facile and versatile procedure.[29] First of all, hydrothiolation reactions can be processed under a wide range of conditions, as well as via a radical pathway, by the use of catalytic processes mediated by nucleophiles, acids and bases, in the apparent absence of an added catalyst in highly polar solvents such as water or DMF (a high-dielectric-constant, the thiolate is achieved due to the polarity of the solvent), or by using supramolecular catalysis such as β-cyclodextrin.[29] In contrast to the typical acid-base type of catalysis, β-cyclodextrin, having hydrophobic cavities,

catalyse reactions via the creation of host-guest complexes by non-covalent bonding.[30] Because their exterior, bristling with hydroxy groups, is polar and hydrophobic cavity, CDs provide a micro-environment for organic reactions, whereby they catalyse reactions through non-covalent interactions.[31] As such as, they have been identified as versatile enzymes that also mimic supramolecular hosts for organometallic complexes.[31]Secondly, a variety of enes serve as appropriate substrates. For example, activated and non-activated species in addition to multiple substituted olefinic bonds.[29] On the other hand, reactivity can vary significantly, depending on reaction mechanisms and substitution patterns with regard to the C=C bonds.[29] Thirdly, fundamentally, any thiol containing highly functional species can be employed.[29] However, reactivity can cover several orders of magnitude, depending on the S-H bond strength and the cleavage mechanism, such as homolytic vs. heterolytic.[29] Lastly, the reactions are mostly extremely rapid, and can occur in a matter of seconds, and proceed with the quantitative formation of the corresponding thioether in a regio-selective fashion.[29] In general, the thiol-ene reaction has been conducted under radical conditions that are frequently photochemically induced.[29]

As has been mentioned previously, thiol-ene chemistry was known in the last century, involving simply a thiyl radical being added to alkene.[29, 32] Historically, in the polymer/materials fields, thiol-ene chemistry has been widely used as a means of preparing near-perfect linear and network polymers via the reaction between di or multifunctional thiols and alkenes (enes). At the present time, this approach to polymer formation has attracted considerable attention because of its ease of use and versatility (it is classed as a form of 'click' chemistry), leading to the production of a variety of functional polymers and macromolecular materials. By the end of the 1970s, thiol-acrylate mixtures underwent rapid polymerization processes due to the fact that

the acrylate copolymerizes with the thiol (thiyl addition to the acrylate bond followed by the hydrogen abstraction of thiol hydrogen) and homopolymerizes (acrylate group propagation). This unique combination of two types of free-radical polymerisation processes leads to the use of a wide range of acrylates with several chemical structures that combine the features of an acrylate network with thiol-ene networks.[33] It is predicted that thiol-ene click chemistry has the promise of being applied in all areas of science and engineering for creating and functionalizing polymers and surfaces for application in an enormous range of disciplines that involves high performance materials.[21] The future appears to indeed be favourable for both a radical- and a catalytically-mediated thiol-ene click reaction.[21]

1.6.2 Thiol-ene photopolymerisation

In recent years, the efficiency of thiol-ene reactions has been used in a wide range of synthetic processes that demonstrate their use as a highly efficient tool for chemical and material synthesis. Thiol-ene reaction is produced by both radical mechanisms and using the base catalysed method (Thiol-Michael Addition).[25] The well-known radical mediate, the thiol-ene reaction, is usually initiated by UV-light in the presence of a photo initiator, or by heat in the presence of a thermal initiator.[25, 34] Thiol-ene polymerisations are reactions between multifunctional thiol and ene (vinyl) monomers that occur through a step-growth radical addition mechanism. Initiation is achieved via the generation of radical centres, the most common method being the photoinitiation of radical centres.[27] Although it is a known fact that there is an example of thermally-initiated or reduction oxidation-initiated thiol-ene reaction, the majority of the literature describes the photo-initiated reaction, in no small part due to the fact

that the special temporal control can be thus completed.[24] Several unique properties have been exhibited by thiol-ene photopolymerisation.[35] This has made them the recent focus of a considerable number of studies.[35] There are many advantages associated with photopolymerisation, including the fact that they do not require solvents for processing, can polymerise rapidly with little or even no added photoinitiators, and that the products have excellent mechanical properties and are optically clear.[35] It is hypothesized that the charge-transfer interaction is essential in the photo-induced generation of radicals in the absence of a photoinitiator.[36] Carmer and Bowman have demonstrated that thiol-ene systems could be initiated with different types of initiators, including photopolymerisation without the assistance of a photoinitiator.[36] They also showed that thiol-acrylate systems could be polymerised without additional photoinitiators.[36] In addition, oxygen and water inhabitation that usually prevent reaction and polymerisation can often be neglected in the thiol-ene reaction that enables radical polymerisation of a wide range of thiol and vinyl functional group chemistries.[35, 37]Thiol-ene photopolymerisation are radical reactions that proceed using a step growth mechanism.[35] The following mechanism indicates that the thiol-ene step growth mechanism consists of the addition of a thiyl radical to a vinyl functional group (Scheme1.4). Subsequently, the radical transfers from the resulting carbon radical to a thiol functional group. In terms of sequences, these propagation/chain transfer events serve as the basis for the polymerisation reaction.[35]

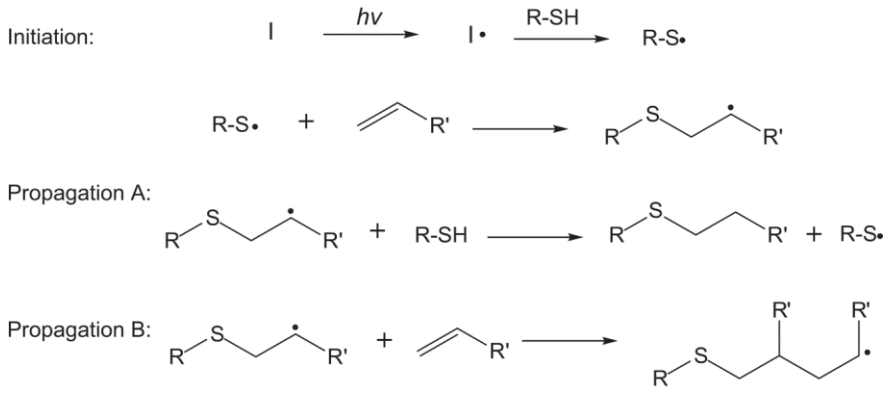

Scheme 1.4. The mechanism for the hydro-thiolation of a C=C bond in the presence of a photoinitiator and *hv*.

Thus, unlike the majority of covalently cross-linked polymer networks which form via a chain-growth or step-growth mechanism, radically-initiated thiol-acrylate photopolymerization is completed using a combination of step and chain growth mechanisms.[38] The unique thiol-acrylate molecular structure develops from this mechanism, and is directly impacted by the thiol:acrylate ratio, transitioning from being more chain-like to more step-like.[38] For example, the ratio of thiol to acrylate groups increases, and there is a shortening of the kinetic backbone chains that are generated during polymerisation.[38] In the presence of oxygen or water, the thiol addition across an ene doubles the radical step growth reaction, and proceeds rapidly with few side products.[38] This is unfortunate because the inclusion of sulphur in a range of molecular formats into polymer matrices continues to attract extensive amounts of attention.[38] There have been a number of studies reporting that thiol-ene photo-polymerisation is widely used for the synthesis of cross-linked functional polymeric micro/nanosphere particles.[25, 39-46]

Recently, there has been a significant interest in the use of photopolymerisation as a curing method for the production of polyHIPE materials which are usually prepared via thermal curing using free radical initiation.[47] Photopolymerisation is usually a very rapid process (complete curing in seconds is common). Therefore, less stable HIPEs can be photopolymerised than can be treated to thermal curing.[47] Also, the number of precursor materials available for polyHIPE preparation is increased.[47] In earlier work it has been demonstrated that the thiol-ene and thiol-yne photopolymerisation, using commercially-available multifunctional thiols with either multifunctional acrylates or alkynes, can also be used for the preparation of polyHIPE materials.[47] Well-defined thiol-ene/yne network materials with mechanical properties that are dependent on the extent of crosslinking, are produced by these methods. Scheme 1.5. shows examples of some components (crosslinked aliphatic polyesters) that are employed to produce a thiolene-network.[47] Emulsion-templated scaffolds have already been reported as scaffolds for tissue engineering. Still, in almost all cases, the products employed contain considerable amounts of non-degradable carbon polymer chains, theoretically limiting their clinical applicability. Furthermore, non-degradable styrene-based polyHIPEs have been employed widely for in vitro 3D cell culture, yet these scaffolds are also not suitable for in vivo applications.[47]

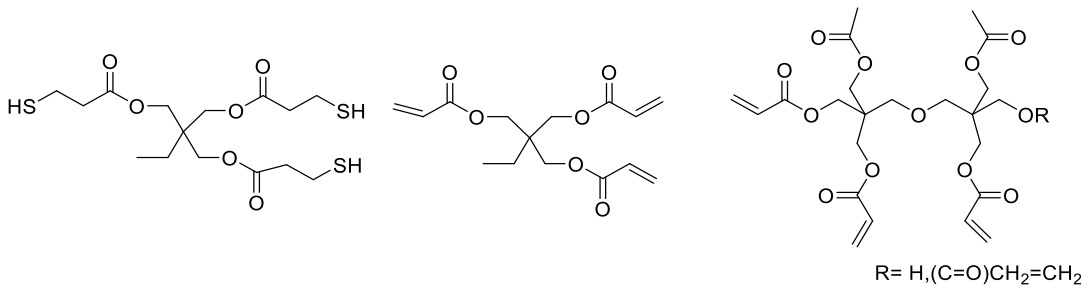

Scheme 1.5. Monomers used to prepare thiol–ene polyHIPE materials.[47]

As pointed out previously , thiol-ene polymerisation has been widely studied over the last century, and is known to proceed through a free-radical step-growth mechanism.[33] Multifunctional thiols will copolymerize with almost any multifunctional ene, and the reaction mechanism affords a high degree of conversion, low shrinkage, uniform crosslink densities, and delayed gelation. This results in the ability to produce products with unique mechanical and physical properties.[33]

1.6.3 Thiol-Michael Addition Chemistry

The **Thiol-Michael** Addition reaction which is analogous to the radical thiol-ene reaction, has garnered considerable attention over the past decade.[24] It is analogous to the radical thiol-ene reaction.[24] Whereas in thiol-ene electron rich are generally favoured, the reaction rate trends with the electron-deficiency of the Michael acceptor in the Thiol-Michael Addition reaction.[24] The reaction mechanism for the Michael reaction can be described as being similar to that of thiol-ene reaction, with anionic species in place of a radical.[24] This powerful facial reaction proceeds via the conjugate addition of the reaction of the Nu-H reactant, a class of reaction that includes the addition of highly reactive thiols or thiolate anions which are Michael donors across the activated C=C bonds. These serve as Michael acceptors and are commercially available.[24, 48-51] The C=C bond reactivity order of reactivity is as follows: maleimide> fumarates >maleates acrylates/acrylamides >acrylonitrile> crotonate >cinnamate ethacrylates/methacrylamides.[24, 48] Over the years, the Thiol-Michael Addition reaction benefits from mild, solvent-less reaction conditions, and minimal by-product formation using mild catalysts to yield a highly efficient, modular click reaction.[24, 49, 50] Generally, the most efficient catalysts that have been used to initiate the Thiol-Michael reaction are the base (e.g. amine) and nucleophile-based catalysts (phosphines).[48] Thus, two distinct mechanistic pathways exist, based on the nature of

the catalysts, the traditional base-catalysed and reactions, and the nucleophile-mediated thiol reactions (see Scheme 1.6) and base catalysed Thiol-Michael Addition and nucleophile character.[48-50] Both base and nucleophile catalysed Thiol-Michael Addition mechanisms are known for their minimal side reactions.[48-50] This ability to proceed to high conversion when optimised without side product formation, such as radical-radical termination products formed in radical mediated thiol-ene reactions, even under dilute conditions, was the reason why the Thiol-Michael Addition reactions are so favourable for many material chemistry applications.[48-50] For example, the Thiol- Michael Addition is used widely in biological research to conjugate maleimide-containing fluorescent dyes to proteins via a reduced disulphide bridge.[24] Great efforts have been given to develop the understanding of the Thiol-Michael Addition reactions mechanism, along with the development of novel catalyst systems capable of achieving high yields from the facial hydrothiolation of an activated C=C bond with readily available reagents such as sodium methoxide, weak organobases such as trimethylamine (NEt_3), and nucleophiles such as phosphines being the most widely-used catalyst systems.[48]

a) Base catalysed Mechanism

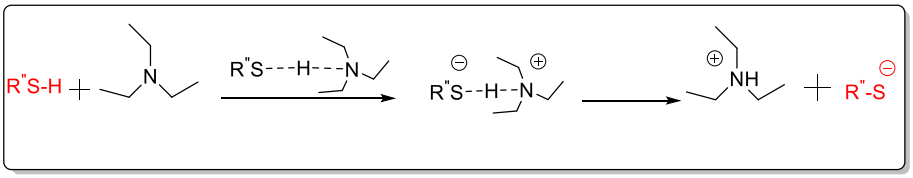

b)Nucleophile-catalysed mechaism

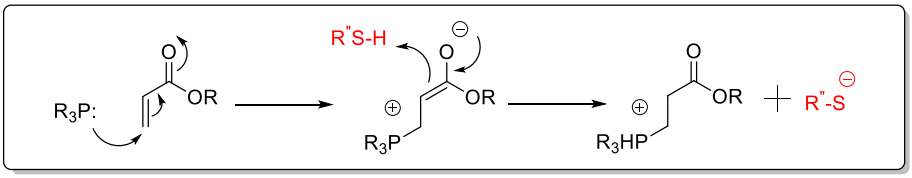

C)Michael type thiol-acrylate cycle

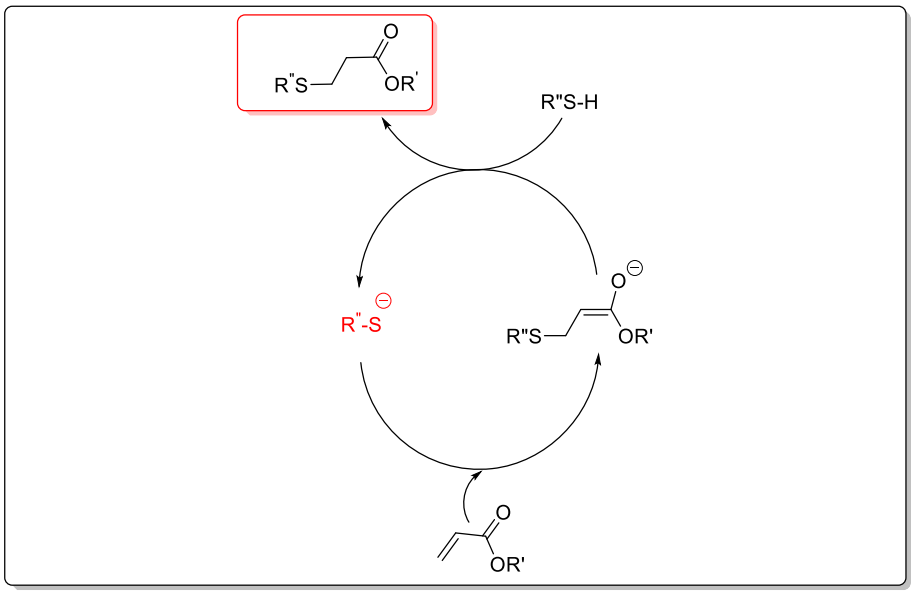

Scheme 1.6. Here we provide a brief description that clearly elucidates the Thiol-Michael Addition base-catalyzed pathway (a), the Thiol-Michael nucleophilic addition pathway (b) and generalized Thiol-Michael Addition reaction cycle mechanism (C).

1.6.4 Application of thiol-ene photo polymerisation in bio-organic chemistry

Thiol-ene click photo polymerisation produces a robust, solvent-less, user friendly, rapid polymerisation platform for making homogenous polymer networks, the mechanism of which involves the step –growth reaction between multi-functional thiol

and ene.[52] A high degree of flexibility has been detected in terms of the thermal and mechanical properties of the resulting network as a large number of thiol crosslinkers and ene monomers have become accessible (commercially and synthetically).[52] Therefore, the thiol-ene UV-photoinitiated system has been utilized in a number of application such as antibacterial materials, non-woven and electrospun fibre, nanoprint/soft imprint lithography, gas barrier and transport membranes, and lithium ion barriers.[52-54] In recent times, several bio-based thiol-ene networks have been reported.[55] Bio-based raw materials such as carbohydrates, vegetable oils and fatty acids, plant-based phenolic acids, eugenol, itaconic acid, isobrid, D-limonene and linalool have been used to synthesize monomers for creating thiol-ene polymers.[55] In particular, there is emerging trend with regard to using natural resource containing allyl group for forming networked polymers using functional thiol monomers and thus renewable materials.[56, 57] It should be noted that the thiol-ene reaction has also been employed in more traditional (bio) organic syntheses. Fiore and his co-workers described the synthesis of a range of unnatural thioglycosides by UV-initiated radical thiol-ene coupling between thiol and ene-functional sugars (see Scheme 1.7 for a general example.[29, 58] After the optimization of the reaction conditions, such facile couplings proceeded rapidly with >97% of conversions as determined by ^{1}H NMR spectroscopic analysis.[29, 58] The scope and flexibility of this approach to novel disaccharides was demonstrated with ten examples using a variety of thiol and ene sugar substrates.[29, 58]

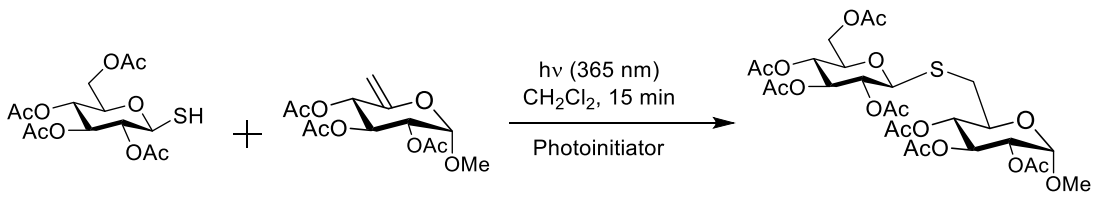

Scheme 1.7. Radical-induced thiol-ene coupling between a peracetylated glucosylthiol and a hex-5-enepyranoside under photochemical conditions.[29, 58]

There are very few previous cases of the use of thiol-ene chemistry to prepare porous materials. Materials have many essential technological uses involving thiol-ene. These include, for example, inter alia, support for several catalysts and reagents, chromatography stationary phases, substrates for 3D cell culture and tissue engineering and hydrogen storage media.[32]

1.7 Aim and motivation of this thesis

In this thesis we synthesis poly thiol allyl microstructure particles and explore their behaviour by comparing their chemical structure, glass transition temperature and morphology, before and after post-polymerisation functionalization. The main purpose of these microparticles is that they can be crosslinked to suit their desired purpose and can be used in vivo (e.g. in the case of drug delivery).[59] The thesis organization start with the introduction in the form of this chapter, followed by experimental details of the project in Chapter 2. In Chapter 3 we describe the synthesis and chemical analysis of multifunctional cross linkers for use in cross-linked microstructure polymer particle preparation. This novel hexa-allyl cross-linker was synthesised by combining epoxy ring opening reactions/ reagents with the Thiol-Michael Addition reaction reagent. Thiol-allyl crosslinked microstructure polymer particles were prepared using the high share suspension polymerisation technique using the thiol-ene click reaction of HA with a selected series of thiol monomers with various degrees of functionality. In addition to this, we functionalize the residual of

the thiol functional group on the surface of micro spherical poly tetrathiol-ally particles using different acrylate monomers. Chapters 4 and 5 investigate the influence of varying the thiol monomer ratio, the homogenizer speed, the crosslink density photo polymerization time, and the thermal curing methods on the glass transition temperature (Chapter 4) and the morphology (Chapter 5) of the poly thiol-allyl compounds before and after post-polymerisation functionalization. In Chapter 6, we discuss the polymerization of water-in-oil (W/O) high internal phase emulsions (HIPEs) containing trimethylolpropane tris(3-mercaptopropionate) (trithiol) and dipentaerythritol penta/hexaacrylate (oil phase) using three methods involving three different pieces of emulsification equipment, and show their influence on the polyHIPEs morphology Finally, in Chapter 7, we conclude and highlight the main achievements and the contribution of this thesis to polymer and colloid science. The supplementary information in Chapter 8 contains the additional characterisation of the chemical structure using EDX analysis.

2 Methods and Instrumentation

2.1 Materials and Equipment

2.1.1 Materials

All chemicals were purchased from Sigma Aldrich, unless otherwise noted, and used as received. Distilled water from Millipore Milli-Q water system (18.2 MQ cm) was used in all experiments. The materials used in the synthesis of Hexa-allyl multifunctional cross-linker were: Trimethylolpropane triglycidyl ether (triepoxide, ≤10 ppm free epichlorohydrin, 99.0 %), diallylamine (99%) and methanol (MeOH, 99.9%).

The materials used in the suspension photo and thermal polymerisation experiment were: Pentaerythritol tetrakis(3-mercaptopropionate) (Tetrathiol, 4T, 95%), Trimethylolpropane tris(3-mercaptopropionate) (trithiol, 3T, ≥95.0%), 2,2′-(Ethylenedioxy) diethanethiol (dithiol, 2T, TEGDT, 95%), 1,6-Hexanedithiol (dithiol, 2T, HDT, 96%), toluene (anhydrous, 99.8%), photoinitiator (a blend of diphenyl (2, 4, 6-trimethylbenzoyl) phosphine oxide/2- hydroxy-2-methylpropiophenone, Divinylbenzene (DVB, 80%) Azobisisobutyronitrile (AIBN) Sodium dodecyl sulfate (SDS, ≥99%, Fisher Scientific), Methanol (≥99.9%), Dichloromethane (DCM, 99+%, Fisher Scientific), Acetone (>99.99%) and Diethyl Ether (DEE, 99.5+%, Fisher Scientific).

The materials used in post-polymerisation functionalisation were: 5.5′-Dithiobis(2-nitrobenzebenzoic acid) (DNTB, ≥98%), Dimethyl Sulfoxide (DMSO, ≥99.9, Fisher Scientific), 2,2′-(Ethylenedioxy) diethanethiol (dithiol, 2T, TEGDT, 95%), Trimethylamine (TEA, 99%, Fisher Scientific), 2-Hydroxyethyl acrylate (HEA, 96%), Methyl arylate (MA, ≥99.5%), Ethylene glycol methyl ether acrylate (EGMEA, 98%) and 2(Diethylamino) ethyl acrylate (DEAEA, 95%).

The materials used in the polyHIPEs preparation were: Monomers Trimethylolpropane tris(3-mercaptopropionate) (trithiol, 3T, ≥95.0%) and dipentaerythritol penta/hexa-acrylate (DPEHA, ≤650 ppm MEHQ as inhibitor), photoinitiator (a blend of diphenyl (2, 4, 6-trimethylbenzoyl) phosphine oxide/2-hydroxy-2-methylpropiophenone, 1,2- dichloroethane (DCE, ≥99.5%) (from MERCK) were used as received. The surfactant Hypermer B246, obtained from Croda, is a triblock copolymer of polyhydroxystearic acid and polyethylene glycol[60] and was used as supplied.

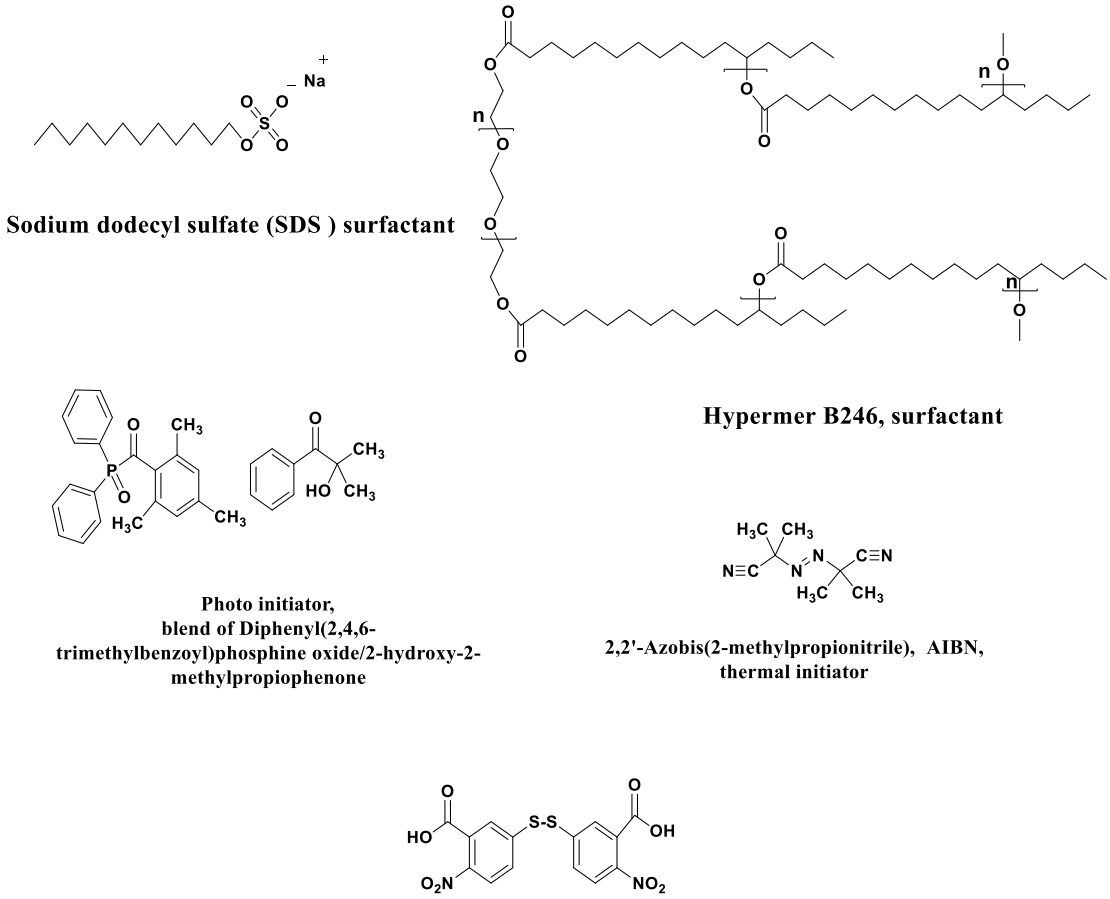

Figure 2.1. The chemical structure of surfactants, initiators and Ellman's reagent were used in this study.

2.1.2 Equipment

All techniques requiring mixing and/or heating were carried out using IKA WERKA magnetic stirrers. All glassware was cleaned and dried before use.

UV-Light Sources. A UV nail gel curing lamp (λ_{max}~360 nm), equipped with four 9W bulbs, was used as the UV-source light for curing thiol-allyl particles via suspension photo polymerisation.

Homogeniser. An Ultra-Turrax homogeniser from IKA, with an 18 mm head at a speed of 8000 rpm or 20500 rpm for 30 sec at room temperature, was used.

2.2 Characterization and analytical techniques

Nuclear Magnetic Resonance (NMR). The following NMR experiments were recorded on Bruker DPX-300 and DPX-400 spectrometers using solvents purchased from Sigma–Aldrich: ^{1}H and ^{13}C NMR and COSY spectra. Chemical shifts (δ) were reported in parts per million (ppm) relative to either the tetramethylsilane (TMS) reference signal located at 0.00 ppm or the residual non-deuterated solvent ($CHCl_3$) signal at 7.26 ppm.

Fourier Transform Infrared Spectroscopy (FTIR). The FTIR spectra were measured on a Bruker VECTOR 22-G1003697 spectrometer that was fitted with a golden diamond attenuated total reflection cell and presser tower; it was analysed using Opus spectroscopy software.

Electrospray Ionisation-Mass Spectrometry (ESI-MS). The ESI-MS analyses were obtained using Agilent 6130B Single Quad electrospray instruments using positive electrospray mode.

Ultraviolet-Visible Absorption Spectroscopy (UV-Vis spectra). The UV-Vis spectra were recorded on a SYNERGY/HTX multi-mode reader, supplied by BioTek Instruments, with a wavelength range of 300-600 nm.

Raman spectroscopic. The Raman spectroscopic measurements were carried out using a Renishaw inVia Raman microscope. All spectra were recorded on neat solid samples with an excitation wavelength of 785 nm using 5x objective. Obtained spectra were 1 accumulation of acquisitions of 10 seconds over a region of 400-4000 cm^{-1}.

Differential Scanning calorimetry (DSC). The T_g of microparticles was analysed using a Mettler Toledo DSC in 40 μL hermetically sealed aluminium pan. The T_g values were recorded with Mettler Toledo STARe software. All test samples were measured using the following temperature programme (two heating/cooling cycles): from -40 ˚C to 50 ˚C at 10 K/ min, a flow of N_2 at 50 mL/min was used and the weight of the samples was 5-8 mg. The T_g was determined from the second heat cycle and taken at the middle of the step-like change in the baseline of DSC.

Energy dispersive X-ray spectroscopy (EDX). The elemental compositions mapping (mass/atomic) of synthesised microcomposite was conducted to determine the presence of various elements in poly thiol-allyl microstructure particles before and

after post-polymerisation functionalisations were performed with energy dispersive X-ray spectroscopy (EDX) in Zeiss SUPRA 55VP FEG/SEM with OXFORD X-ray **analysis system.**

Scanning Electron Microscope (SEM). The surface morphology of synthesised samples of poly thiol-allyl microstructure particles before and after post-polymerisation functionalisation were investigated using a scanning electron microscope with a field emission electron gun (Zeiss Supra® 55VP-23-99 FEG/SEM).

The samples to be analysed were placed on aluminium pin stubs with Leit adhesive carbon tabs 12mm (electrically conductive), and the loose or excess material was removed by compressed air. In order to increase the electron conduction and to improve the quality of the micrograph, a conductive layer of Au/Pd was made with Polaron sputter coater prior to SEM investigation. Thereafter, the samples were placed in a sample holding vacuum chamber and operated at an accelerating voltage of 10 KV. Images were captured by signal SE2 detectors with a working distance of 8.4 mm. The spot sizes varied from 10 μm to 20 μm depending on the applied magnifications. All particle diameter size measurements on micrographs were performed using ImageJ software. A statistical correction factor was employed to provide accurate particle diameters

2.3 Synthetic procedures

2.3.1 Multifunctional cross-linker via combining epoxy ring opening reactions/reagents with Michael's addition reaction reagent

The synthesis of hexa-allyl cross-linker was done via reaction of triepoxide with diallyl amine (surface allylation) using a previously reported method with minor modification.[61] A 250 mL round-bottomed flask (RBF), charged with a stirring bar, contained a solution of 2.3 mL (3.6 g, 12 mmol) trimethylolpropane triglycidyl ether in 10 mL of methanol; a solution of 10.3 mL(8 g, 83.43 mmol) of dially amine in 40 mL of methanol was added and continuously stirred for 10-15 min. After that, the flask was immersed in the oil bath and the mixture was stirred at 60 ˚C for three days. After the reaction had finished, the solvent was removed using a rotary evaporator to give a clear viscous oil (78%). ^{1}HNMR (300 MHz, $CDCl_3$): δ 0.992 (t, 3H), 1.67 (m, 2H), 2.67(m, 4H), 4.27(m, 30H), 5.47 (m, 10H), 6.35(m, 5); ^{13}CNMR (75.74 MHz, $CDCl_3$): δ 7.76, 23.17, 43.37, 55.87, 57.10, 66.91, 72.01, 74.03, 117.86, 135.24. Based on ^{1}HNMR integrals, it is estimated that we have between 90-99% of allylation of epoxides (5.72/6 =0.99; 10.81/12 = 0.90). IR : υ (cm^{-1}) 3450 (O-H), 2970 (stretch C-H), 1646 (stretch C=C), 1240 (stretch C-N), 1146 (stretch, C-O), MS (ESI) m/z: 594.4477$[M+H]^+$ $C_{33}H_{60}N_3O_6$.

2.3.2 General procedure for the synthesis of cross-linked poly thiol-allyl microsphere particles via thiol-ene click suspension photo polymerisation

The conditions for synthesis of poly thiol-allyl microsphere particles via thiol-ene click suspension photo-polymerise was adopted from a modification of previously published procedures.[40, 62] Our model consisted of two multifunctional monomer

(hexa-allyl, which was synthesised by us, and thiols), and used stoichiometric ratios of double bond of ene monomer (hexa-allyl) and thiol functionality. All reactions were carried out with 9.45 wt.% of total weight of monomer relative to the water and all quantities were carried with regard to the total monomer weight.

In the typical procedure of equal ratio between tetra thiol and hexa-allyl (1:1), the first mixture (organic/dispersed phase) was prepared by adding a total of 2.96 g (2 mmol, 44.71 wt.%) of HA, 3.66 g (3 mmol, 55.36 wt.%) of tetrathiol, 1.466 g (0.7 mL, 11.84 wt.%) of photo initiator is soluble in the organic phase and 4.32 g (92.14 mmol, 65 wt.%) of toluene into a 50 mL glass jar equipped with a magnetic stirrer bar; it was then wrapped with aluminium foil to avoid light and stirred. The second mixture (aqueous/continuous phase) was prepared by dissolving 3.5 g (12.13 mmol, 5 wt.% relative to water) of SDS in 70 mL distilled water in a 250 mL glass jar; this was also covered with aluminium foil. After introducing the first mixture to the second one, the high speed homogeniser was used to mix the two mixtures for 30 sec to obtain uniform distribution of the dispersed phase, which immediately turned milky and resulted in the third mixture (suspension).

The preparation of the suspension mixture was repeated twice to produce particles at homogeniser speeds of 8000 rpm and 20500 rpm after being mixed by the homogeniser, the suspension was irradiated by continuous UV light (λ =360 nm) for either 1 or 5 hours, using continuous magnetic stirring at room temperature, with a stirring rate of 600 rpm, to maintain fairly uniform drops that formed during the intensive homogenisation. Finally, the content was poured slowly through a Buchner funnel attached to a vacuum pump containing filter paper in the top, which was

moistened with methanol; methanol was also added to the suspension mixture during filtration through the Buchner funnel to loss of solid polymer particles. Then the products were washed successively with methanol, DCM, acetone and DEE. The resultant pale yellow/white powder was dried in a vacuum oven at 25 °C for 48 hours. The resulting particles were characterised and used without further purification.

For the synthesis, polymeric microsphere particles with excess of thiol functionality based at molar ratio 1.5:1 and 2:1 of tetrathiol: HA were carried out as described. All other conditions of suspension photo-cured network composition, containing trithiol: HA or dithiol: HA, were identical to the one used for microsphere particles via the use of tetrathiol: HA.

2.3.3 General procedure for the synthesis of cross-linked poly thiol-allyl microsphere particles via suspension thermal polymerisation

For the thermal-initiated reaction, the suspension (third mixture) was accomplished in accordance with the previous procedure. In this part 10 mol% of AIBN (relative to monomers) was used as thermal initiation. The reaction mixture was poured into a 50 mL 3-necked RBF containing a magnetic stirring bar. The mixture was then immediately purged with nitrogen in an ice-cold bath on stirrer plate and stirred at 600 rpm for 30 min to flush-out the dissolved oxygen in the mixture and provide inert atmosphere. The RBF was sealed with rubber septa and one side was connected to a nitrogen line with a venting needle placed in the other side (The nitrogen line was placed above the liquid so as to avoid SDS foaming). The venting needle was then removed and the RBF was immersed in an oil bath (preheated to 75 °C) for 2 hours, stirring at 600 rpm was continued throughout. Afterward, the sample was removed

from the oil bath and allowed to cool to room temperature on a stirrer plate, still set to stir at 600 rpm. Once cooled, the particle suspension was poured into a Buchner funnel attached to a vacuum pump to collect the particles. The particles were then washed with sequential volumes of water, methanol, DCM and DEE. Finally, the particles were collected into a glass jar and placed in a vacuum oven to dry overnight.

All other thermal-induced reactions of poly tetrathiol-allyl microsphere particles with molar ratio of 1:1 (with DVB, 3 mmol), 1.5:1 and 2:1 were carried out similar to the above method.

2.3.4 Determination of available thiol using Elman's reagent/UV analysis

Before functionalisation, the residual of thiol groups on the microsphere polymer particles' surface was determined by Ellman's assay. For Ellman's assay, 50 mg of dry particle samples were re-suspend in 275 mL DMSO and reacted with 100 µL of Ellman's reagent solution (4 mg of DNTB in 1 mL DMSO) for 10 to 15 min. Then, 250 µL aliquots were placed into 96 well microplates and the absorbance of the relative particles measured at 498 nm using a BioTek Epoch plate reader. Thiol concentration was calculated by calibrating the curve of 2,2′-(Ethylenedioxy) diethanethiol (dithiol) solution that was used as standard from 40 µL to 244.1 µL (See Table 2.1). Figure 2.1 displays the standard curve prepared by adding 250 µL of each dithiol standard into a test tube, each containing 50 µL of Ellman's reagent solution and 2.5 mL of DMSO.

Table 2.1. A Set of Dithiol Standards were Prepared by Dissolving Dithiol at the Following Concentration of DMSO

Standard	Volume of DMSO	Dithiol (M.W=182.30)	Final concentration
A	9.755 mL	0.2441 mL	1.5 m
B	9.796 mL	0.203 mL	1.25 mM
C	9.837 mL	0.162 mL	1.0 mM
D	9.878 mL	0.122 mL	0.75 mM
E	9.918 mL	0.081 mL	0.5 mM
F	9.959 mL	0.040 mL	0.25 mM
G	10.000 mL	0.000	0.0 mM

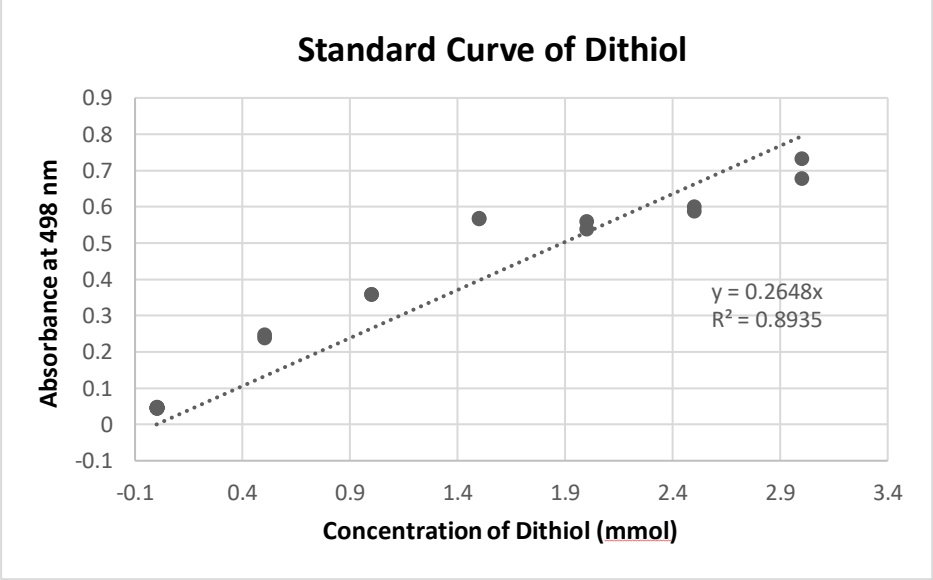

Figure 2. 2 Standard curve from Ellman's assay.

The number of moles of thiol for true weight of the particles was calculated as follows (Table 2.2): Thiol group concentration = absorbance of relative particles/0.265

Table 2.2. Thiol Concentration in Particles

Mass	**Sample code**	**Samples: [tetrathiol]:[allyl]/homogenizer speed/UV for 5h**	**Absorbance (nm)**	**thiol group concentration (mmol)**
50mg	TAP57	1:1 / 800 rpm	0.403	1.52
50 mg	TAP58	1:1/ 20500 rpm	0.257	0.969
50 mg	TAP59	1.5:1/8000 rpm	1.02	3.87
10mg	TAP60	1.5:1/20500 rpm	1.58	5.96
10mg	TAP61	2:1:1/8000 rpm	0.395	1.49
10 mg	TAP62	2:1/ 20500 rpm	0.267	1
5mg	TAP35	1.5:1 / 8000 (uv for 1h)	1.637	6.177

2.3.5 General procedure for the post-polymerisation functionalisation of cross-linked poly tetra thiol-allyl microparticles with acrylate monomers

The post-functionalisation was based on the reaction between the thiol group on the surface of microsphere particles and acrylate monomers using a previously published protocol. That is, thiol Michael addition of 1.5 eq. HEAMA, EGMEA, DEAEA) with 1 eq. microsphere polymer of thiol-allyl particle using 0.5 eq. catalyst, trimethylamine.

In a typical experiment, 50 mg of sample particles were mixed in glass vial with 1 mL of DMSO. The desired acrylate and TEA monomer were used at 1.5 and 0.5 molar equivalent, respectively, relative to the calculated thiol group residual. The

functionalised reaction was allowed to proceed at ambient temperature overnight without stirring. Each reaction was vacuum filtered and washed three times with 5 mL methanol, 5 mL DCM, 5 mL acetone, and 5 mL DEE. The particles were dried thoroughly in a vacuum oven at 25 ˚C for 48 hours a few days prior to analyses.

2.3.6 Preparation of polyHIPEs using an overhead stirrer

An overhead stirrer with a fixed stirring rate was chosen. The stirrer paddle was made out of PTFE which perfectly fits the inner bottom of a 250 mL 3 neck RBF In the dropping funnel attached to the continuous carrier phase, 70 mL of the internal phase (water) was added wisely to form a HIPE. The emulsion was then poured into seven cylindrical PTFE moulds with a diameter of 15 mm and a depth of 20 mm. The moulds were secured between two glass plates and passed under a UV irradiator (Fusion UV systems Inc. Light Hammer® 6 variable power UV curing system with LC6E benchtop conveyor) and were polymerised fifteen times on each side at a belt speed of 4.0 m min^{-1}. The polymerised emulsion was purified using Soxhlet extraction overnight with DCM and dried in a vacuum oven at room temperature for 4 hours.

2.3.7 Preparation of emulsion or polyHIPEs using a vortex mixer

The oil phase consisted of a mixture of trithiol and DPEHA (cross-linkers), a blend of diphenyl (2, 4, 6-trimethylbenzoyl) phosphine oxide/2- hydroxy-2-methylpropiophenone (initiator) and surfactant Hypermer B246. HIPEs were prepared by stirring using a vortex mixer at 30 hertz. Typically, the emulsions were obtained by mixing 2 ½ mL of organic solvent or monomers and the slow gradual addition of 14 mL of the internal phase (water) using plastic pipette droppers. The polymerised emulsion was soaked in acetone, then purified using Soxhlet extraction overnight with DCM, and dried in a vacuum oven at room temperature for 4 hours.

2.3.8 Preparation of emulsion of polyHIPEs using a homogeniser

The oil phase consisted of a mixture of trithiol and DPEHA (cross-linkers), a blend of diphenyl (2, 4, 6-trimethylbenzoyl) phosphine oxide/2- hydroxy-2-methylpropiophenone (initiator) and a surfactant Hypermer B246. HIPEs were prepared by stirring the homogeniser with an 18 mm head at speeds up to 8000 rpm. The emulsions were obtained by mixing 2½ mL of organic solvent or monomers and the slow gradual addition of 14 mL of the internal phase (water) using plastic pipette droppers. Also, an equal ratio of oil phase and water phase, with a total volume of 5 mL, were emulsified using the homogeniser at speeds up to 8000rpm for 1 min at room temperature.

3 Novel poly thiol-allyl particles via thiol-ene suspension polymerisation

3.1 Introduction

Cross-linked micro-structured polymeric particles have received great research interest due to their application in industrial and biomedical fields such as paint coating, chromatography columns, catalysis, ionic exchange processes, enzyme immobilisation, cosmetics and drug delivery.[17, 39, 63-66]

Recently in drug or vaccine delivery fields, cross-linked polymeric microparticles have attracted growing interest as using microbead system proteins delivery has successfully demonstrated class I antigen presentation with macrophages through the activation of cytotoxic T cells, which is a necessary step in vaccine development.[67] As it brings about using a cross-linked microparticle, this will enable encapsulating plasmids physically, rather than electrostatically, and without the use of polycations, which also allows this delivery system to be compatible with biomolecules of other charged states such as proteins.[67] It has been demonstrated that plasmid DNA is directly encapsulated into biocompatible polymer microparticles via radical polymerisation in an inverse emulsion system.[67] In addition to this, Frechet et al. (2004) published a paper in which they described polymers how were synthesised by applying an AA-BB type step of growth polymerisation in which AA is the acid-degradable diamine monomer and BB represents a variety of bis-electrophilic monomers with different hydrophobicities; they synthesised a library of polymers and identified those polymers that could both form suitable microparticles and degrade sufficiently quickly to be used as delivery vehicles.[63] This can potentially be used in a wide range of commercially available or easily synthesised bi-functional monomers to readily prepare polymers with variable physical properties, which further highlights the versatility of their approach.[63]

Over the past decade, there has been a dramatic increase in the development of many synthetic approaches to the synthesis of various polymeric microsphere particles.[17, 40, 64, 68] Generally, heterogeneous polymerisation systems are used to produce polymer particles including dispersion, emulsion and suspension polymerisation.[40, 42] Ship et al. (2013) have reported the use of thiol–ene suspension polymerisations.[40, 42] In addition, thiol cross alkene has recently become a popular approach to the synthesis of microsphere polymer particles.[64] It is one of the most important click chemistry reactions, known as thiol-ene reaction, which was reported in about 1905.[55] Thiol-ene chemistry is attractive in the fields of biomedical application, optics, electronic devices, coating and film. Due to its flexibility and fast robust platform for the formulation of polymer network, and because of lake of water and oxygen sensitivity, it has high conversion and yield, negligible by-products, is solvent-free, and has a rapid reaction rate and photo polymerisation even at ambient temperatures.[55, 69, 70] These features are essential given short processing time and are suitable for manufacture scale environments.[70]

The allyl group provides a handy chemical handle with many promising chemical pathways, and has been examined as a possible derivatization route in different variations.[71] One way of utilising the allylated epoxide is through thiol−ene reactions.[71] The radical thiol-ene reaction has been effectively exploited as a facile and suitable tool for polymer functionalisation and the construction of complex macromolecules such as dendrimers and polymer networks.[72] Apart from the radical mediated thiol-ene reaction, when activated olefins with electron accepting groups are

used, the Michael-type addition of a thiol to the activated C=C bond were proceed in the presences of nucleophilic or basic catalyst.[72]

The novelty of our design surface allylation for commercially available trieopxide is by combining epoxy ring opening reaction with Michael addition reaction reagent, forming a cross-linker with six allyl group HA followed by photo cross-linking by tetrathiol, trithiol and dithiol (TEGDT, HDT) monomers by thiol-ene suspension click polymerisation, which is reported here for first time. Then, various acrylate monomers (HEA, MA, EGMEA, DEAEA) were used for post-polymerisation functionalisation of unreacted thiols on the surface of the cross-linked tetra thiol-HA microsphere polymer particles by base-catalysed thiol Michael addition reaction. The main aims of the current chapter are to determine the structural changes of a chemical nature in the poly thiol-allyl microstructure particles before and after post-polymerisation functionalisation using FT-IR Raman spectra and EDX to examination structure and functionality before post-polymerisation functionalisation. Figure 3.1 shows the schematic routes for thiol-ene suspension polymerisation applied in cross-linked microparticles.

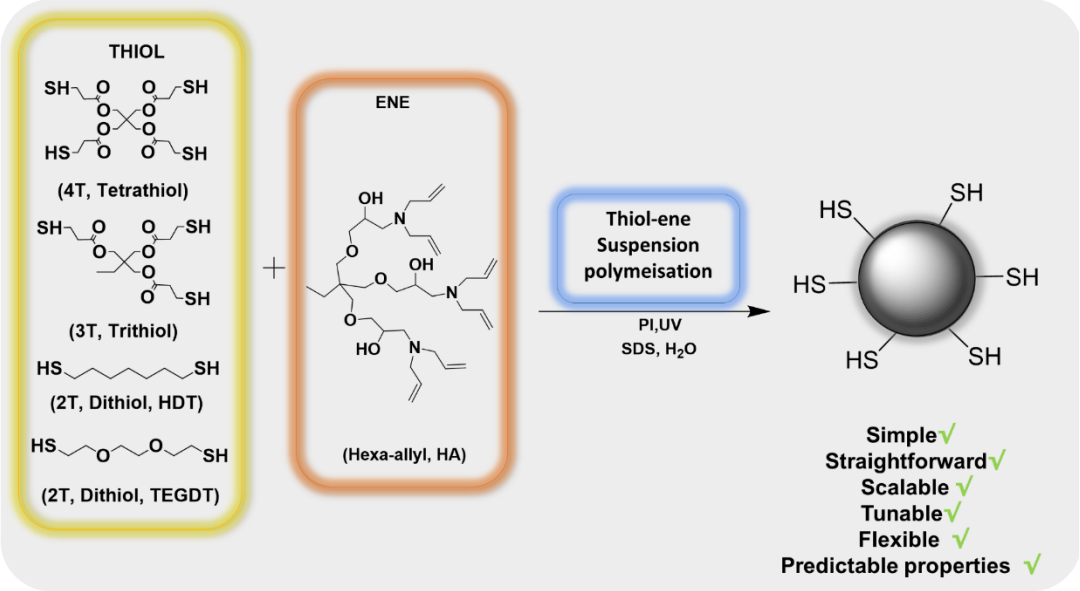

Figure 3.1. Schematic representation of the approach employed to prepare thiol-allyl cross-linked.

It is significant that these particles can be easily engineered to tailor their glass transition temperature, shape and size by tuning the molar ratio between thiol and allyl functional groups, homogeniser speed, network cross-linking density, photo polymerisation time or curing method, which will be discussed in detail in chapters 4 and 5.

3.3 Results and Discussion

3.3.1 **Synthesis and characterisation of hexa-allyl multifunctional cross-linker via the combining of epoxy ring-opening and Michael addition**

Preparing branched polymer systems via ring opening reaction, known as polymerisation using ring opening, is well known, particularly using cyclic ethers, amides, sulphides, aziridenes, siloxanes and others with ether cationic, anionic or other

mechanisms.[61] Yet, synthesis of highly branched polymers via ring opening polymerisation is less well known. Although work has been done on the use of ring opening polymerisation in the synthesis of several hyper-branched polymers, mostly it is of the traditional type, resulting in hyper-branched polymers with broad poly-dispersal ties.[61] Herein, we use the ring opening reaction that was used to prepare hyper branched polymers. This new method for synthesis of a multifunctional cross-linker is suitable as a starting material, particularly for preparing the polymer particles via suspension polymerisation if the oil phase consists of stoichiometric formulation of thiol-ene system in addition to the initiator and solvents. This method is simple and there is no need for further purification steps that cause low yield product. The ring opening reaction of diallyl amine with triepoxide affords the multifunctional cross-linker with six allyl groups. Figure 3.2 shows the scheme methodology of synthesis of HA. The method was straightforward using methanol as a solvent. The mechanism that indicates the addition of diallyl amine to the epoxy group.

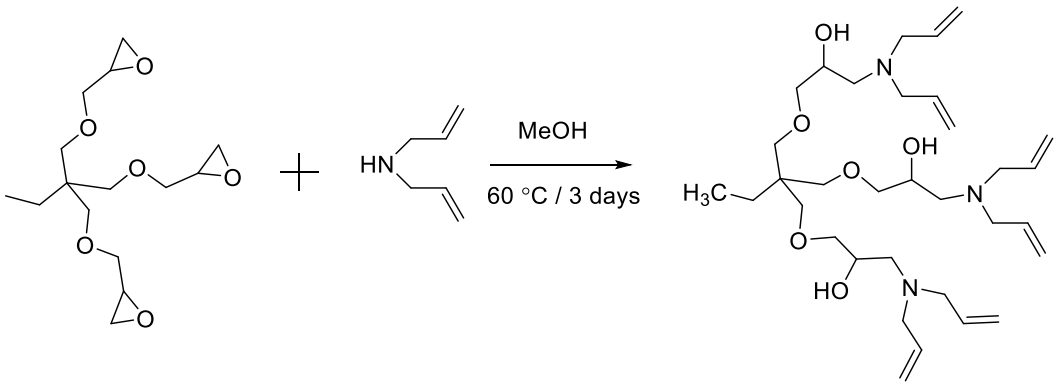

Figure 3. 2. Synthesis of multifunctional cross-linker.

The experimental procedures and conditions used in the synthesis are described in chapter 2. This surface allylation provides good control of the number of functional

groups. It was analysed by ^{1}H NMR, ^{13}CNMR, ^{1}H COSY NMR and mass spec. Confirmation of successful FTIR were all in agreement with the anticipated product. Figure 3.3 represents the ^{1}HNMR with each peak assigned. The peaks located in the region of 5-6 correspond to the allyl groups in the epoxy/allyl, allylated by ring opening functionalisation process. The 1D ^{1}H-NMR spectrum, shown with the 2D H-NMR correlation spectrum (COSY) in Figure 3.4, indicates that the peaks located in the region of 5-6 correspond to the allyl groups of allylated triepoxide. 2D COSY NMR spectrum analysis has proven the formation of the product of HA monomer and the cross-peaks, which are observed in the 2D COSY when there is spin-spin coupling between the hydrogen as a consequence of the connectivity between the following carbons h/I, h/g, i/g, e/OH, e/d and a/b. The ^{13}C NMR spectrum is shown in Figure 3.5, and the mass spectrum is displayed in Figure 3.6. These show the correct [M+H] + molecular ion peak at 594.4477 m/z. The peaks in the mass spectrum all relate to the product.

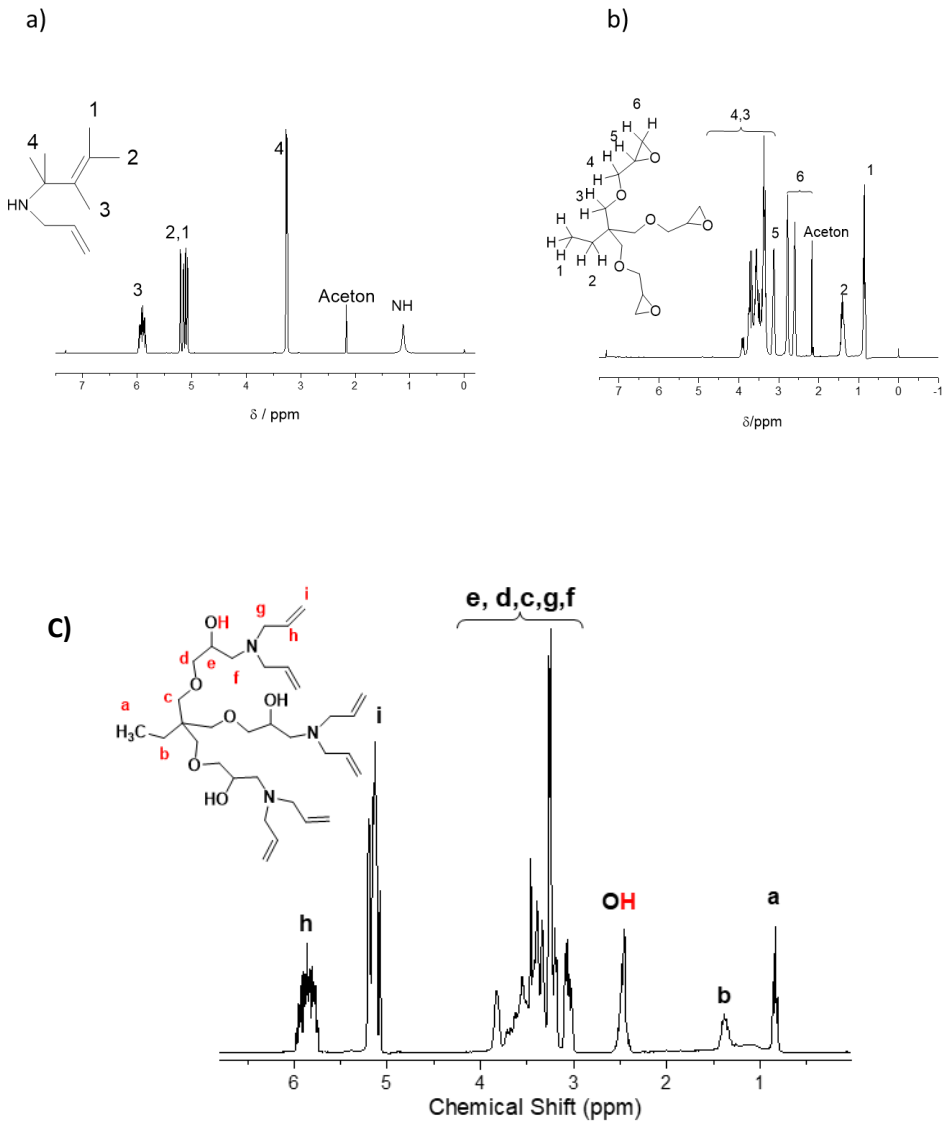

Figure 3. 3. ^{1}H NMR spectrum ($CDCl_3$, 300 MHz) of a) diallylamin, b) triepoxide and c) the HA cross-linker.

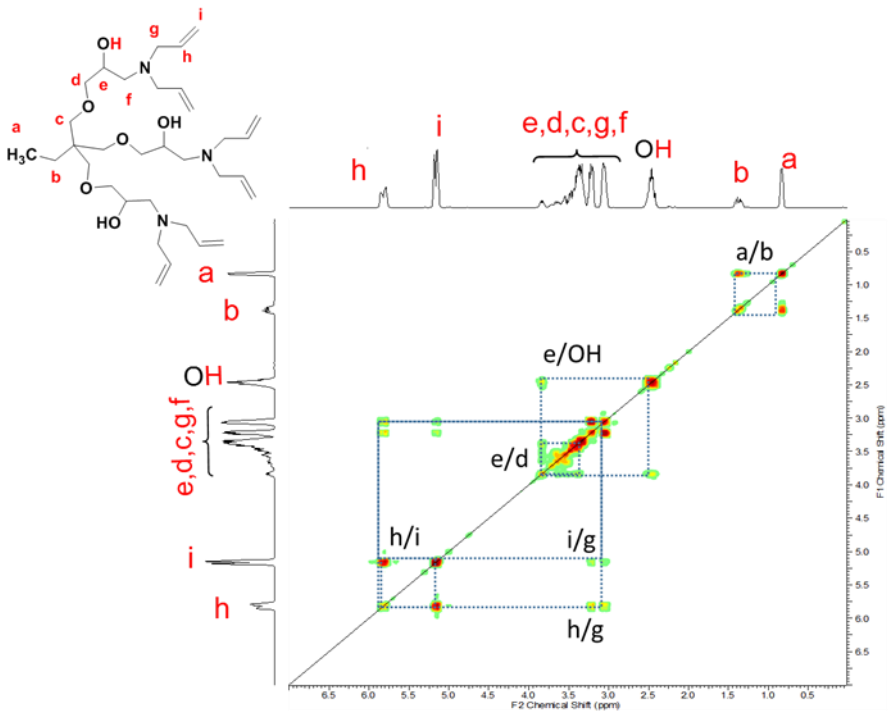

Figure 3. 4. ^{1}H-^{1}H COSY NMR spectrum ($CDCl_3$, 300 MHz) of HA.

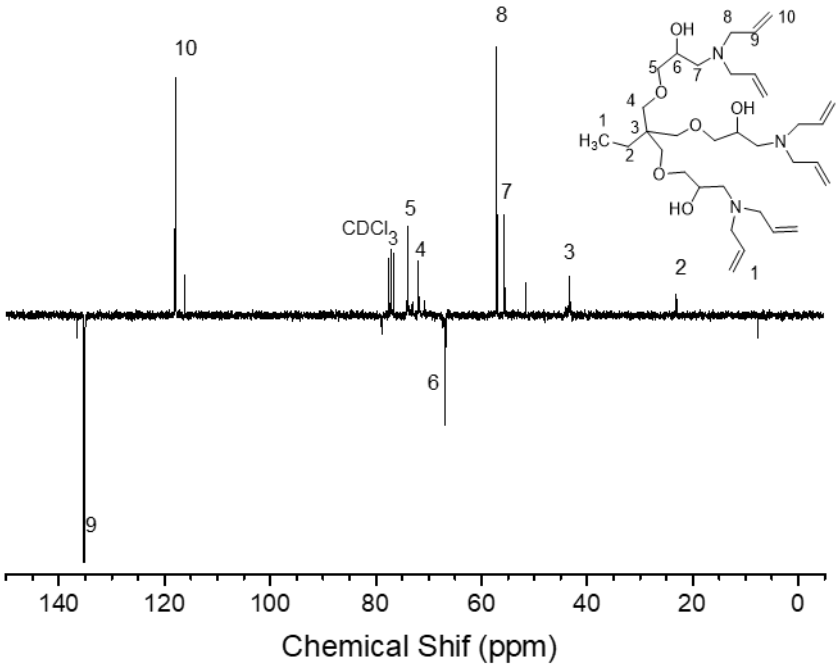

Figure 3. 5. ^{13}C NMR ($CDCl_3$, 300 MHz) spectrum of the product of HA cross-linker.

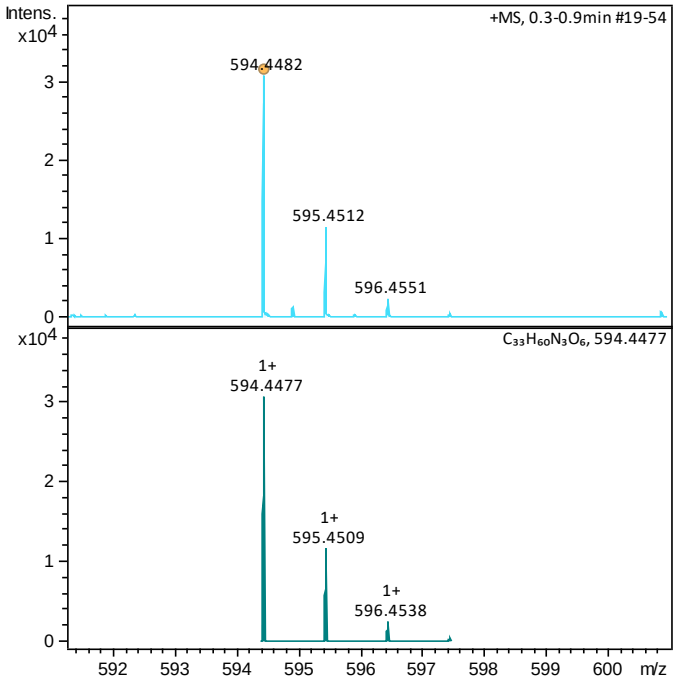

Figure 3. 6. ESI-MS spectra of HA cross-linker.

FT-IR spectra of HA is shown in Figure 3.7. The bands at 3010 and 3075 cm-1 are described as =C-H2 and =C-H, respectively, stretching vibrations of the alkenes group. Furthermore, the sharp band at 1635 cm^{-1} corresponds to C=C. The doublet bands at 2780 and 2830 cm^{-1} are assigned to the C-H stretching vibration of CH_2-N and CH_2-O, respectively. Also, a sharp band near 1625 cm^{-1} associated with stretching vibrations of C-N appears. Notice that C-O vibrations of CH-OH and C-O-C are generally located at around 1000 and 1085 cm^{-1}. The broad band ranging from 3250 to 3600 cm^{-1} with a peak centred at 3423 cm^{-1} is attributed to the O–H stretching vibrations of adsorbed hydroxyl groups resulting from the ring opening reaction between triepoxied and allyl amine. These results confirm the success of using this approach for synthesis multifunctional cross-linker.

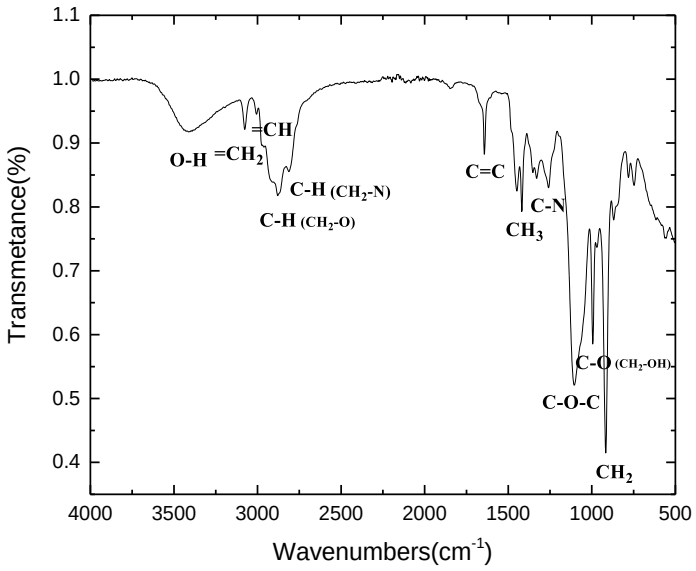

Figure 3. 7. FTIR spectra of HA cross-linker.

3.3.2 Synthesis and characterisation of poly thiol-allyl particles with surface thiol groups

Previously, mercapto group (SH) was incorporated into cross-linked particles by mercapto allylation with allyl functional cross-linker.[41, 43, 44, 46, 73-75] We aspired to develop poly thiol-allyl microsphere particles as presented by Ship et al.(2013) They reported a straightforward synthetic approach to making thiol-allyl cross-linked microsphere polymers using thiol-ene suspension click polymerisation, which resulted in microsphere particles.[40, 42, 45, 62]

We investigated the synthesis of thiol-allyl microstructure polymer particles using variable synthesis parameters: a series of thiol monomers of various functionality (cross-linking density), 2T, dithiol HDT, 2T dithiol (TEGDT), 3T (trithiol) and 4T (tetra thiol) were reacted with HA monomer (see Figure 3.8). These combinations serve the purpose of examining the different network properties based on varied cross-linking densities.[40, 76]

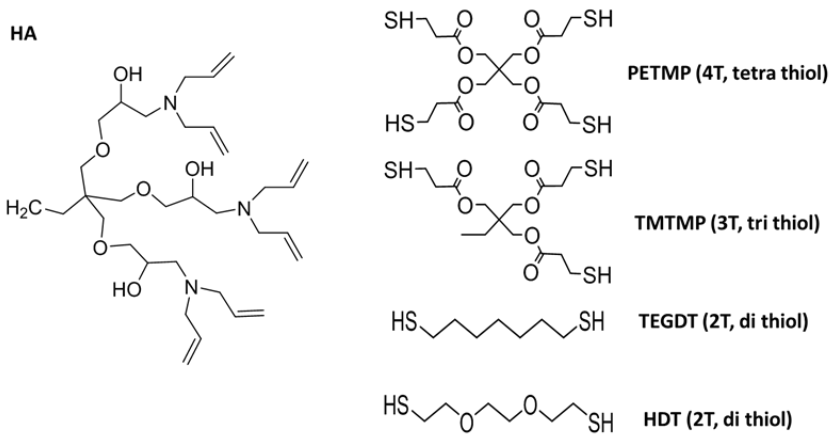

Figure 3. 8. Chemical structure of monomers used for poly thiol-allyl micro-structure particles.

The synthetic approach for heterogonous thiol-ene photo-polymerisation involves high-shear of the organic phase, consisting of monomers, initiator and solvent in aqueous solution of 5 wt. % SDS. In general, cross-linked thiol-allyl microstructure polymer particles were prepared by combining a 1:1, 1.5:1 and 2:1 molar equivalent of allyl and thiol functional groups at two types of mechanical agitation to create micro droplets. One before UV irradiation, which involves intensive power speed (8000 or 20500 rpm) to form droplets, followed by moderate magnetic stirring in the presence of ultraviolet light for 1 or 5 h or heating by oil bath using thermal initiators. The synthetic reaction for cross-linked thiol-allyl polymer particles is depicted in Figure 3.9.

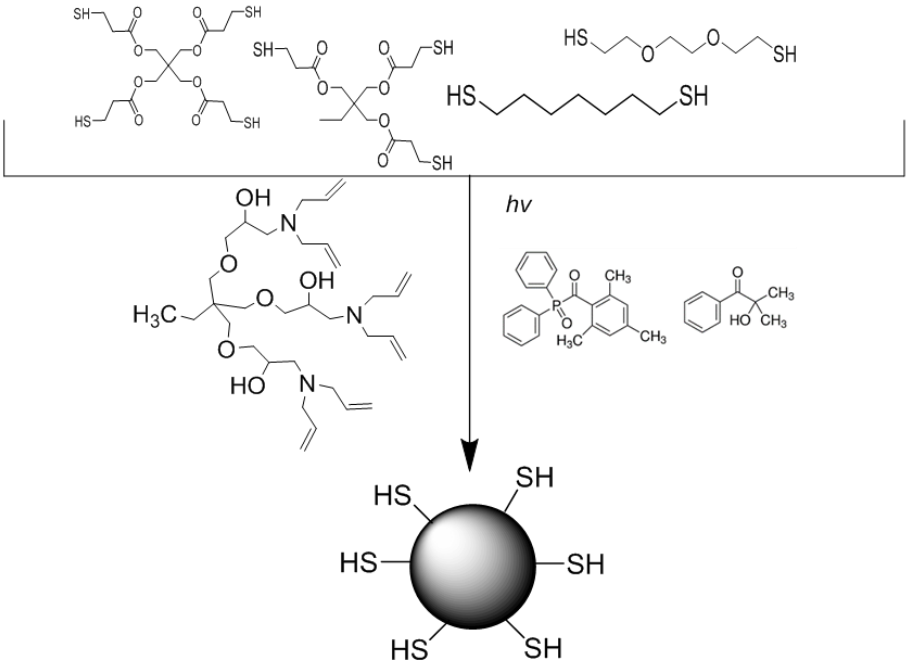

Figure 3. 9. Synthesis of poly thiol-allyl microstructure particles.

3.3.3 EDX analysis

Studying the chemical nature of the cross-linked polymer particles is one of the most important characteristics of analysis for some applications, especially where

functionalisation is need.[4] EDX and elemental mapping is a powerful tool that has been used widely in nano/microanalysis; it is also one of the most suitable techniques for characterising the surface chemistry of particles.[4, 77-91] Elemental analysis in scanning electron microscopy (SEM) is achieved by measuring the energy and intensity distribution of X-ray signals produced by focused electron beam.[77] The EDX and elemental mapping for the prepared poly thiol-allyl microstructure particles were recorded and their corresponding chemical scheme reactions are shown in Figures 3.10 to 3.16. From Figures 3.11 to 3.18, several observations can be made. First, the existence of C, N, O and S peaks in the EDX spectra of these microcomposites confirm the synthesis poly thiol-allyl microstructure particles. Second, the distribution of S and O, N and C in all samples was further confirmed by EDX elemental mapping from the prepared microcomposite thiol-allyl particles. In addition, EDX mapping indicates homogenous element distributions of C, N, O and S throughout the samples, thus confirming the purity of the compound and the absence of any secondary phase.[79, 82] Finally, although the elemental composition showed that the amount of C, N, O and S in the structure differed significantly during varying thiol monomer ratio, homogeniser speed, cross-linking density, photo polymerisation time and thermal curing method, no particular trend could be followed regarding the influence of varying these conditions on the average chemical composition. Further investigations are required to evaluate the cause of this non-followed trend. The EDX results of photo polymerised poly thiol-allyl particles at higher ratios of thiol monomer and thermal initiated particles are presented in the appendix.

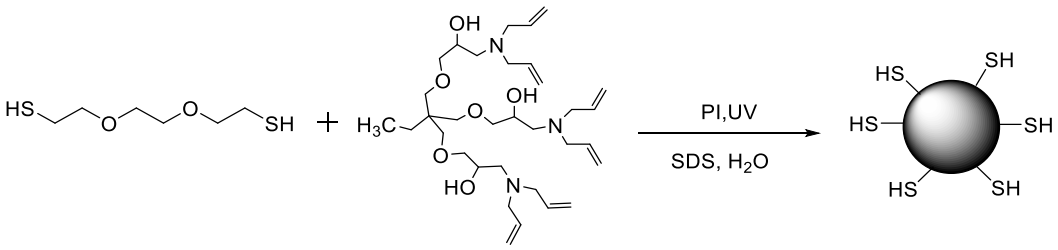

Figure 3. 10. Hexa-allyl-2,2′-(Ethylenedioxy)diethanethiol particles.

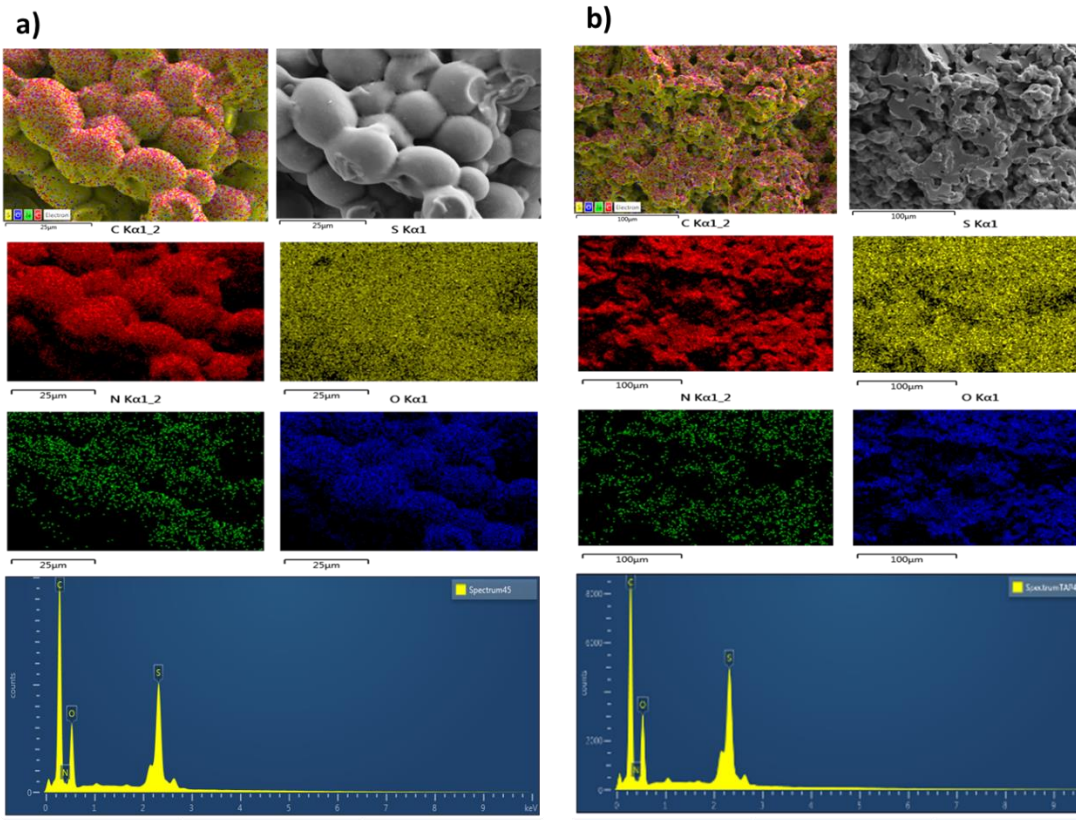

Element	Wt%	Atomic %
C	94.21	96.55
N	0.15	0.13
O	3	2.31
S	2.64	1.01
Total:	100	100

Element	Wt%	Atomic %
C	94.84	96.93
N	0.09	0.08
O	2.73	2.09
S	2.34	0.9
Total:	100	100

Figure 3. 11. SEM image, element distribution and EDX data for poly dithiol-allyl particles consisting of equal ratios of TEGDT and HA at (a) 8000 rpm and (b) 20500 rpm.

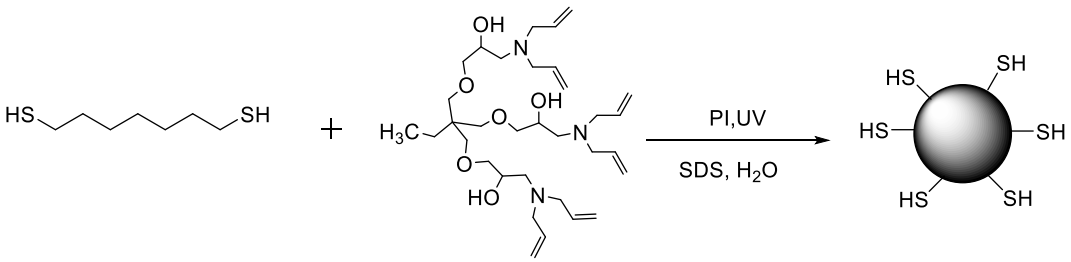

Figure 3. 12. Hexa-allyl-1,6-hexane dithiol particles.

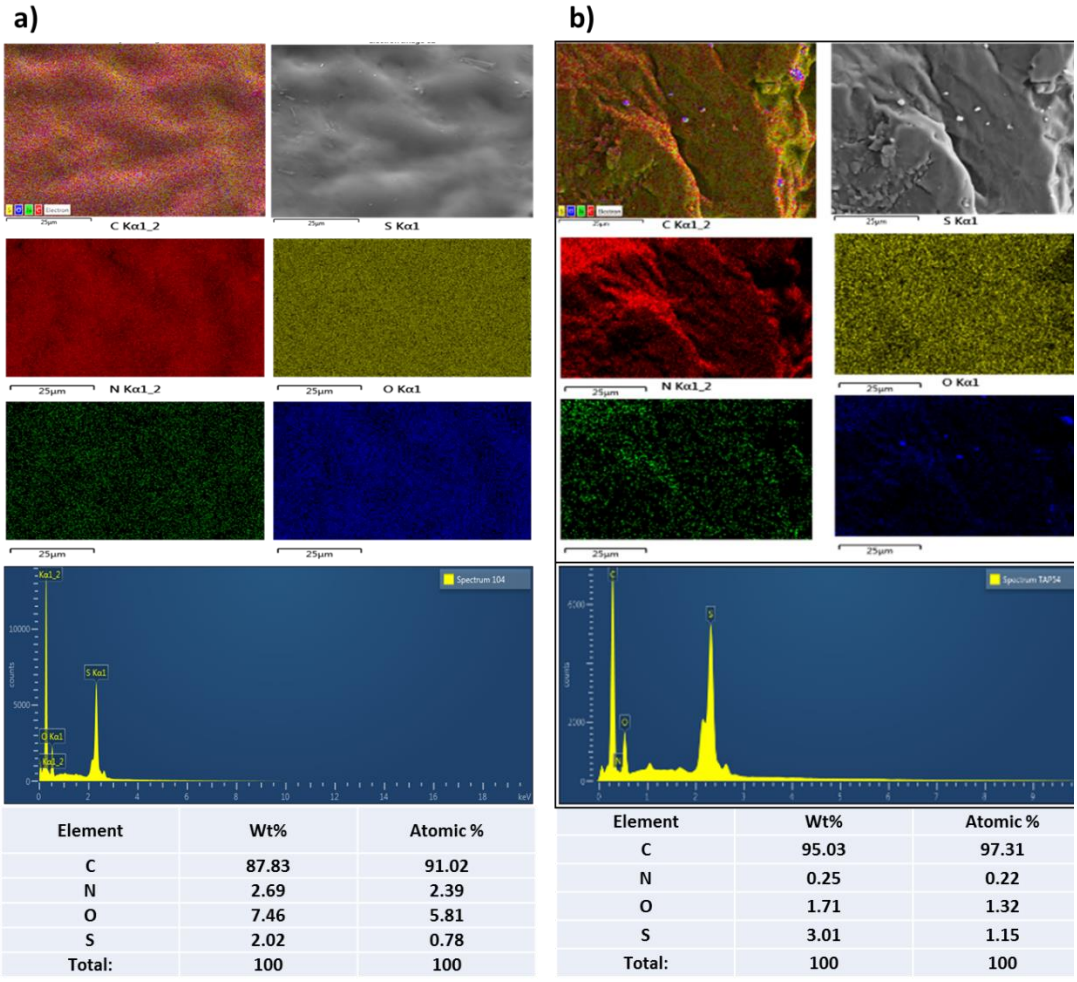

Element	Wt%	Atomic %
C	87.83	91.02
N	2.69	2.39
O	7.46	5.81
S	2.02	0.78
Total:	100	100

Element	Wt%	Atomic %
C	95.03	97.31
N	0.25	0.22
O	1.71	1.32
S	3.01	1.15
Total:	100	100

Figure 3. 13. SEM image, element distribution and EDX data for poly dithiol-allyl particles at consisting of equal ratio of HDT-thiol and HA at (a) 8000 rpm and (b) 20500 rpm.

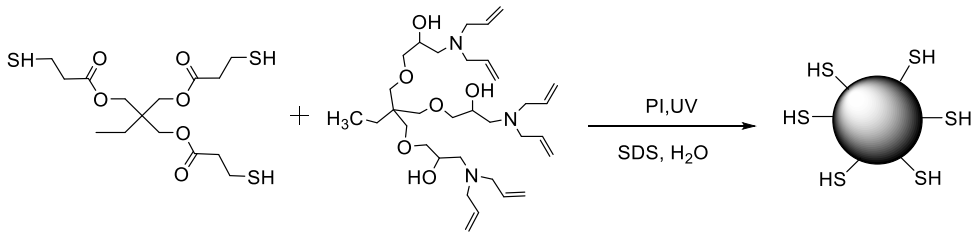

Figure 3. 14. 2-Hexa-allyl-trimethylolpropane tris(3 mercaptopropionate) particles.

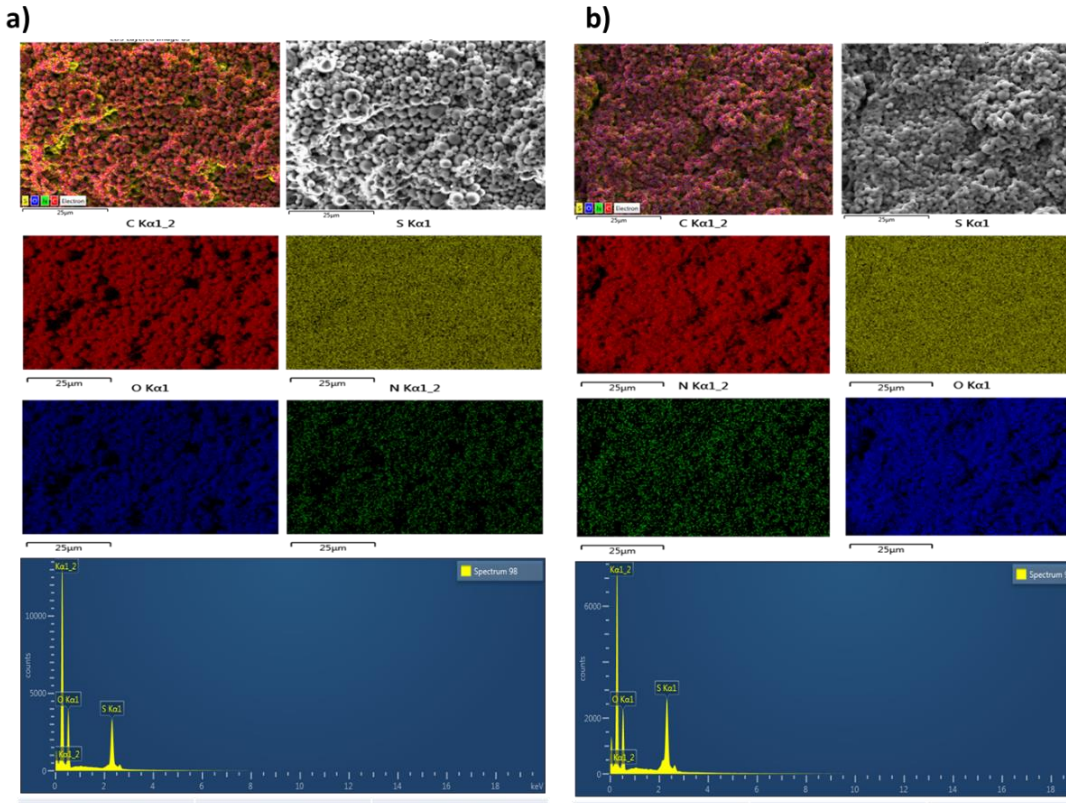

Element	Wt%	Atomic %
C	85.37	88.97
N	0	0
O	13.55	10.6
S	1.08	0.42
Total:	100	100

Element	Wt%	Atomic %
C	84.68	88.57
N	0	0
O	13.8	10.84
S	1.52	0.59
Total:	100	100

Figure 3. 15. SEM image, element distribution and EDX data for TMTMP-HA (1:1) microsphere polymer particles at (a) 8000 rpm and (b) 20500 rpm.

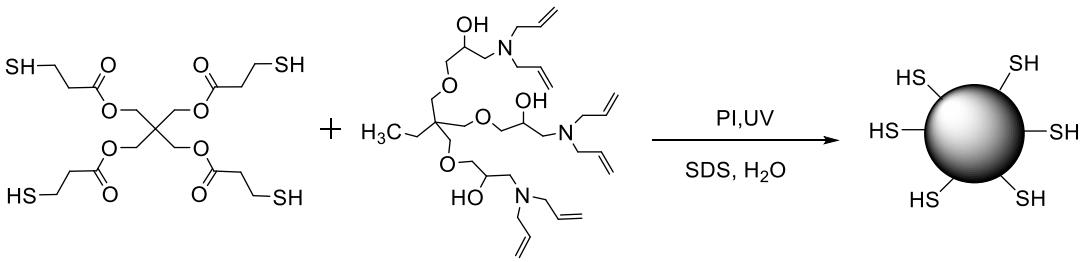

Figure 3. 16. Hexa-allyl-pentaerythritol tetrakis(3-mercaptopropionate) particles.

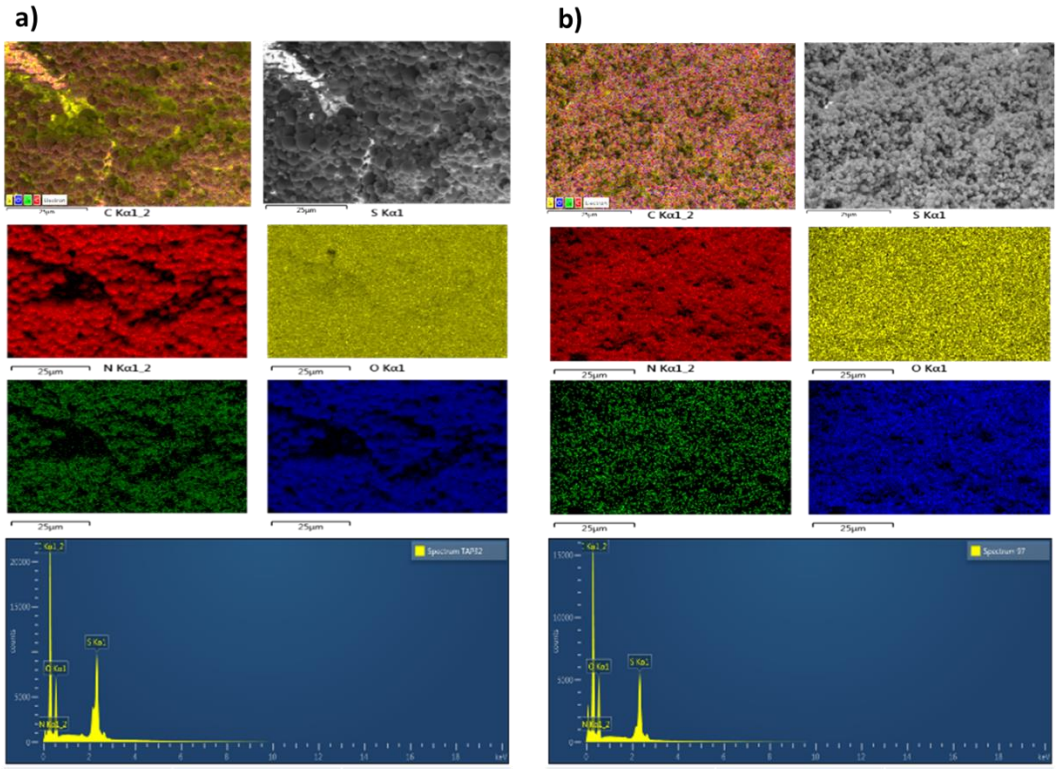

Element	Wt%	Atomic %
C	83.86	87.93
N	0.73	0.65
O	13.59	10.7
S	1.82	0.72
Total:	100	100

Element	Wt%	Atomic %
C	84.15	88.12
N	0	0
O	14.39	11.31
S	1.45	0.57
Total:	100	100

Figure 3. 17. SEM image, element distribution and EDX data for PETMP-HA (1:1) microsphere polymer particles. Synthesised under UV for one hour at (a) 8000 rpm and (b) 20500 rpm.

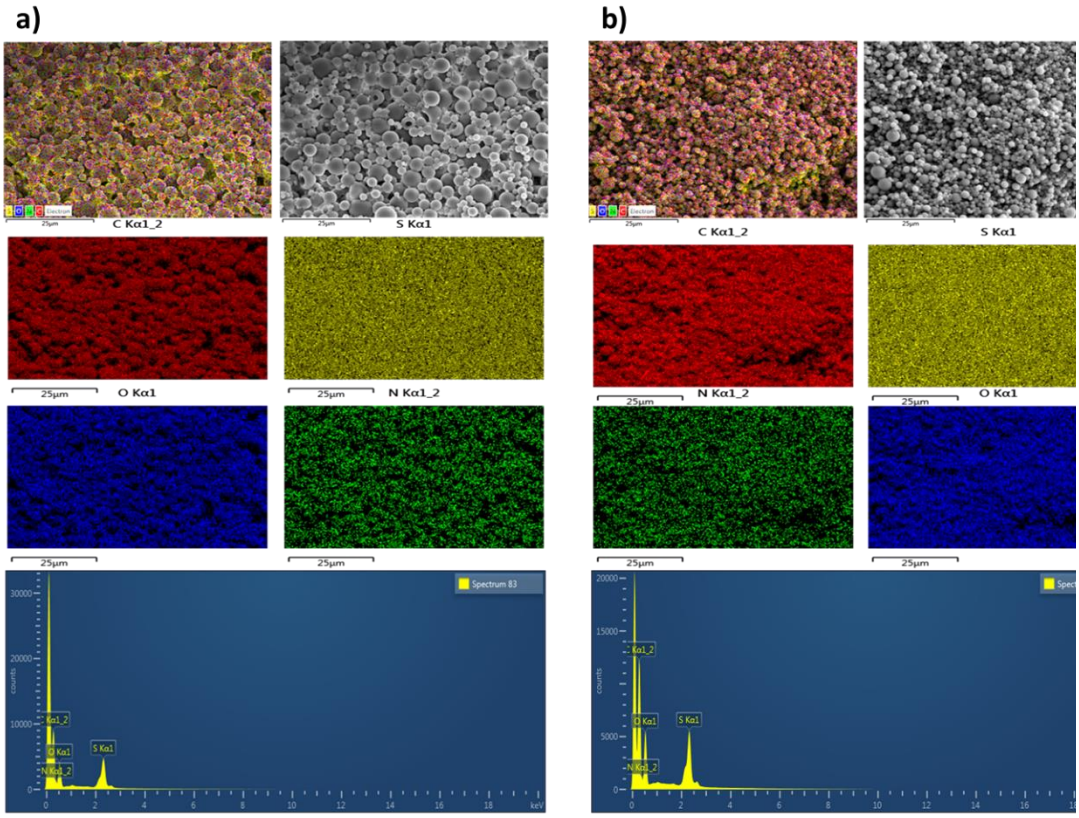

Element	Wt%	Atomic %
C	58.99	64.66
N	29.31	26.92
O	10.94	8.1
S	0.76	0.32
Total:	100	100

Element	Wt%	Atomic %
C	72.97	77.6
N	11.23	10.24
O	14.66	11.7
S	1.14	0.45
Total:	100	100

Figure 3. 18. SEM image, element distribution and EDX data for PETMP-HA (1:1) microsphere polymer particles. Synthesised under UV for five hours at (a) 8000 rpm and (b) 20500 rpm.

3.3.4 FTIR and Raman analysis

While EDX analysis provides elemental distribution, analysis of functional group in poly tetra thiol-allyl particles was performed by FTIR and Raman spectroscopy. Raman and FTIR was used to determine the compounds collected from the surface of tetra thiol-allyl microstructure particles before and after post-polymerisation functionalisation. Figure 3.19 shows the FTIR (lower curve) and Raman spectra (upper curve) of unfunctionalised poly tetra thiol-allyl microsphere particles under UV

for 5 hours with various ratios of thiol monomer (PETMP) at 8000 rpm and 20500 rpm. Both spectra show bands around 3200-3650, 2540-2600 and 1765-1645, which can be assigned to O-H starching, C-H stretching, S-H stretching and C=O starching, respectively. The results of FTIR, Raman spectrum analysis and EDX analysis are in agreement. The FTIR and Raman analysis, shown in Figure 3.19 confirms the structure of cross-linked thiol-allyl particles. It is believed that the peak at around 2540 cm^{-1} can be assigned to the residual of the thiol group.

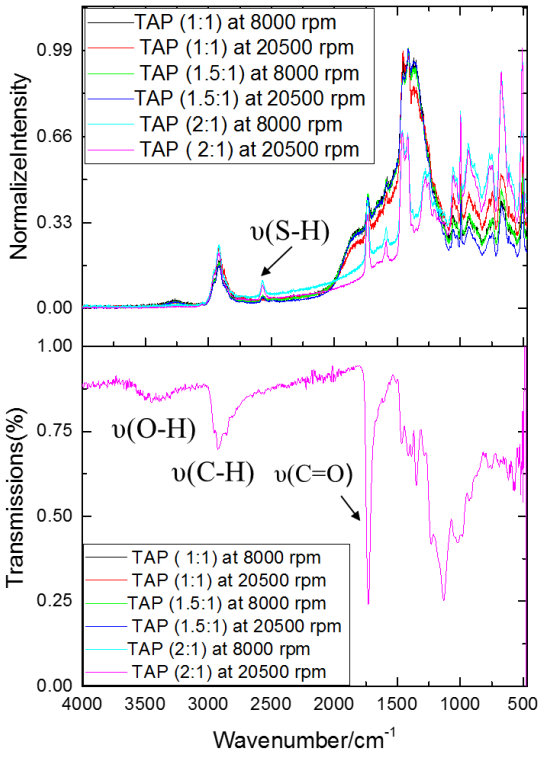

Figure 3. 19. Raman spectra (upper curve) and FTIR spectra (lower curve) before post-polymerisation functionalisation for solid poly tetra thiol-allyl microsphere particles under UV for 5 hours with various ratios of thiol monomer (PETMP) at 8000 rpm and 20500 rpm.

3.3.5 Post-polymerisation functionalisation of particles with Michael addition

Here, we outline post-polymerisation functionalisation for acrylate monomers on microsphere particle surfaces by adapting the procedure used by GZ Li et al.[49] The Michael addition was used with vinyl groups of different types of acrylate monomers, i.e. HEA, MA, EGMEA and DEAEA, and residual outline thiol functional group on the microsphere polymer particles of PETMP-HA 1:1, 1.5:1 and 2:1; it was synthesised under UV for 5 hours at 8000 rpm and 20500 rpm. Figure 3.20 presents the scheme for using HEA, MA, EGMEA and DEAEA in the presence residual of the thiol functional group in the surface of microsphere solid particles and trimethylamine as catalyst at ambient temperatures. Their chemical structure was analysed using FTIR and EDX.

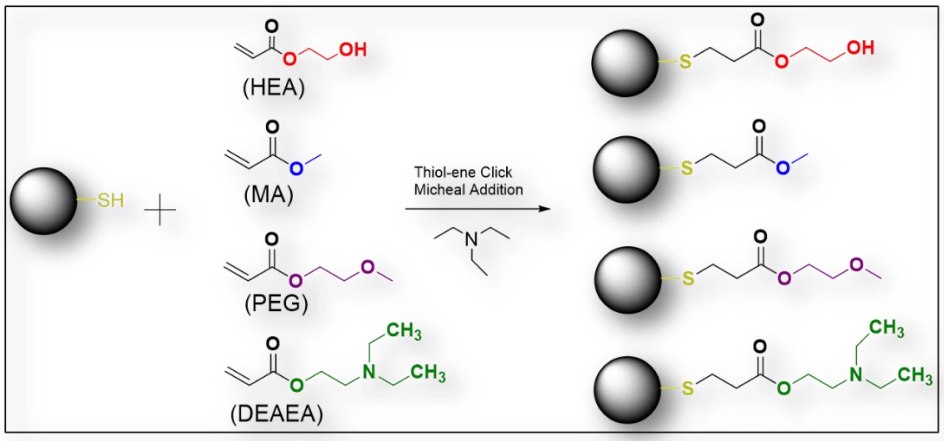

Figure 3. 20. General scheme of synthesis of functionalised poly thiol-allyl microsphere particles

As can be seen from Figure 3.21, the TEA hydrogen attached to the proton in the thiol generates a stronger nucleophile (thiolate anion), which then attacked the electron deficient vinyl group forming the thioether linkage.[48, 92]

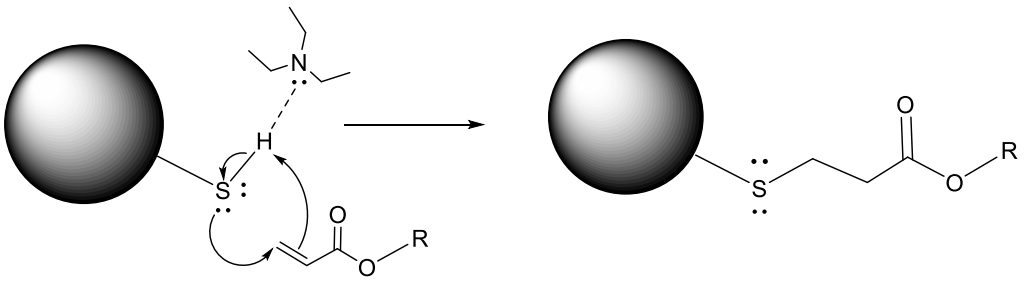

Figure 3. 21. Proposed reaction mechanism for the functionalisation of microsphere poly tetrathiol-allyl particles.

Similar to the result of un-functionalised poly tetra thiol polymer particles, the EDX data, shown in Figure 3.22, confirms that C, N, O and S and are uniformly spread over particles after post-polymerisation functionalisation via thiol-acrylate Michael addition reaction using acrylate monomers (HEA, MA, EGMEA and DEAEA).

In order to reveal the changes in the chemical structure of poly tetra thiol allyl- allyl microsphere particles after post-polymerisation functionalisation, FTIR and Raman analysis were conducted for the neat solid particles. Figure 3.23 suggests all samples were fully functionalised, so no traces of thiol or acrylate could be seen in the spectra around 2540-2600 cm^{-1} or 1600, respectively. The peak around 1720 cm-1 corresponds to carbonyl stretch in the structure of the thiol monomer. The absence of an intensity peak in thiol bands around 2540 cm-1 FTIR and Raman spectra indicates that the presence of sulfur in EDX data is present as a thiolate.[93] Thus it can be said that the poly thiol-ally microsphere particles were successfully functionalised with acrylate monomers (HEA, MA, EGMEA and DEAEA) via thiol Michael addition reaction.

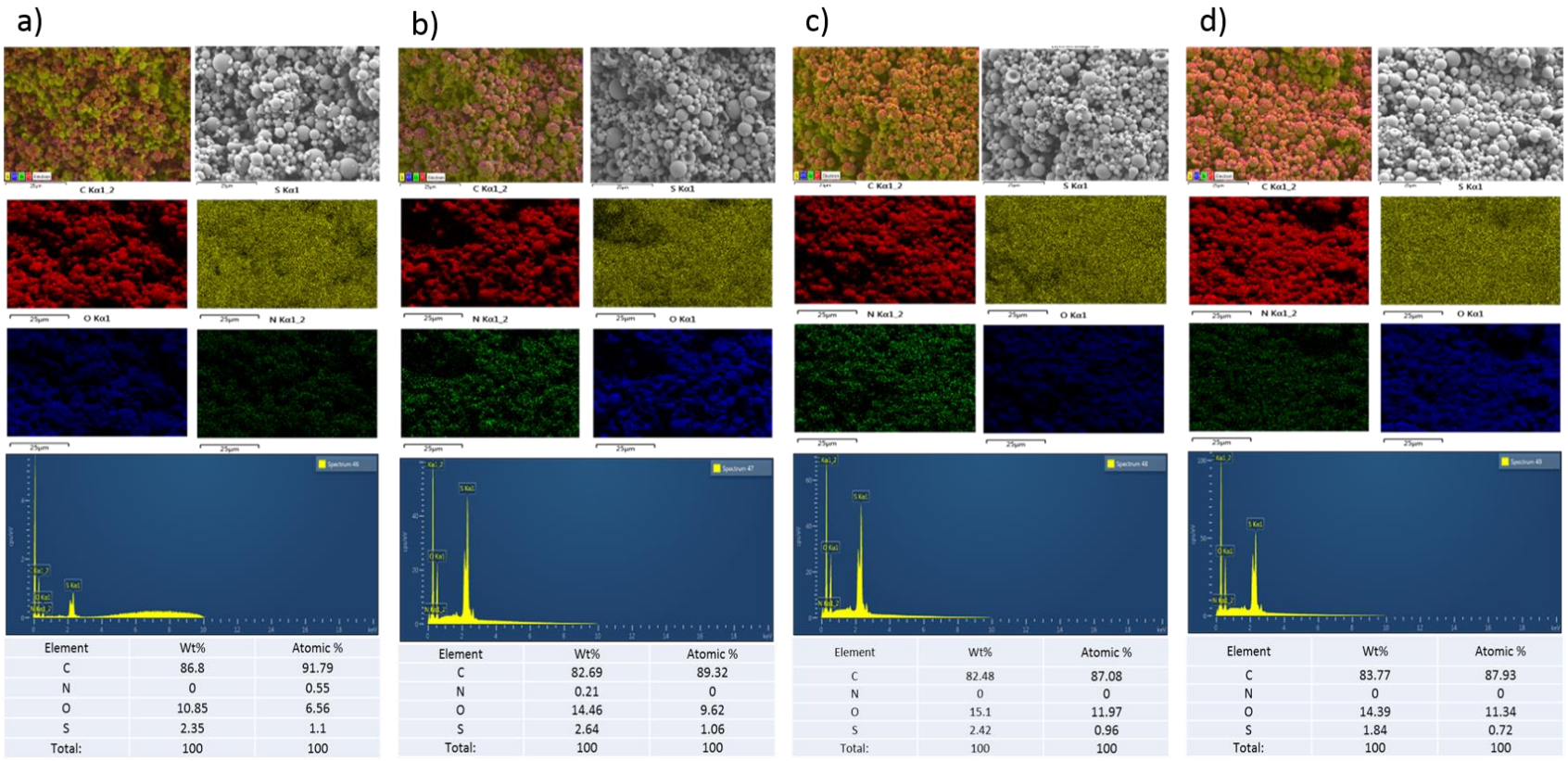

Element	Wt%	Atomic %
C	86.8	91.79
N	0	0.55
O	10.85	6.56
S	2.35	1.1
Total:	100	100

Element	Wt%	Atomic %
C	82.69	89.32
N	0.21	0
O	14.46	9.62
S	2.64	1.06
Total:	100	100

Element	Wt%	Atomic %
C	82.48	87.08
N	0	0
O	15.1	11.97
S	2.42	0.96
Total:	100	100

Element	Wt%	Atomic %
C	83.77	87.93
N	0	0
O	14.39	11.34
S	1.84	0.72
Total:	100	100

Figure 3. 22. SEM image, element distribution and EDX data after post-polymerisation functionalisation via thiol acrylate Michael addition reaction using different acrylate monomers: (a) HEA, (b) MA, (c) EGMEA and(d) DEAEA for PETMP-HA (1:1) microsphere polymer particles, synthesised under UV for 5 hours at 8000 rpm.

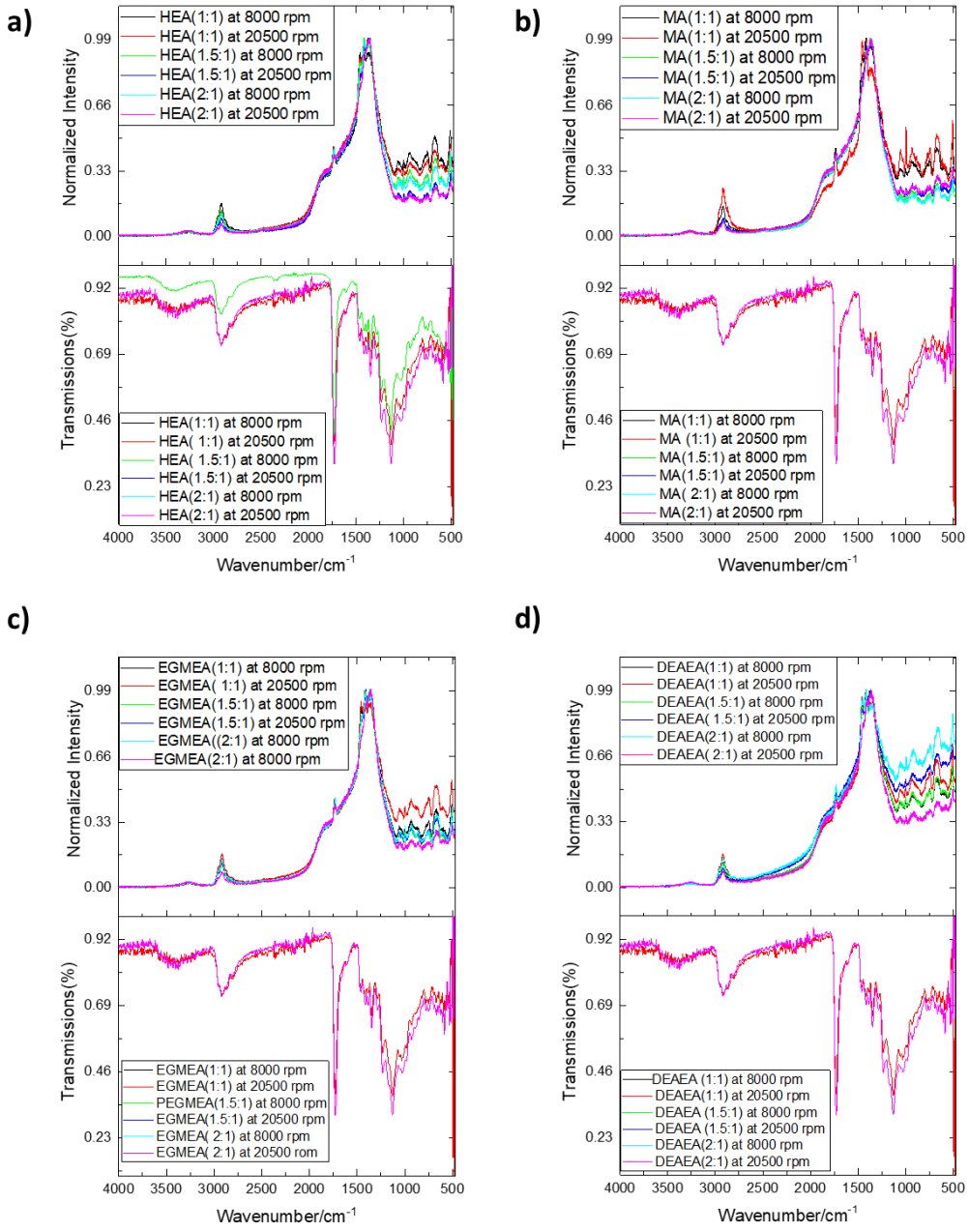

Figure 3. 23. Raman spectra (upper curve) and FTIR spectra (lower curve) after post-polymerisation functionalisation via thiol acrylate Michael addition reaction using different acrylate monomers: (a) HEA, (b) MA, (c) EGMEA and (d) DEAEA for synthesised solid poly tetra thiol-allyl microsphere particles under UV for 5 hours with various ratios of thiol monomer (PETMP) at 8000 rpm and 20500 rpm.

3.4 Conclusions

In conclusion, a novel HA cross-linker was successfully synthesised by combining epoxy ring opening reactions/reagents with Michael's addition reaction reagent. We emphasise that this highly efficient method offers ready access to the formation of a wide range of functional polymeric materials. We have successfully synthesised step-growth poly thiol-allyl microstructure particles using thiol-ene click suspension polymerisation by varying the molar ratio of thiol monomer to HA monomer, homogeniser speed, the number of thiol functional groups (cross-linking density), photo polymerisation time and the thermal polymerisation method. Then, several acrylate monomers (HEA, MA, EGMEA and DEAEA) were introduced into the residual of the thiol functional group in the surface of PETMP-HA microsphere polymer particles via thiol-Michael addition reaction. Without doubt, the newly developed synthetic procedures will find application in a wide variety of fields.

EDX mapping confirms that C, N, O and S and are uniformly spread over particles before and after post-polymerisation functionalisation. Further investigations are required regarding the changes on the average chemical composition in the elemental mapping for the prepared poly thiol-allyl microstructure particles.

FTIR and Raman measurements proved that the synthesis of poly tetrathiol-allyl particles with residuals of the thiol functional group achieved excellent structure and functionality before post-polymerisation functionalisation. Our results show that the absence of an intensity peak of thiol in FTIR and Raman spectra after post-

polymerisation functionalisation indicates that the presence of sulfur in the EDX data is present as a thiolate.

The aim of this chapter was to explore the preparation of poly thiol-allyl microstructure particles and their chemical characterisation. In the following chapters, we investigate glass transition temperature and the morphological control of the micrometre length scale of poly thiol-allyl microstructure particles before and after post-polymerisation functionalisation, and how they can be dependent on the molar ratio of thiol monomer to HA monomer, homogeniser speed, cross-linking density, photo polymerisation time and thermal curing method.

4 Glass Transition Behaviour of Poly Thiol-Allyl Particles before and After Post-Polymerisation Functionalisation

4.1 Introduction

The glass transition temperature (T_g) is one of the most important characteristics in the thermoset of the polymeric world.[94, 95] It is a critical property when considering a polymer's final application and characteristics such as modules, hardness and fragility.[95, 96] T_g is commonly relevant to wholly or partially amorphous polymeric materials. There are several ways to define the glass transition temperature; for instance, it is defined as the temperature at which the physical properties of plastics change from a glassy or crystalline state. Further, T_g is the value of the change in the thermodynamic properties .T_g is also the transitional start of freezing (during decreases of temperature) or movement from a frozen state (during increasing the temperature).[96, 97] It is critical parameter in the characterization of amorphous polymers and can be strongly influenced by molecular parameters such as tacticity and molecular weight (M_W).[98]

The term "glass transition" has acquired a broader meaning in recent years and is now often used to describe "…any phenomenon that is affected by a time scale (on which some interesting degrees of freedom equilibrates) becoming longer than the timescale on which the system is being observed". For convenience, the glass transformation region is usually represented by a single value, denoted as the "glass-transition temperature" is very reproducible and has become recognized as one of the most important properties, directly related to several other thermophysical and rheological property processing parameters, and fields of potential application.[99]

Indeed, polymer physical properties such as hardness and volume can be very varied according to their T_g values.[96, 100] For example, above the glass transition temperature,

polymeric materials behave as rubbery substances that the molecules can cooperatively relax; below the glass transition temperature, polymeric materials have a less flexible mobility.[96, 101] In fact, polymer chain segments are treated in a statistical manner, for instance, a specified polymer in a specified environment has a particular statistical segment length.[102] In stiffer polymer chains, higher T_g are observed, with the larger and smaller segment leading to softer polymer chains, therefore a lower T_g.[102] Accordingly, the direct measurement of the segment movement is the physical meaning of T_g.[102] The T_g is an important property in determining the suitability of a polymeric for an engineering application because its value determines the upper limit of the temperature range of material application [95, 103, 104] Despite its essentiality, determining the implicating mechanisms that govern the T_g phenomenon is still one of the outstanding challenges in studying the physical properties of polymers.[104]

In recent years the plasticizers which are added to provide the needed workability to biopolymers have become the focus of materials scientists. The importance of plasticizers is that they improve the flexibility and processaability of polymers by lowering the T_g.[105] In the production of biopolymer-based films and coatings, plasticizers are also an important additive since they can improve the flexibility and handling of films, maintain integrity, and avoid pore cracks in the polymeric materials.[105] A typical case is PVC plasticized with acrylonitrile butadiene rubber or copolymers of ethylene vinyl acetate.[99] Table 4.1 shows an example of four selected commercial plasticizers that have been investigated by Přemysl Menčík and co-workers.[106]

Table 4. 1 Commercial and chemical names of the some plasticizers.[106]

Commercial Name	Chemical Name	Molecular Wight ($g.\ mol^{-1}$)
Citroflex® 4	Tributyl Citrate	360.4
Citroflex® 4	Acetyl tributyl Citrate	402.5
Citroflex® 4	Acetyl trihexyl Citrate	486
Citroflex® 4	n- Butyryl tri-n-hexyl Citrate	514

The T_g of two mixtures of compatible or plasticized polymers usually occurs in a temperature region that is intermediate between the transition temperature regions of the two components. It is possible to compute and plot the representative T_g versus the weight fraction of one component (e.g., the plasticizer's). The M_W is related to the glass transition temperature through the Fox-Flory equation.[104, 107] This is as follows:

$$\frac{1}{T_g} = \frac{1}{T_{g,\infty}} - \frac{K}{M_n}$$

where $T_{g,\infty}$ is the maximum glass transition temperature that can be achieved for a theoretical infinite M_n, and K is an empirical parameter that is related to the extra free volume that is present in the sample due to the chain end.[108]

Over the past few decades, the characteristics of T_g have received significant attention for resultant micro/nanostructure polymeric particles materials.[17, 40, 76, 98, 103, 104, 109-116] Polymer microstructure particles, which enclose only one or a small number of high molecular weight polymer chains, are different to the bulk polymer and some unusual thermal behaviour could be anticipated.[114]

Gaining such knowledge of thermal behaviour is an important step toward full understanding of widespread polymer microsphere particles' properties that are relevant for applications. The T_g plays a crucial role in the applications of synthetic materials.[117] In fact, the range of different purposes such as intelligent medical devices, implants for minimally invasive surgery, the production of "breathable clothing", or fabricating devices with high ionic conductivity using soft (low T_g) polymers featuring rapid segmental motion and low rigidity is a reflection of the great potential for varying the T_g values.[117]

Herein, our findings suggest that the ability to tailor or even predict the T_g. This motivation comes from the dependence of the T_g on factors such as the size or chemical composition of the particle, which has been widely studied. Few, however, have focused on extending investigation beyond the size or chemical content to more visible, flexible, variable and adjustable approaches.

In the next section, we characterise the T_g of the polythiol-allyl microstructure particles that were synthesised in chapters 2 and 3. The T_g was measured using differential scanning calorimetry (DSC). We then discuss in detail the influence of several factors, which are thiol monomer ratio, homogeniser speed, cross-linking density, photo polymerisation time and thermal curing method on the T_g for poly thiol-allyl microstructure particles before and after post-polymerisation functionalisation can. Finally, a large body of this work has focused on studying the correlation between the T_g and the structures of acrylate monomers as well as the solvent type and volume applied during the functionalisation of these poly thiol-allyl microsphere particles; this offers insight into the importance of monomer and solvent selection after post-polymerisation functionalisation. This provides prior knowledge of simple techniques

in controlling the thermal behaviour before and after post-polymerisation functionalisation for the resulting poly thiol-allyl microsphere particles. Our chapter ends with a brief conclusion of the effects of the above mentioned factors on the T_g.

4.4 Results and Discussion

For meaningful comparison of and to determine more accurately the influence of the operational parameters, DSC was used to identify the T_g changes in the microparticles, as described in Chapters 2 and 3. All DSC results are summarised in Table 4.1. Figure 4.1 shows representative DSC thermograms of suspended thiol-allyl micro structure polymer particles before post-polymerisation functionalisation. In all cases, poly thiol-allyl microstructure particles' DSC curves exhibit only one single glass transition, which was shown to be visible.[118]

Table 4. 2. Summary of the T_gs (°C) of Poly Thiol-Allyl Microstructure Particles before Post-Polymerisation Functionalisation

Ratios [thiol]:[HA]	***homogenizer speed***	***Dithiol TEGDT***	***Dithiol HDT***	***Trithiol***	***Tetrathiol (1h)***	***Tetratiol (5h)***
1:1	8000	-18.23°C	-16.18 °C	7.26°C	20.93 °C	32.85 °C
1:1	20500	-17.49 °C	-14.40 °C	4.73 °C	22.7 °C	35.26 °C
1.5:1	8000			-5.49 °C	1.29°C	26.23°C
1.5:1	20500			-2.74 °C	3.92 °C	24.10 °C
2:1	8000			-2.18°C	-2.35 °C	26.41 °C
2:1	20500			-3.94°C	1.59 °C	16.78°C

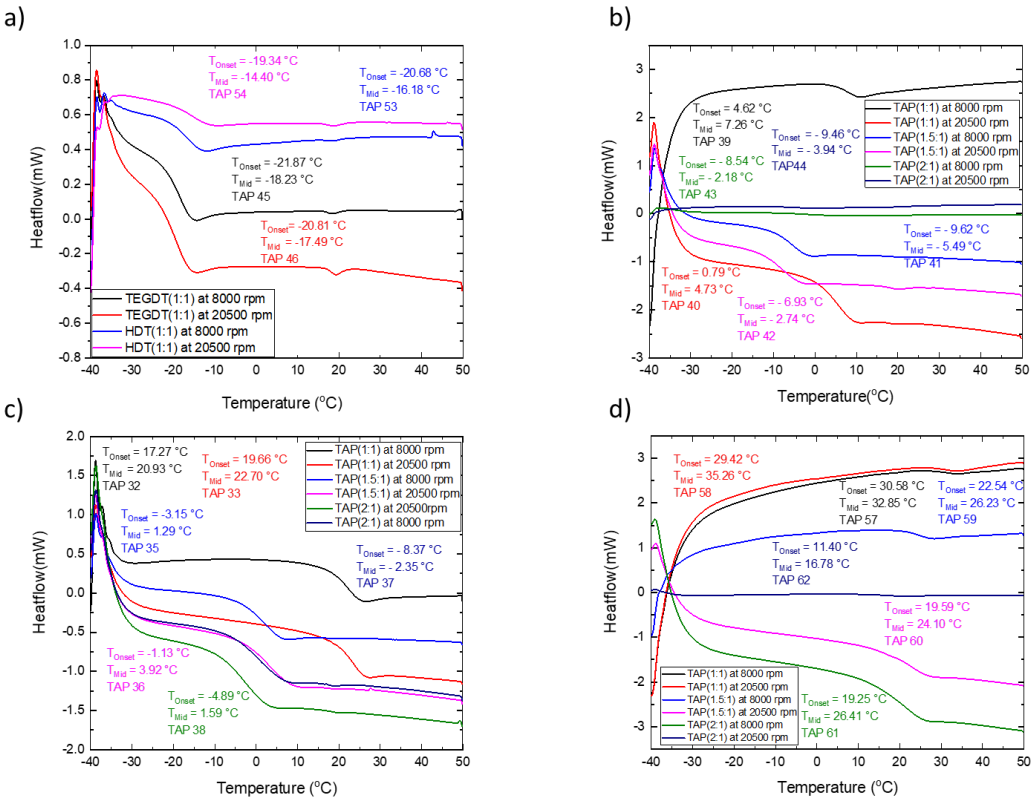

Figure 4. 1. Second heating DSC curves scans for photo initiated poly thiol-allyl microstructure particles before post-polymerisation functionalisation. All scans at 10 K/min. (a) dithiol, (b) trithiol, (c) tetrathiol (1h) and (d) tetrathiol (5 h).

4.4.1 Influence of thiol monomer ratio of T_g

Overall, the Tg of the photo cured sample decreased by increasing the thiol monomer ratio. As the thiol hexa-allyl molar ratio varies from 1:1 to 2:1, the T_g of the cured particles using tetra thiol at 8000 rpm decreased from 20.93 ˚C to -2.35 ˚C. In addition, the T_g of the cured sample using tetra thiol at 20500 rpm decreased from 22.7 ˚C to 1.59 ˚C. The DSC measurements (see Figure 4.2c) showed that the cured sample of tetra thiol with equal ratios of HA [1:1]; 4t:HA and 8000 rpm, had T_g of 20.93 ˚C; this was considerably higher than the T_g of 1.29 ˚C and -2.35 ˚C of the cured sample tetra

thiol with HA at both ratios of 1.5 mole 2 mole, respectively. However, as we can see from Figure 4.2, the T_g value decreases slightly by around 4 ˚C when the ratio of tetra thiol monomer increases from 1.5 to 2 mole, respectively. The DSC result of tri thiol at 8000 rpm (Figure 4.2b) shows similar behaviour in the tetra thiol regarding an increase in the thiol monomer ratio from 1 to 1.5 mol: the T_g values decreased significantly from 4.62 ˚C to -5.49 ˚C, and then decreased slightly to -2.18 ˚C after the thiol monomer ratio was doubled (2 mol). This result is attributed to the fact that the formation of the flexible poly thiol-ether limits the thermal motion of the formed polymer, thus leading to lower T_g values. In other words, increasing the concentration of the thioether linkage increases the mobility of cross-linked particles, which provide lower T_g.[20, 119, 120]

In contrast to the above results, the T_g values increased by increasing the thiol monomer ratio of samples of trithiol at 8000 rpm as its T_g value based at molar ratio 2:1 of trithiol:HA exhibited exclusively higher T_g (-2.18 ˚C) than the network based on 1.5:1 of tri thiol: HA, (-5.49 ˚C); this was, however, still lower than the T_g value (4.62 ˚C) of equal ratio of tri thiol with HA. In addition, the T_g value of the molar ratio [tetra thiol]: [HA] at 8000 rpm, under UV for 5 hours, increased slightly from 26.23 ˚C to 26.41 ˚C by increasing the thiol monomer ratio from 1.5 mol to 2 mol, which was still lower than the T_g (35.26 ˚C) of the cured sample with equal ratios of tetra thiol and hexa-allyl.[120, 121]

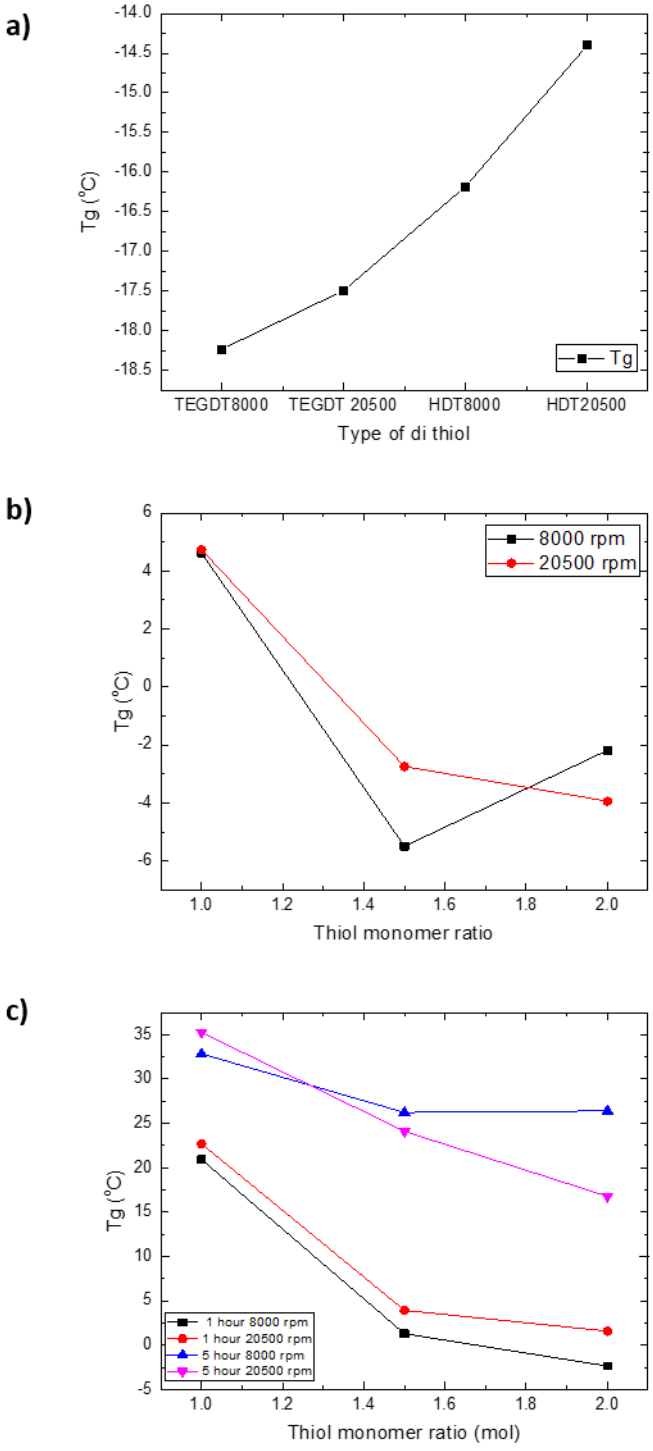

Figure 4. 2. Changes in the T_gs with respect to the thiol monomer ratio for photo initiated poly thiol: (a) dithiol, (b) trithiol, and (c) tetra tetra thiol, allyl microstructure particles from second heating at 10 K/min.

4.4.2 The influence of homogeniser speed

Figure 4.2 shows as well the variation of T_g with homogeniser speed at 8000 rpm and 20500 rpm for all photo-cured experiments of poly thiol-allyl particles using thiol monomer. It also indicates a different number of thiol functionality Di (Figure 4.2a), tri (Figure 4.2b) and tetra (both for 1 and 5 hours) cured time (see Figure 4.2c).

In most cases, the increase of the homogenisation power speed led to a visible increase in the T_g values of poly thiol-allyl. These trends can be explained by considering the effect of mixing power. Davon Ship et al. (2013) demonstrated that higher homogenization power produced smaller particles.[42] We looked further into the effect of homogenisation power by investigating its influence on the T_g value of the resulting particles. In our case, the difference was that we changed the speed of the homogeniser and not the duration time of mixing; this was because the organic and aqueous phases were homogenised for only 30 sec prior to curing, whether under UV or thermally, followed by continuous gentle magnetic stirring. The following section explains the effect of changing the power mixing speed in more detail.

First of all, the T_g value rises consistently for thiol-ally particles consisting of equal ratios of di-thiol and HA, as particles of both TEGDT and HDT increased from -18.23 ˚C and -17.49 ˚C to -16.18 ˚C and – 14.40 ˚C, respectively, when the homogeniser speed increased from 8000 rpm and 20500 rpm (Figure 4.2a).

Next, the T_g value of poly thiol-allyl microsphere particles consisting of equal ratios of tri-thiol and HA remained similar at 4.62 ˚C and 4.73 ˚C at 8000 rpm and 20500 rpm, respectively. With the microsphere particles with ratios of 1.5:1 of thiol: HA, the

T_g value increased significantly from -5.49 ˚C to -2.74 ˚C when the homogeniser speed increased from 8000 rpm and 20500 rpm. Contrary to expectations, the T_g value notably reduced from -2.18 ˚C to -3.94 ˚C after increasing the speed power from 8000 rpm to 20500 rpm (Figure 4.2b).

Lastly, increasing the speed power of the homogeniser led to a steady increase in the T_g values for all poly thiol-allyl microsphere particles consisting of tetra-thiol and HA that has been photo-cured for one hour, in conjunction with the gap between the two speeds rising gradually by the increasing thiol monomer ratio (Figure 4.2c). Whereas, in the case of particles left under UV for 5 hours, the increase of the homogeniser power led to increases in the T_g values only for microsphere particles with equal ratios of tetra-thiol and HA. Furthermore, there was a decrease in the rest of the T_g values of microsphere particles consisting of higher ratios of thiol monomer. This was more noticeable for the microsphere particles with double ratios of tetra thiol monomer because the gap of the T_g value increased between two speeds of about 10 ˚C.

Exceptional cases of T_g values were found in the following poly thiol-ally microparticles: Firstly, microparticles consisting of 2:1 tri-thiol:HA, as T_g drops nearly 2 ˚C; secondly, poly tetra-thiol- allyl microsphere particles, which were photo-cured for 5 hours at 1.5:1 of tetra-thiol:HA, whereby T_g values decreased by 2 ˚C; thirdly, at double the thiol monomer ratio to HA, there was a significant drop in the T_g values. The T_gs of these polymer decreased as the speed of the homogeniser increased from 8000 rpm to 20500 rpm.

4.4.3 Influence of cross-linking density

Cross-linking density is the crucial parameter which substantially influences the thermal properties of the based polymer particles depending on the type of monomer and cross-linker.[122] It is known from the literature that the T_g value depends on the amount of cross-linked unit.[123] Herein, particles with controlled cross-link density were determined by the number of thiol functional group and thiol monomer was applied. Cross-link density clearly impacted on the T_g, with higher cross-link density leading to higher T_g values.[40]

Figure 4.3 demonstrates that at both homogeniser speeds of (a) 8000 rpm and (b) 20500 rpm, 1:1 thiol- allyl of tetra thiol-ene materials, which had a greater cross-link density than trithiol-ally and dithiol-allyl, achieved T_g values greater than the corresponding di and tri thiol-ally network. In general, T_gs were found to correlate well with the literature: cross-link density clearly impacted on the T_g, with higher cross-link density leading to higher T_g values.[40, 73]

Interestingly, at 8000 rpm and the thiol:HA molar ratio of 1:1, T_g was found to strongly depend on the monomer functionalities. As the number of the functional groups increased, the T_g values increased. As we can see from Figure 4.3, at 8000 rpm, the T_g (20.93 ˚C) of tetra thiol-HA (1:1) was higher than that (4.62 ˚C) of trithiol-HA (1:1) and (18.23 ˚C, 16.18 ˚C) of di thiol-HA (1:1), reflecting the difference in cross-linking density. These results match those of modified thiol-HA networks at 20500 rpm, observed in (Figure 4.3b), which is due to an increase in cross-link density. These results evidently demonstrated that while basic features of tetra thiol-ene microspherical particles formation are similar to those of tri thiol-ene and di-thiol-ene,

it offers a direction of microstructure material with variable thermal properties (physical). The findings observed in this study mirror those of the previous studies that have examined the effect of cross-link density of polymeric particles materials on the T_g, which corroborates the findings of a great deal of the previous work on thermal properties of this field.[20, 40, 73, 76, 120, 124-127]

Indeed, thiol modified network of the liner thiol monomers of TEGDT and HDT had noticeably cross-linked materials with lowest T_g values of -18.23 ˚C and -16.18 ˚C at 8000 rpm as well as -17.49 ˚C and-14.40 ˚C at 20500 rpm. This corresponded very well with literature, as the photo polymerisations did not produce particles for higher molar ratios (1.5 and 2) of di thiol monomer at same conditions of the rest of the monomers, tetra thiol and tri thiol. The linear dithiol monomer, which were considered to be cross-linked with HA, were expected to have T_g values below the reaction temperature. Hence, they would not be expected to form particles.[44]

A more interesting observation is that as the thiol:HA molar ratio varies from 1:1 to 2:1, when the molar ratio of thiol monomer has increased to 1.5:1 and 2:1 of thiol-HA system, the T_g was found to be less affected by monomer composition after increasing the thiol monomer ratio, equal T_g values of tri and tetra were obtained with little difference and or similar (Figure 4.3a). This suggests that the cross-link density decreases by increasing the ratio of thiol monomer. A possible explanation for these results may be that the molar fraction of flexible thiol-ether linkage in the 1.5 and 2 molar ratio is higher than that for the equal ratio.

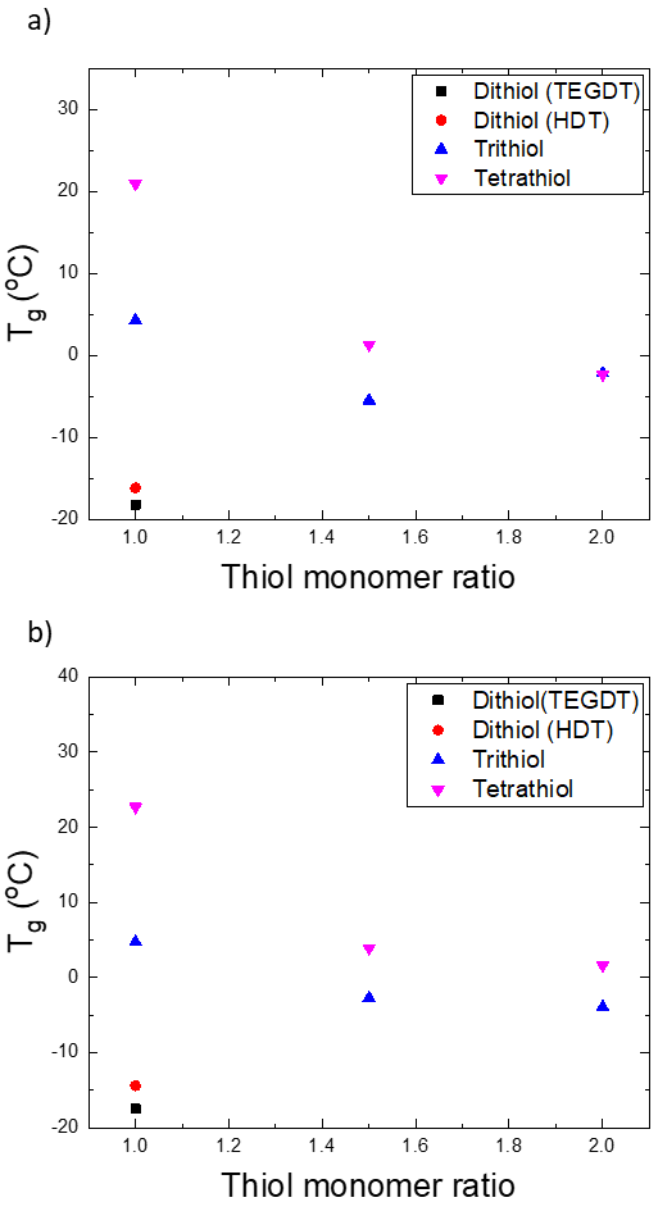

Figure 4. 3. The comparison of Tg values at various thiol monomer ratios and thiol functional density of photo initiated poly thiol-allyl microstructure particles from second heating at 10 K/min, using homogeniser at speed (a) 8000 rpm and (b) 20500 rpm.

4.4.4 Influence of photo-polymerisation time

Figures 4.4a and 4.4b demonstrated that the duration time of UV curing clearly impacts on the T_g, with longer hours under UV leading to higher T_g values. By leaving

the suspension mixture under UV for 5 hours with similar components, we were able to increase the T_g values to produce some samples with glassy network (i.e. T_g is greater than room temperature). The influence of photo-polymerisation times on the T_g were monitored by measuring the change in the T_g values of the tetra thiol-HA network, which consisted of various molar ratios of the tetra thiol monomer at 8000 rpm (Figure 4.4a) and 20500 rpm (Figure 4.4b) upon UV exposure for 1 and 5 hours. Figure 4.4 illustrates that at 8000 rpm, as the molar ratio of the thiol monomer increased, the T_g dramatically increased from 20. 93 ˚C to 32.85 ˚C for tetrathiol-HA (1:1), from 1.29 ˚C to 26.23 ˚C for tetrathiol-HA (1.5:1), and from -2.35 ˚C to 26.41 ˚C for tetrathiol-HA (2:1). The greatest gap was between the two samples at a ratio of 2:1 thiol:allyl and 8000 rpm, which was 28.76 ˚C, and the narrowest gap was between the samples at ratio of 1:1 thiol:allyl (11.5 ˚C). Hence, the efficiency of increasing the curing time increased by raising the thiol monomer ratio (11.59<24.94<28.76, 1<1.5<2, respectively). Different result behaviour was observed at 20500 rpm, when the gap increased from 12.56 to 20.18 ˚C by increasing the thiol:allyl ratio from 1:1 to 1.5:1; it then dropped to 15.19 ˚C when the thiol:allyl monomer ratio increased to double 2:1.[39, 125, 128]

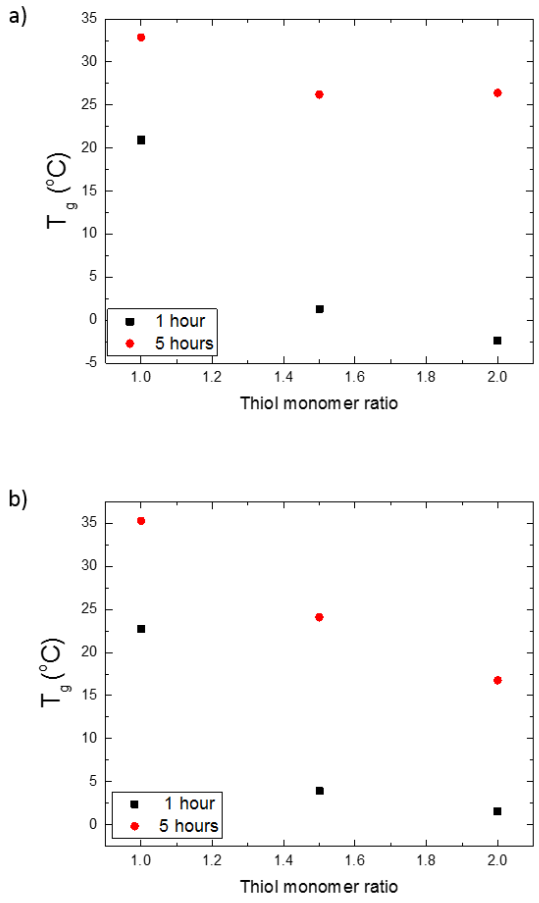

Figure 4. 4. T_gs versus thiol monomer ratio of photo initiated poly thiol-allyl microstructure particles from second heating at 10 K/ min, using homogeniser at speed (a) 8000 rpm and (b) 20500 rpm, showing the increased T_g due to increased photo polymerisation time.

4.4.5 Influence of the thermal curing method

The thermal properties of the resulting thermal polymerisation network of poly thiol-allyl microparticles with various tetra thiol monomer ratios behaved oppositely to that provided by photo initiation. As shown in Figure 4.5, the glass transition of microparticles prepared by thermal polymerisation of poly tetrathiol-ally microparticles decreased slightly from 5.18 ˚C of tetrathiol-HA (1:1) to 4.3 ˚C of

tetrathiol-HA (1.5:1). In contrast to the thermal curing process, the majority of photo initiated poly thiol-allyl particles decreased rapidly when the tetra thiol monomer increased from the equivalent to 1.5 molar ratio. It is worth noting that thermally cured network of tetrathiol-HA (2:1) showed interesting thermal behaviour, as a dramatic increase to 8.66 ˚C was observed when examining the T_g value of tetra thiol-HA (2:1) molar ratio. Additionally, the formation of thermal initiated network worked significantly different as consequence of adding divinylbenzene. It is expected that by adding DVB in the precipitation polymerisation leads to high transition temperature (T_g). However, the resulting thermal cross-linking gave a lower T_g value -0.50 ˚C relative to the tested T_g value (5.18 ˚C) of thermal polymerisation network without using DVB.

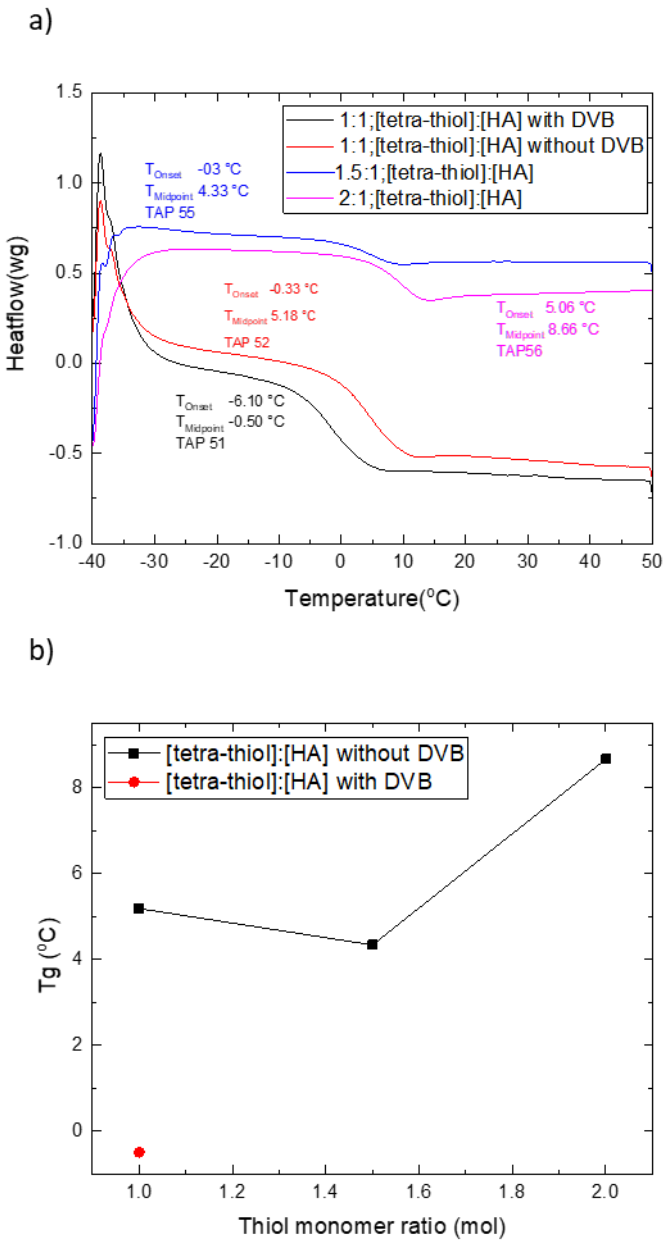

Figure 4. 5. (a) Second heating DSC scans of thermal initiated poly thiol-allyl microstructure particles. All scans at 10 K/ min; (b) T_gs of thermal initiated poly thiol-allyl microstructure particles from second heating at 10 K/min, using homogeniser at speed 8000 rpm and adding DVB.

4.4.6 After post-polymerisation functionalisation

There were advantages to using thiol Michael addition for post functionalisation polymerisation already known from recent studies. Acrylate monomers such as HEA, MA, EGMEA and DEAEA were chosen. However, changing polymer structures has an effect on the thermal properties of the product. In respect of post-polymerisation functionalisation, using acrylate monomer leads to change in T_g values depending on the nature of the acrylate monomer. It was also required to investigate the impact of incorporating each type of acrylate monomer to understand the variability of the thermal properties with changed types of monomer. The effect of polymer backbone chemistry on the glass transition of the poly-thiol-allyl microsphere particle after post-polymerisation functionalisation was examined by DSC. Herein, we focused on determining the alternation of T_g of poly thiol-allyl microsphere particles after post-polymerisation functionalisation.

The curves obtained from DSC are presented in Figure 4.6; in all cases of poly thiol-allyl microspheres particles after post-polymerisation functionalisation, curves showed only one single transition. Consequently, it was confirmed that were cross-linked. Table 4.2, on the other hand, summarises the T_g value of poly tetra thiol-allyl microsphere particles before and after post-polymerisation functionlisation.[123]

To directly compare acrylate monomers, chemical structures were chosen to functionalise poly thiol-allyl microsphere particles; Figure 4.7 plots the dependence of T_g on the chemical structure of acrylate monomers. Also included in Figure 4.7 are T_gs of functionalised microsphere polymer particles consisting of tetra thiol monomer with molar to HA ratio of 1, 1.5 and 2, as well as at two homogeniser speeds of 8000

rpm (Figure 4.7a) and 20500 rpm (Figure 4.7b). We noted that the majority of functionalised polymer particles materials have lower T_g than the thiol-allyl particles before post-polymerisation functionalisation, thus reflecting the higher thiol-ether linkage availability of the former.

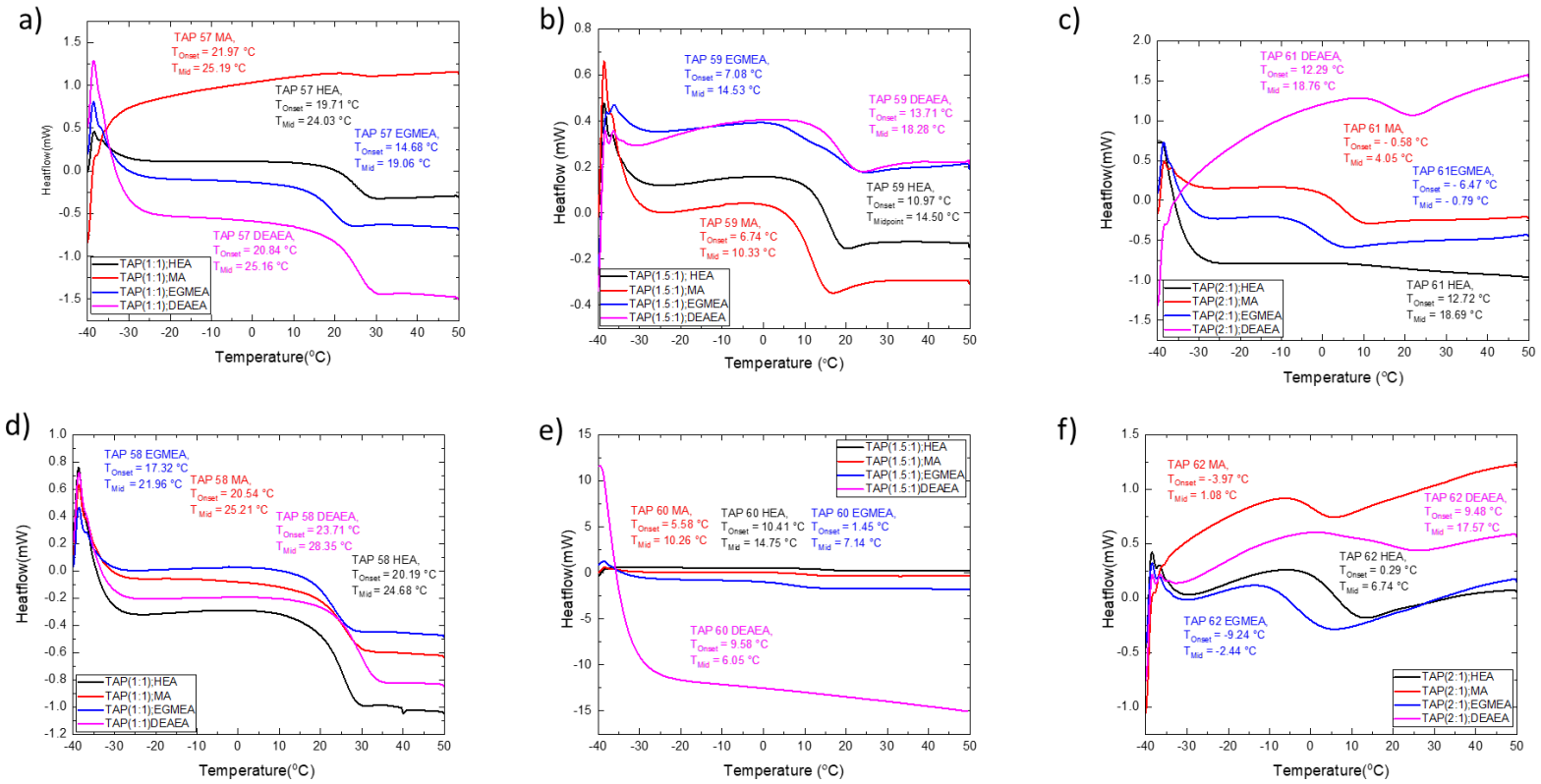

Figure 4. 6. Second heating DSC scans of thermal initiated poly thiol-allyl microstructure particles after post-polymerisation functionalisation. All scans at 10 K/min. Upper row using homogenizer speed at 8000 rpm, 1:1(a) 1.5:1(b) and 2:1(c), lower row using homogenizer speed at 20500, (d)1:1, (e)1.5:1and (f) 2:1 20500 rpm.

T_g for given functionalised particles using HEA, MA, EGMEA and DEAEA decreased dramatically from 24.03 ˚C, 25.19 ˚C, 19.06 ˚C and 25.16 ˚C to 14.50 ˚C, 10.33 ˚C, 14.35 ˚C and 18.28 ˚C, respectively, when the thiol monomer ratio increased from 1 mol to 1.5 mol at 8000 rpm. After increasing the thiol monomer ratio to 2 mol, both T_g values of particles functionalised with HEA and DEAE rose to 18.69 ˚C and 18.76 ˚C, respectively, whereas T_g values of particles functionalised with MA and EGMEA declined markedly to 4.05 ˚C and -0.79 ˚C, respectively.

At 20500 rpm, apart from particles produced by the post-polymerisation using DEAE monomer, where T_g values decreased sharply from 28.35 ˚C to 6.05 ˚C, then the T_g value elevated massively to 17.57 ˚C, which was higher than the T_g of the thiol-allyl microsphere particles before post-polymerisation functionalisation (16.57 ˚C). The rest of that obtained by post-polymerisation functionalisation using HEA, MA and EGMEA behaved correspondingly as they clearly decreased with a T_g range between 24.68 ˚C and -2.44 ˚C. The decrease in the T_g can be explained by the presence of the thiol-ether linkage in the resulting post-polymerisation functionalisation reaction. Consequently, the increase in thiol-ether linkage quantity leads to increased flexibility in the polymer backbone and decreased T_g.[123]

It is accepted that the T_g value obtained by post-polymerisation functionalisation of acrylate monomer follows the sequence given in Table 4.3.

Table 4. 3. T_gs of the Poly Tetra Thiol-Allyl Microstructure Particles after Post-Polymerisation Functionalisation Measured by DSC.

Ratios [thiol]:[HA]	homogenizer speed	Before functionalization T_g (°C)	Reactant (1.5 eq)	T_g (°C)
1:1	8000	32.85	HEA	24.03
			MA	25.19
			EGMEA	19.06
			DEAEA	25.16
1:1	20500	35.26	HEA	24.68
			MA	25.21
			EGMEA	21.96
			DEAEA	28.35
1.5:1	8000	26.23	HEA	14.50
			MA	10.33
			EGMEA	14.53
			DEAEA	18.28
1.5:1	20500	24.10	HEA	14.75
			MA	10.26
			EGMEA	7.14
			DEAEA	6.05
		26.41	HEA	18.69
2:1	8000		MA	4.05
			EGMEA	-0.79
			DEAEA	18.76
2:1	20500	16.78	HEA	6.74
			MA	1.08
			EGMEA	-2.44
			DEAEA	17.57

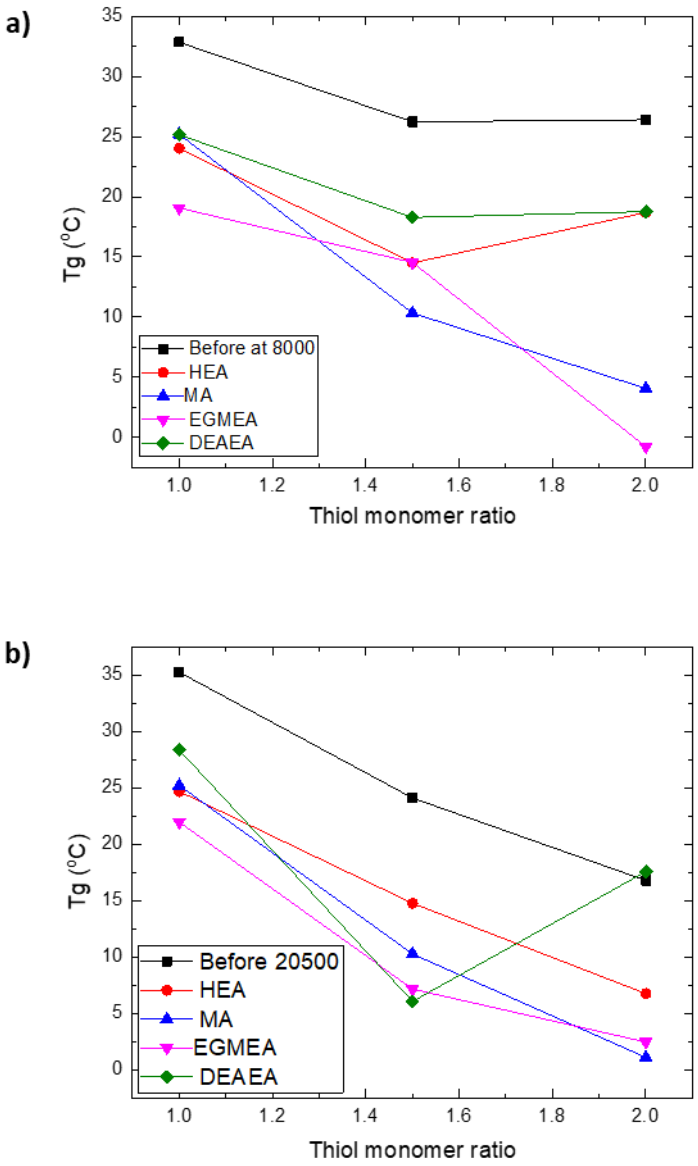

Figure 4. 7. T_gs of photo initiated poly tetra thiol-allyl microstructure particles before and after post-polymerisation functionalisation from second heating at 10 K/min.

To further evaluate the correlation between the chemical structure of acrylate monomer homogeniser speed and thiol monomer ratio, Figure 4.8 represents the

influence of increasing the homogenisation speed on T_g values for each type of acrylate: HEA (Figure 4.8a), MA (Figure 4.8b), EGMEA (Figure 4.8c) and DEAE (Figure 4.8d), separately at several thiol monomer molar ratios. In general, there were significant, weak or no homogeniser speed-dependence of functionalised poly thiol-allyl microsphere particles as described below: first, at 1:1 molar ratio, similar T_g values were observed after post-polymerisation functionalisation using HEA and MA monomers, however it was increased using EGMEA and DEAEA monomers. Secondly, at 1.5:1 molar ratio system, increasing the homogeniser speed led to similar T_g values as in the case of using HEA and MA monomers, whereas it was significantly decreased after post-polymerisation functionalisation using EGMEA and DEAEA monomer. Finally, at 2:1 molar ratio system, T_g values noticeably decreased after functionalisation with HEA and declined slightly when functionalisation occurred with MA, EGMEA and DEAEA.

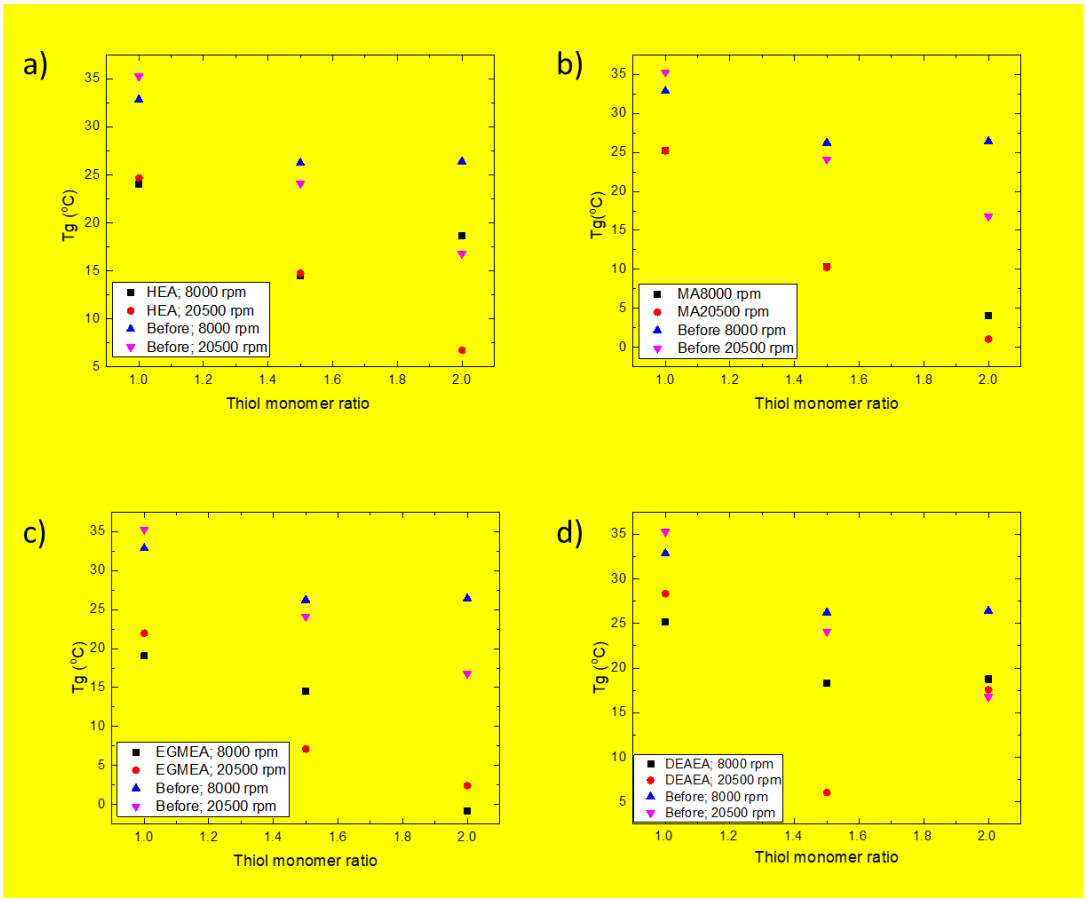

Figure 4. 8. T_gs versus thiol monomer ratio of photo initiated poly tetra thiol-allyl microstructure particles before and after post-polymerisation functionalisation depending on acrylate monomer structure from second heating at 10 K/min.

More interestingly, Figure 4.9 and Table 4.4 show curious observations about the T_g for poly thiol-ally microparticles after post-polymerisation functionalisation: they are not only affected by the acrylate monomers structure, but are also influenced by the solvent type and volume used during the functionalisation process.

Table 4. 4. T_gs of the Poly Tetra Thiol-Allyl Microstructure Particles after Post-Polymerisation Functionalisation using Different Solvent Type and Volume Measured by DSC

Ratios [tetra-thiol]:[HA]	homogenizer speed for 1 hour	T_g (°C)	Reactant (1.5 eq)	Solvent	Solvent volume	T_g (°C)
1.5:1	8000	1.29	EGMEA	DMSO		-4.61
				Ethanol		-4.46
				DMF	5ml	-5.73
					1 ml	-1.18

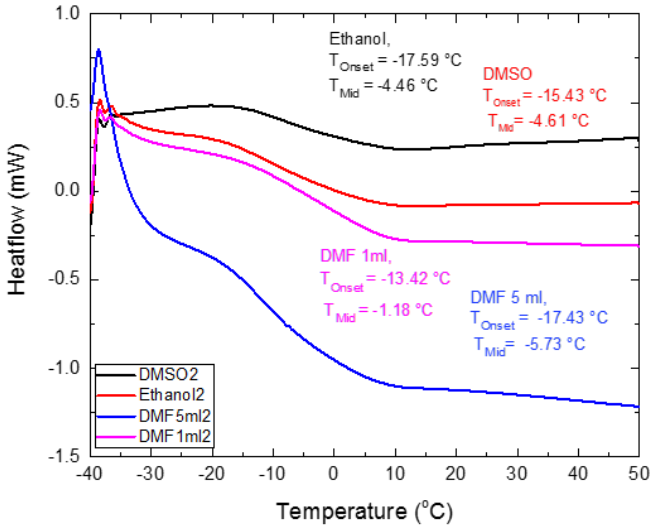

Figure 4. 9. Second heating DSC scans of photo initiated poly thiol-allyl microstructure particles after post-polymerisation functionalisation using different solvent types and volume. All scans at 10 K/min.

4.5 Conclusions

Overall, we have experimentally investigated the T_g dependence on the following factors: thiol monomer ratio, homogeniser speed, cross-links density, photo polymerisation time and thermal curing method for poly thiol-allyl microstructure particles before and after post-polymerisation functionalisation in great detail using DSC. We found a striking and weak differentiation /similarity of the effect in the above mentioned factors on the T_g.

Based on these preliminary results we have found that a higher **thiol monomer** ratio for poly thiol-allyl microparticles leads to decreases in the T_g because of the increasing number of thiol-ether linkages in the system. Changing the **homogenisation speed** was considered as in most cases the increase in the homogenisation power speed led to a visible increase in the T_g values of the poly thiol-allyl; the exception was for trithiol-allyl polymer particles at 2:1 molar ratio and tetrathiol-allyl polymer particles at 1.5:1 and 2:1, which were under UV for 5 hours. While the higher **cross-link density/thiol group functionality** generates higher T_g at equal molar ratios of thiol monomer and HA cross-linker, the T_g was slightly increased or nearly the same at higher thiol monomer when increasing the number of the thiol functional group and cross-link density.

A remarkably strong effect of the **photo-polymerisation time** on the T_g was observed at all thiol monomer ratio ranges. Indeed, it showed a strong affect particularly at 2:1 (thiol:allyl) and 8000 rpm, which increased the T_g by around 28 ˚C while increasing the duration time under UV for 5 hours. Furthermore, thermal curing method of poly thiol-allyl microparticles represents a unique system to explore **thermal**

polymerisation influences on the T_g, as they behave oppositely from the photo-polymerised thiol-ally micro-particles regarding the dramatic increases in the T_g at higher thiol monomer ratios.

Our exploration underscores the importance of the use of the thermal analysis as comparable methods provide useful and valuable information of the resulting thermal behaviour **after post-polymerisation functionalisation.** The fact that within functionalisation of poly tetrathiol-ally microspherical particles via thiol acrylate Michael addition there was a significant decrease in the T_g by nearly half, hypothesises that the increase in thiol-ether linkage quantity in the system leads to increased flexibility in the polymer backbone and decreased T_g. Besides that, the T_g for poly thiol-allyl particles after post-polymerisation functionalisation showed similar trends in behaviour to the particles before post-polymerisation functionalisation regarding the influence of thiol monomer ratio and homogeniser speed on the T_g with the exception of particles functionalised with DEAEA at 1.5:1 and 2:1 molar ratios and 20500 rpm as well as particles functionalised with EGMEA and MA at 2:1 (tetrathiol:HA) and 8000 rpm. In addition to the influence of the acrylate monomer structure on the T_g, the effect of the solvent type and volume on the T_g for the functionalised poly thiol-allyl microspherical particles has also been detected.

5 Morphological Studies of Poly Thiol-Allyl Particles Before and After Post-Polymerisation Functionalisation

5.1 Introduction

Within several biomaterials, polymeric colloids are unique in the breadth of potential applications.[129] Owing to the ability to control architecture, size, surface functionality and degradations profiles, many biomedical and pharmaceutical application include polymer colloids.[129] In the last two decades there has been increased interest in drug delivery using biodegradable polymeric microsphere.[130] The efficiency of the medication not only depends on its chemical compositions, but particles size can also significantly affect a drug's bioavailability.[7] The morphology of polymeric colloids is vital for their use.[51] Changes in the morphology leads to changes in their ability to suit their desired purpose.[51]

As mentioned in the introductory chapter with regard to emulsion or suspension polymerization, there are two heterogeneous phases: a continuous phase and a dispersed phase. Usually, the continuous phase transfers energy into the dispersed phase (when the reaction takes place). The polymerisation reaction creates a particle that has the same size and shape as the parent droplet. The advantage of suspension and emulsion polymerisation is their capacity to control the size and shape of the resulting polymer particles. Several parameters can influence the particle size distribution (PSD) and the mean size in emulsion and suspension. These include agitation speed, temperature initiator, cross-linked and diluent, ultrasonic introduction and the addition of surfactants and pigments.[45, 131, 132]

Based on the literature survey, PSD depends upon the balance between the break-up and the coalescence of droplets, which is then controlled by the type and speed of the agitator, monomer and surfactant.[133]

In addition, the literature results indicate that a good solvent has both a smaller and greater miscibility in the water and monomer phases, respectively, which allow the later phase separation between the water and the monomer phase. On the other hand, a bad solvent allows earlier phase separation. Consequently, miscibility is not preferred in the case of a bad diluent, and it is separated in the early stage.[133] Toluene, THF, n-hexane, n-heptane, and MEK are examples of solvents that may be used to form polymer particles as an insertion of the diluent in the organic phase.[133]

Although as is typical in the case of suspension polymerisation, agitation energy has a greater impact on particle size. Surfactants are also noteworthy with regard to other methods of thiol-ene polymer particles synthesis.[45] Indeed, Durham and Shipp have already demonstrated the effect of surfactant type and concentration on the final particle size distribution of thiol-ene polymers. They examined the variation in terms of surfactant concentration and variation in surfactant species (anionic, cationic and non-ionic surfactants) beside the structural analogues. They found that using a stabilizing agent or surfactant is important in order to prevent extensive aggregation and agglomeration of cross-linked thiol-ene polymer particles. In general, smaller particles are obtained with a higher concentration of the stabilizing agent, particularly for ionic surfactant species. In addition, they confirmed that particle size is strongly influenced by variations in surfactant structures when reactions are stabilized using non-ionic surfactants.[45]

Looking for easy to control techniques has already attracted research. The morphology, shape, and size of microsphere and nanosphere of polymer particles have

been extensively investigated.[39, 134, 135] The synthesis of micro/nano particles with controlled shape, size and composition has long been of scientific and technological consideration.[135] This chapter is part of an overall study of the effect of process variables of the particulate suspension photo-polymerisation system. These studies have shown that chemical composition/structure and T_g depend on these process variables. In addition, we observed that particle size and shape (morphology) could be easily tuned in this system. Therefore, the purpose of this chapter is to study the effect of thiol monomer ratio, homogeniser speed, cross-linking density, photo polymerisation time, thermal curing method and acrylate monomer structure on the chemical composition/structure, T_g and the morphology obtained by thiol-allyl suspension-polymerisation system before and after post-polymerisation functionalisation using thiol-acrylate Michael addition reaction. Crossed-linked poly thiol-allyl microsphere particles contain surface thiol groups, which are useful for post-polymerisation functionalisation. However, some influences distort the morphology of microsphere. The advantages of microspheres such as high uniformity (narrow size distribution), large specific surface area, high diffusibility and mobility, stable dispersions and variety in surface chemistry texture, have been widely applied in the fields of photonics, electronics and biotechnology.[15, 136] Uniform microscopic particles are required for many applications.[136] More generally, the purpose of uniformity of surface properties, morphology/internal structure and composition is to synthesise a well-defined product.[136]

The methodologies for uniform particle synthesis have a long history in colloid chemistry, which has been under renewed attention.[136] In spite of the fact that synthesis of dispersion of uniform colloid particles of numerous chemical composites and

shapes have been reported, the challenge of explaining uniformity of shape and morphology remains mainly unanswered.[136] To answer the question why do we have different shape and size of poly thiol-allyl microstructure particles, we need to examine the real scientific reasons behind the changes in the morphology of thiol-allyl microstructure particles before and after post-polymerisation functionalisation. Thus, the SEM was used to assess the shape and surface morphology of micro suspension results of the effect of varying the following factors: thiol monomer ratio, homogeniser speed, cross-link density photo polymerisation time and thermal curing methods as well as the influence of acrylate monomer structure and solvent type and volume on the particles' shape and size before and after post-polymerisation functionalisation. Hence, we were able to adjust and identify when and how unwanted outcomes such as aggregation and agglomeration may occur during the formation process.

The remainder of this chapter is organised as follows. An experimental section describes the use of SEM to characterise poly thiol-allyl particles. We then discuss the result of the SEM images, which provides clues to the influence of the molar ratio of thiol monomer, homogeniser speed, cross-linking density, photo-polymerisation time, and thermal curing methods before and after post-polymerisation functionalisation using different structures of acrylate monomers on the morphology. In conclusion, we provide an overview summarising and emphasising that the adaptation of these experimental conditions leads to controlling the shape and size of poly thiol-allyl microstructure particles.

5.3 Results and Discussion

Although suspension polymerisation is not a new method, if small sized monodispere-porous polymer particles could be produced using this technique this would be a cost-effective system which would have the ability to scale up in industry.[133] Thus, in this thesis, we focus on determining the morphology of poly thiol-allyl microstructure particle materials by altering various synthesis parameters (thiol monomer ratio, homogeniser speed, cross-link density photo polymerisation time and thermal curing methods) as well as considering the influence of the acrylate monomer structure and solvent type and volume.

The morphology of poly thiol-allyl microstructure particles materials was observed by SEM. They generally have a spherical shape and non-porous morphology. Average particle diameters were calculated from SEM images by taking over 25 measurements (five measurements from each corner. and five measurements from the middle of the images). Average diameter size measurements of tri/tetra thiol-allyl particles before post-polymerisation functionalisation are presented in Table 5.1.

5.3.1 Influence of thiol monomer ratio on particle morphology

The relationship between the thiol monomer ratio and morphology of poly thiol-allyl polymer particles was examined using SEM. The morphology and particle size can be influenced by this change; as expected, the results reveal that as the molar ratio of thiol-ene monomer increases, morphologies of polymer particles prepared at 8000 rpm and 20500 rpm changed. Figures 5.1, 5.3 and 5.5 show SEM photographs of the surface of the poly thiol-allyl particles with different thiol monomer ratios of thiol:HA. These were confirmed further by the corresponding particle size-distribution analysis (Figures 5.2, 5.4 and 5.6). The images and data shown in Figures 5.1-5.6 clearly

illustrate that the molar ratio of thiol to HA can have an important effect on morphology development in photo cured poly thiol-allyl microstructure particles, which have received relatively little attention.

Table 5. 1. Summary of the Average Particles Diameter (µm) of Poly Thiol-Allyl Microstructure Particles Before Post-Polymerisation Functionalisation.

Ratios [thiol]:[HA]	**homogenizer speed**	**Trithiol (1h)**	**Tetrathiol (1h)**	**Tetra thiol (5h)**
1:1	8000	2 µm	3 µm	3 µm
1:1	20500	1 µm	1 µm	2 µm
1.5:1	8000	3 µm	5 µm	4 µm
1.5:1	20500	-	2 µm	3 µm
2:1	8000	-	3 µm	3 µm
2:1	20500	-	2 µm	3 µm

Figure 5.1 displays photomicrograph samples of poly trithiol-allyl particles formed at 8000 rpm (Figure 5.1) which initially consisted of equal ratios of tri-thiol and HA, in relatively uniform spheroidal particles of 2µm in diameter (Figure 5.1a). Under this condition, the network based on 1.5:1 of trithiol:HA is prepared: the particles are larger ,3 µm in size (Figure 5.1b). In fact, it is unclear from SEM if the assemblies are groups of particles or a larger particle formed by the coalescence of smaller particles. However, it is encouraging to compare this figure (5.1b) with that found by Su-Cheol Park et al. (2013) they found that it is probably related to the photo polymerisation rate as the slow photo cure rate of 60:40 molar ratio of SH:AE thiol-ene would prolong

the phase separation between molecules and prepolymer, thus leading to the larger droplet size than the droplet size of molar ratio of thiol-ene monomers at balance of SH:AE = 50:50, which is the smallest.[137] After increasing the thiol monomer ratio to 2:1 of trithiol:HA, the microsphere particles were completely coalesced into a solid, elastic mass, which are clearly visualised (Figure 5.1c). Subsequent experiments at 20500 rpm demonstrated that the aggregation of the smallest microsphere (1 μm) began at trithiol-HA (1:1), and they were completely coalesced by molar ratio 2:1 of trithiol:HA (Figure 5.1d, e and f). Figure 5.2a, band c, shows histograms of the particle size distributions from the SEM images.

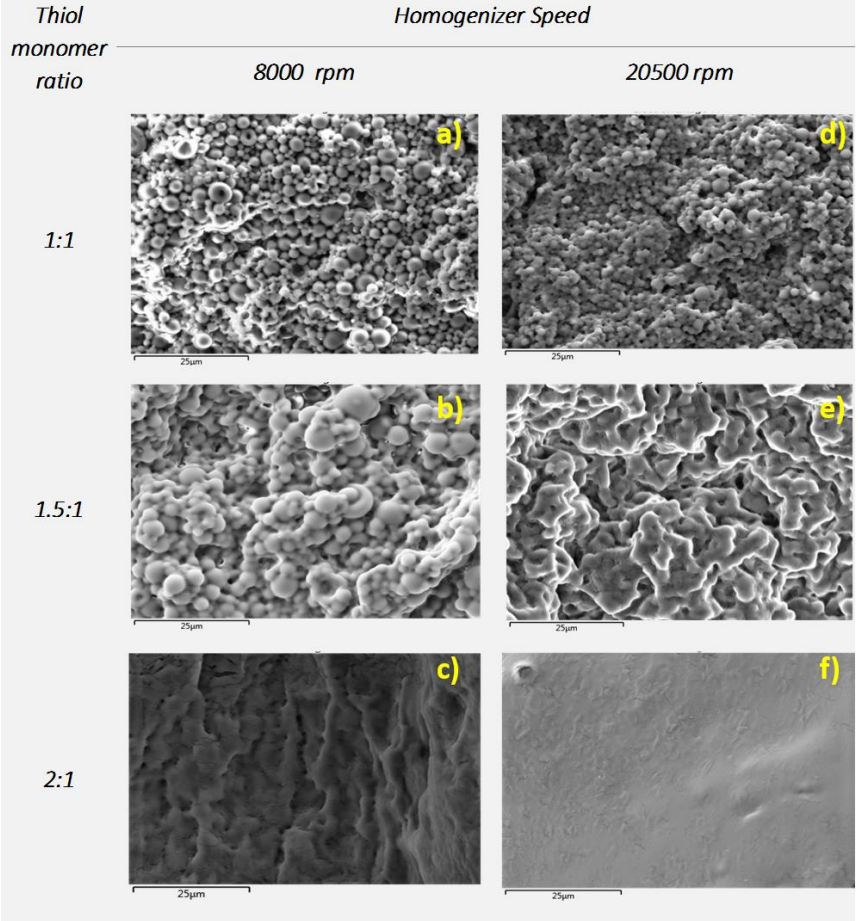

Figure 5. 1. SEM images of synthesised Poly trithiol-allyl microstructure particles synthesised with a variety of thiol monomer (TMTMP) at 8000 rpm: a (1:1), b (1.5:1), and c (2:1); at 20500 rpm: d (1:1), e (1.5:1) and f (2:1). All the scale bars are 25µm.

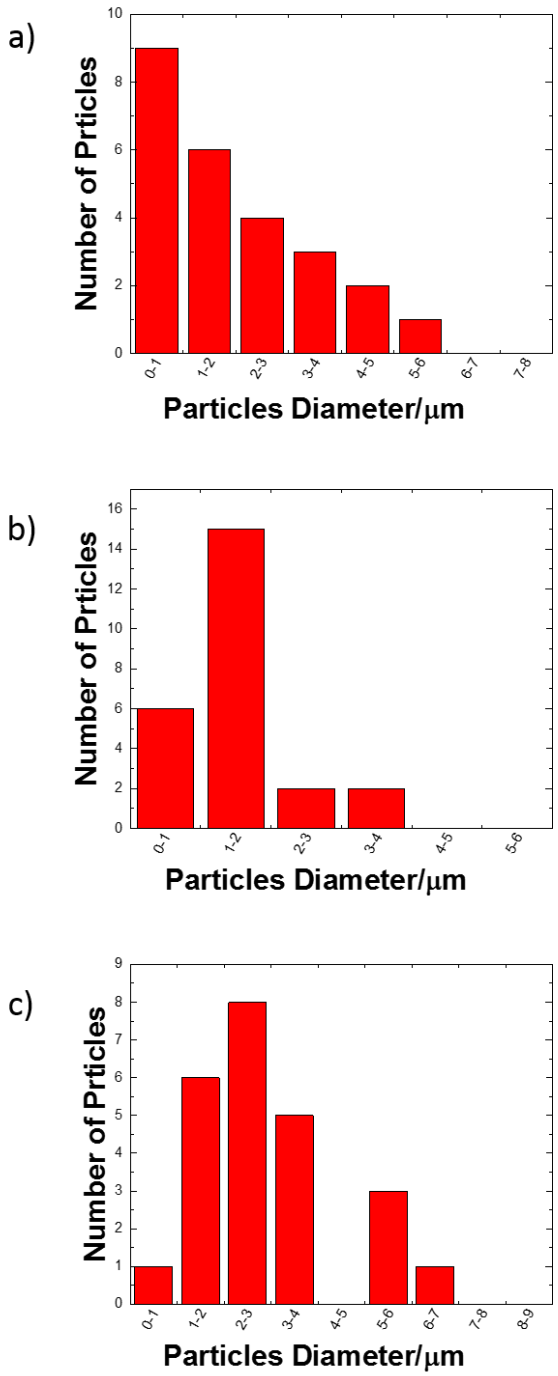

Figure 5. 2. The corresponding particle size distributions of poly trithiol - allyl particles: a) trithiol-HA (1:1) at 8000 rpm; b) trithiol-HA (1:1) at 20500 rpm; and c) tri thiol-HA (1.5:1) at 8000 rpm.

Figure 5.3 shows the SEM images of poly tetrathiol-allyl microsphere particles formed after exposure to UV for 1 hour with different ratios of thiol monomer at 8000 rpm (Figures 5.3a, b and c) and 20500 rpm (Figures 5.3d, e and f). The micrograph in Figures 5.3a and d displays a typical example of spherical particles so obtained: the diameter of which is 3 µm and 1 µm, respectively. It was found that the particles tended to be aggregated when the molar ratio of thiol monomer increased to 1.5:1 and 2:1 of thiol-HA system (see Figures 5.3c-f). The range of size distribution of the above mentioned particles are shown in Figures 5.4. Figure 5.5 present SEM images of the tetrathiol-allyl microsphere particles formed after exposure to the UV for 5 hours. It is clear that all samples display a well-defined microsphere morphology. Moreover, Figures 5.5c and 5.5f fully shows that using thiol monomer ratio of 2:1 of tetra-thiol:HA provides typical monolithic morphology consisting of globuli fused together with an average size of 3 µm and the range of relative obtained particle diameter distribution are shown in Figure 5.6.

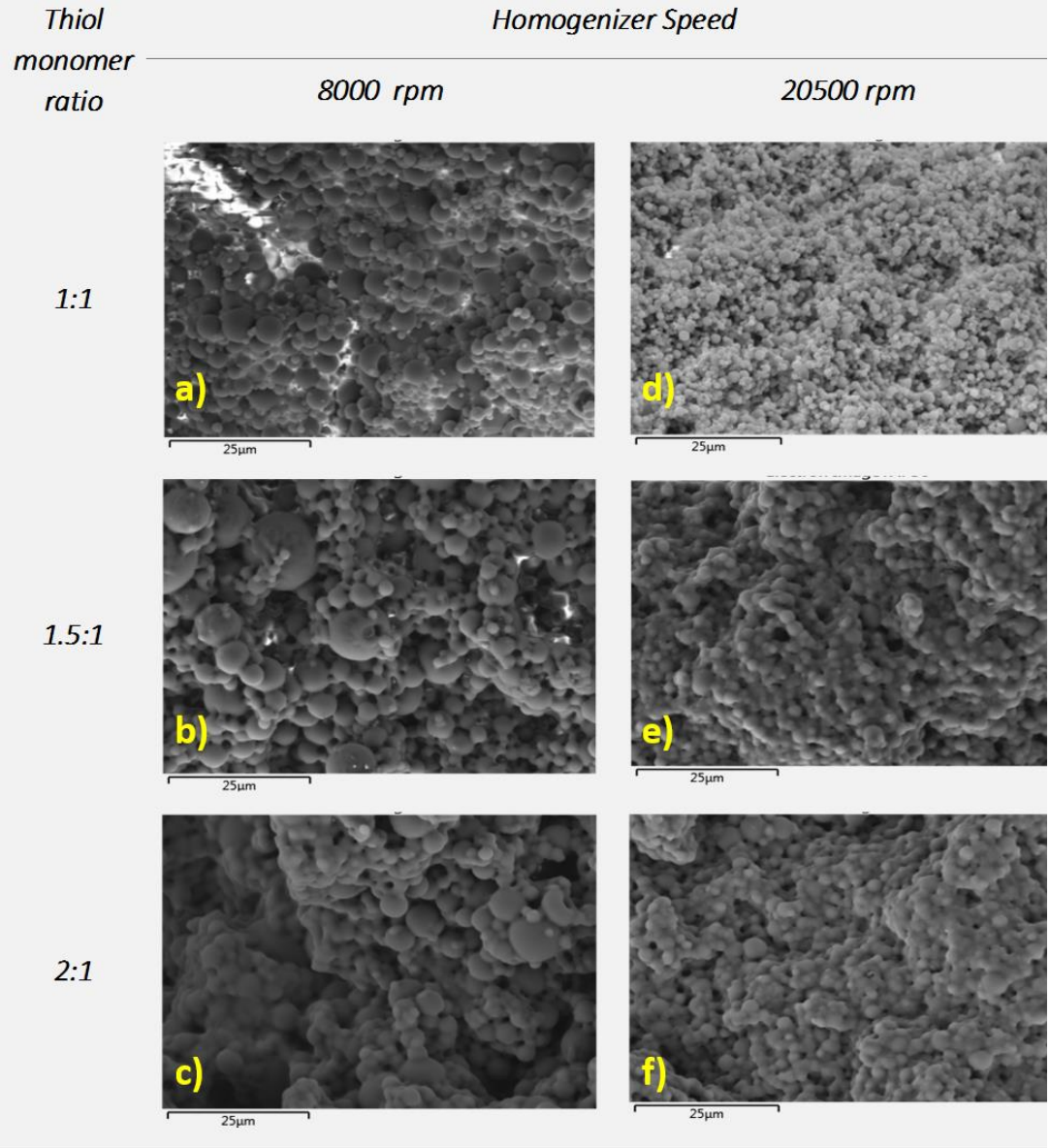

Figure 5. 3. Typical SEM images of poly tetrathiol-allyl microsphere particles. Synthesised under UV for 1 hour with various ratios of thiol monomer (PETMP); at 8000 rpm: a (1:1), b (1.5:1) and c (2:1); at 20500 rpm: d (1:1), e (1.5:1) and f (2:1). All the scale bars are 25µm.

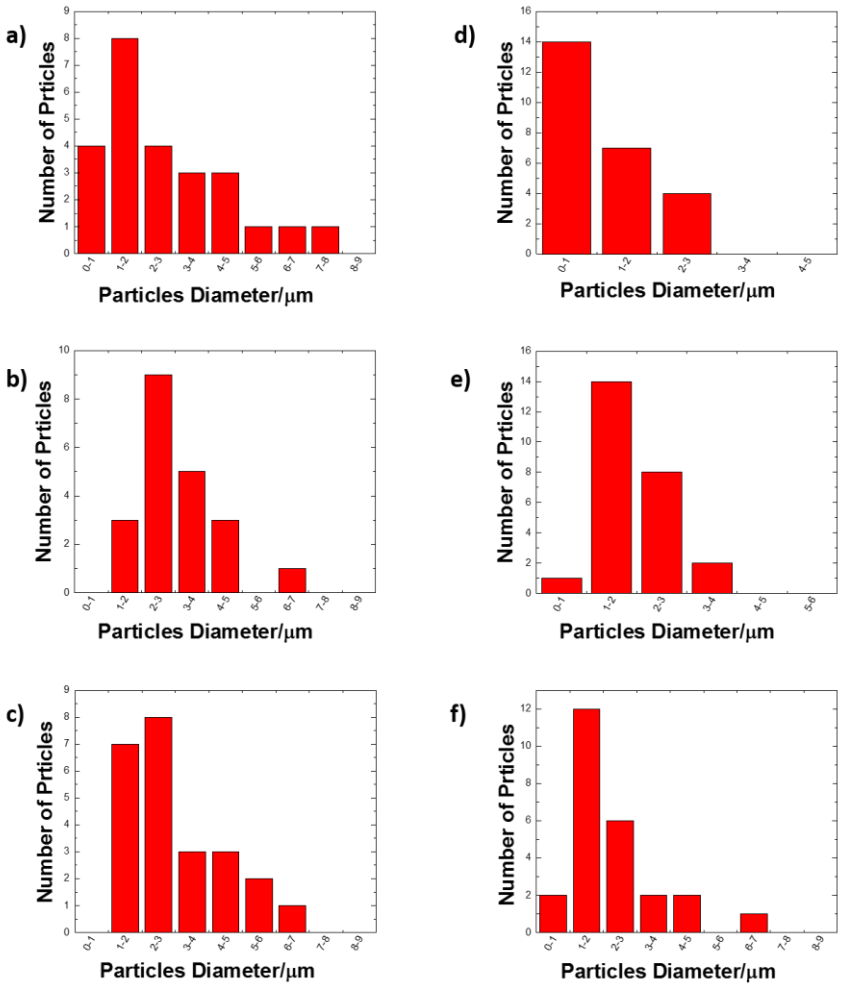

Figure 5. 4. Size-distribution analysis of poly tetrathiol-allyl microsphere particles with various thiol monomer ratios; at 8000 rpm: a (1:1), b (1.5:1) and c (2:1); at 20500rpm: d (1:1), e (1.5:1) and f (2:1). All had 1 hour under UV.

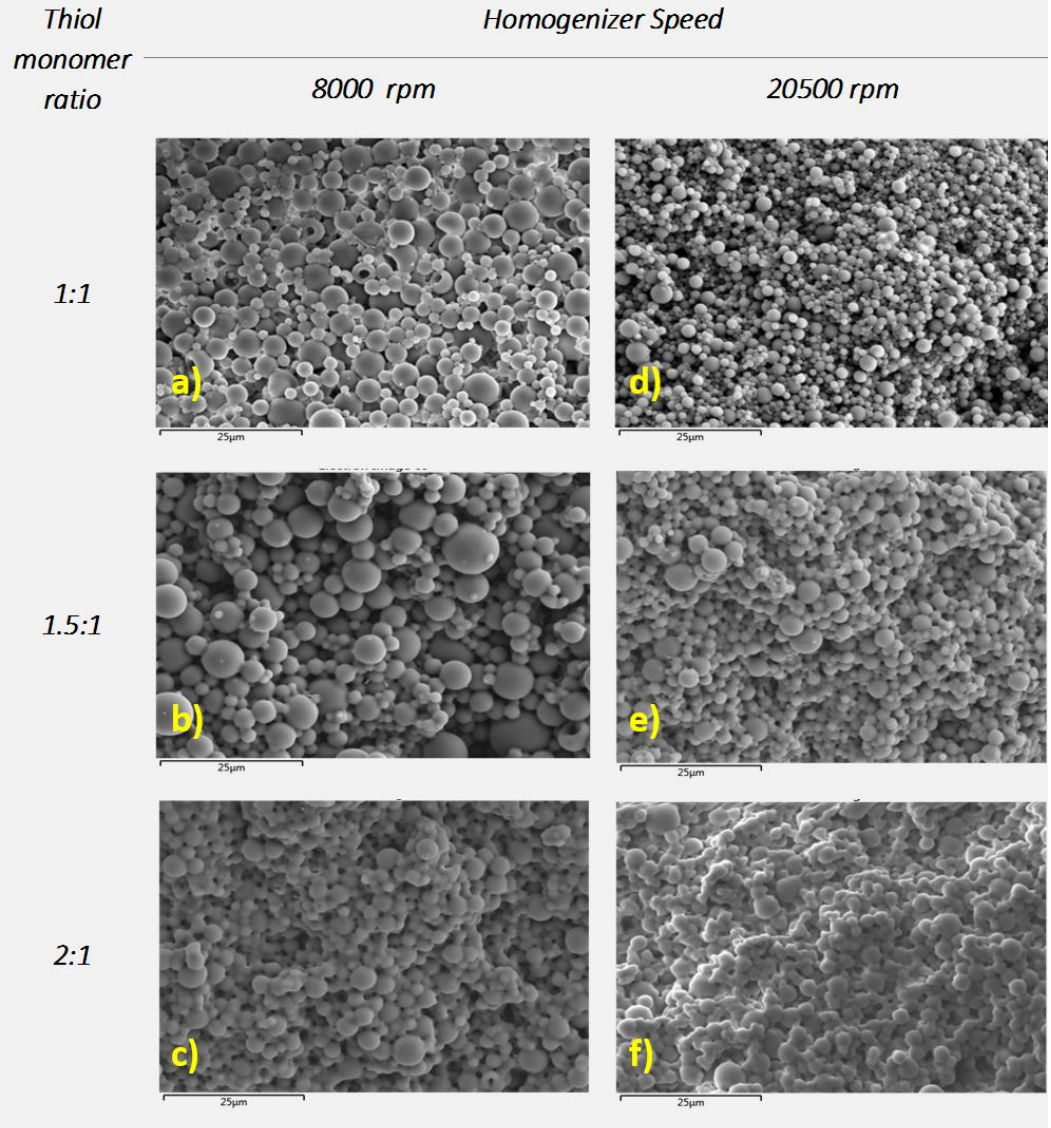

Figure 5. 5. Typical SEM images of synthesised poly tetrathiol-allyl microsphere particles under UV for 1 hour with various ratios of thiol monomer (PETMP); at 8000 rpm: a (1:1), b (1.5:1) and c (2:1); at 20500 rpm: d (1:1), e (1.5:1) and f (2:1). All the scale bars are 25µm.

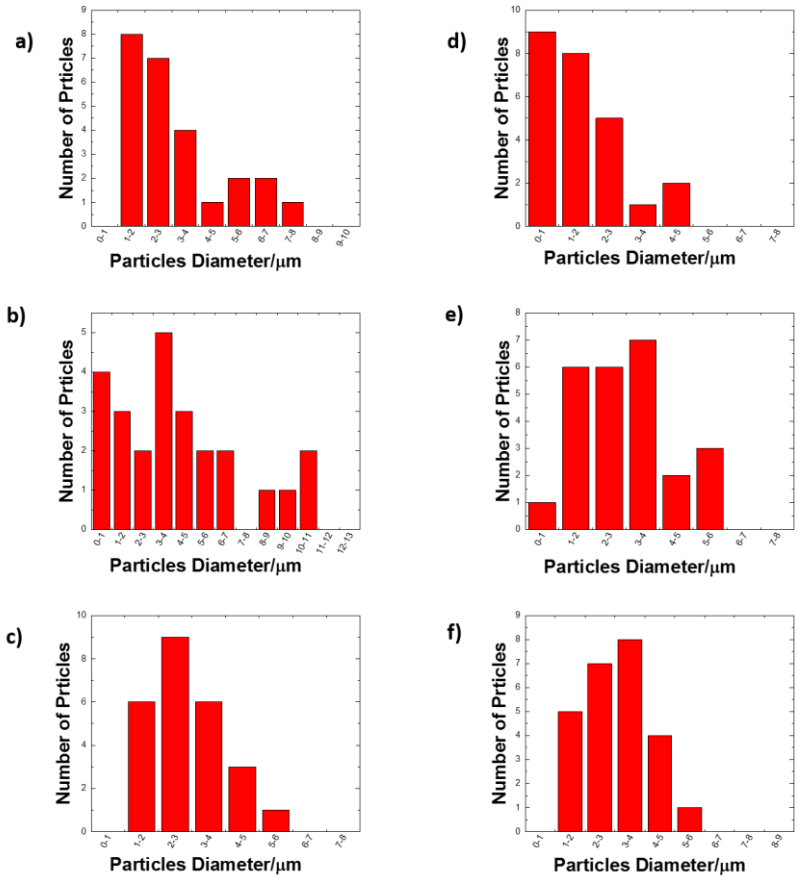

Figure 5. 6. Size-distribution analysis of poly tetrathiol-allyl microsphere particles with various thiol monomer ratios; at 8000 rpm: a (1:1), b (1.5:1) and c (2:1); at 20500 rpm: d (1:1), e (1.5:1) and f (2:1). All had 5 hours under UV.

It is clear that most samples display a well-defined microsphere morphology. However, at higher thiol monomer ratios (1.5:1) and (2:1), samples appeared as agglomerations of smaller or larger particles. Interestingly, there was a marked difference among the previous three types of particles' average size diameter: tri thiol with HA, tetra thiol with HA during both 1 and 5 hours polymerisation time (see Figure 5.7). Overall, the average particle diameter of the photo cured sample increased by increasing the thiol monomer ratio. As the thiol: hexa-allyl molar ratio varied from

1:1 to 1.5:1, the average diameter of the cured particles using tri thiol at 8000 rpm increased from 2 µm to 3 µm. In addition, the average diameter of the cured sample, under UV for 1 hour and using tetra thiol at 20500 rpm, increased from 1 µm to 2 µm when the ratio of tetra thiol monomer increased from 1 to 1.5 and 2 mole. The average diameter size measurements of the cured sample under UV for 5 hours of tetra thiol with equal ratio of HA (1:1:4t:HA) and 20500 rpm, showed similar behaviour in that they had average diameter of 2 µm, which was lower than the average diameter of 3 µm of cured sample tetra thiol with HA at both ratios of 1.5 and 2 mole. In contrast to the above results, the average particle diameter size decreased by increasing the thiol monomer ratio of samples of tetrathiol at 8000 rpm under UV for 1 hour. The average diameter of the particle based at molar ratio 2:1 of tetrathiol:HA exhibited a lower average diameter (3µm) than the network based on 1.5:1 of tetrathiol:HA (5 µm); however, it was similar to the average diameter size of an equal ratio of tetrathiol:HA. Further, the average diameter size of molar ratio tetrathiol:HA at 8000 rpm, and under UV for 5 hours, decreased from 4 µm to 3 µm by increasing the thiol monomer ratio from 1.5 mol to 2 mol. This was still, however, similar to the average diameter size (3 µm) of the cured sample with equal ratios between tetrathiol and hexa-allyl. These results indicate that homogeniser speed influences the formation of poly thiol-allyl microstructure particles, causing different morphologies and average diameter size, which will be explained in detail in the next section.

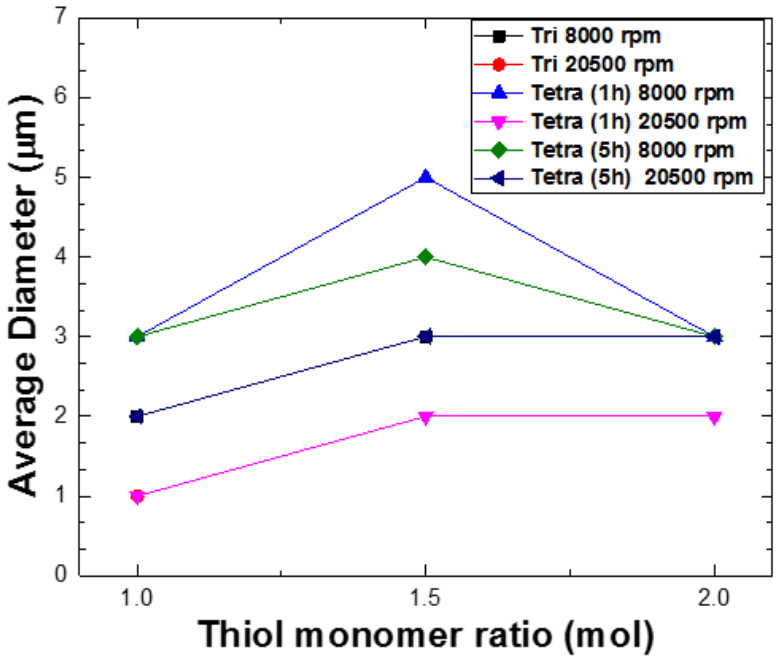

Figure 5. 7. Changes in the average particle diameter size with respect to the thiol monomer ratio for photo initiated poly thiol microstructure particles.

5.3.2 Influence of homogeniser speed

Another factor influencing the morphology and particle size of poly thiol-allyl microstructure particles is the amount of share energy introduced by homogenisation. Wang and Xia have demonstrated that monodispersed spherical colloids of several low melting-point metals could be conveniently synthesised using bottom-up and top-down approaches. A fixed starring rate was used in their preparation. They demonstrated this with a plot showing the relationship between diameters and the stirring rate used in the emulsification process. They proved that, depending on the stirring rate, the diameters of these uniform spherical colloids could be readily varied from 100 to 600 nm.[13] Durham and Ship also found that a higher homogenization power yields smaller particles.[42] In addition, from Sušec et al.'s studies, it is evident

that the stirring rate in addition to other factors, have asignificant effect on the morphological features of polymerised high internal phase emulsion materials.[135]

Moreover, Yang and co-workers investigated PSD and morphology in the case of in situ suspension polymerisation.[131] From their analysis, it is inferred that the droplet size can be decreased by increasing the agitation speed. In their experiments they used agitation speeds ranging from 800 to 2000 rpm, and have plotted the size distribution of the droplets against the agitation speed. This shows that the average size of the corresponding droplets decreases from 113.62 to 66.41 μm and all curves have two peaks, which are in the submicron range and the tens of micron range, respectively. They also show that although a high agitation speed can reduce the droplet size significantly, the average droplet size is still much larger than 10μm.[131]

Thus, the suspensions of the same composition were prepared by homogenising the mixture at different intensive homogenising speeds, namely 8000 rpm and 20500 rpm. From the all previous figures, several observations can made. First, the SEM images of trithiol-HA (1:1) shows spherical particles with narrow size distribution in micrometre ranges, as can be seen in Figures 5.1a and b (see also Figures 5.2a and b). From Figure 5.7, it can be seen that the average particle diameter size reduced slightly from 2 μm to 1μm when the homogeniser speed increased from 8000 rpm to 20500 rpm. The microsphere particles with ratios of 1.5:1 of tri-thiol:HA exhibited a rough surface (Figure 5.1d), and particles consisting of 2:1 of tri-thiol:HA (Figure 5.1f) were completely flat coalesced after increasing the homogeniser speed to 20500 rpm.

Second, Figures 5.3 and 5.5 show SEM images of poly tetrathiol-allyl microsphere particles with various thiol monomer ratios under UV for two different duration polymerisation times: 1 hour (Figure 5.3) and 5 hours (Figure 5.5), at two different homogeniser speeds: 8000 rpm and 20500 rpm. In all cases, it was noted that the resulting microspherical particles become smaller and uniform after increasing the homogeniser speed to 20500 rpm.

Moreover, it is apparent from Figures 5.3b, c, e and f that microsphere polymer particles of tetra thiol with HA at both ratios 1.5 mole and 2 mole, under UV for 1 hour, started to become fused together after increasing the homogeniser speed from 8000 rpm to 20500 rpm. Whereas, microsphere polymer particles that were exposed to UV for 5 hours started to fuse together after increasing the homogeniser speed from 8000 rpm to 20500 rpm only at a tetrathiol-HA ratio of 2:1 (see Figures 5.4c and f).

Interestingly, the average particle diameter size and size distribution of the poly tetrathiol-allyl microsphere particles was also found to be dependent on the homogeniser speed. As is evident from Figure 5.7, increasing the speed of the homogeniser led to a trend of decreasing in the average particle diameter size for all poly tetrathiol-allyl microsphere particles that had been photo-cured for 1 hour; this was more noticeable for the microsphere particles with equal ratios between tetrathiol and HA, as the gap between two speeds was the 2µm. Then, the gap between the two speeds was increased by increasing thiol monomer ratio to 3 µm at tetrathiol-HA 1.5:1. At tetrathiol-HA 2:1, the gap between the average particle diameter size of the two speeds reduced to 1 µm. What is more, in the case of the particles left under UV for 5 hours, increasing the homogeniser speed led to a decline in the average particle

diameter size for all tetrathiol microsphere particles. However, the gap between the two speeds did not change when the thiol monomer ratio increased from 1 mole to 1.5 mole. At tetrathiol-HA 2:1, the average particle diameter size of the two speeds was similar. Dithiol composites consisting of equal ratios of TEGDT/HDT with HA exhibited an extremely rough surface after increasing the homogeniser speed from 8000 rpm to 20500 rpm (see Figure 5.8). Particle diameter distribution results of TEGDT-HA 1:1 are given in Figure 5.9. Our results seem to follow the same trends that several researchers have been put forward to explain this observation.[13, 42, 135, 138, 139]

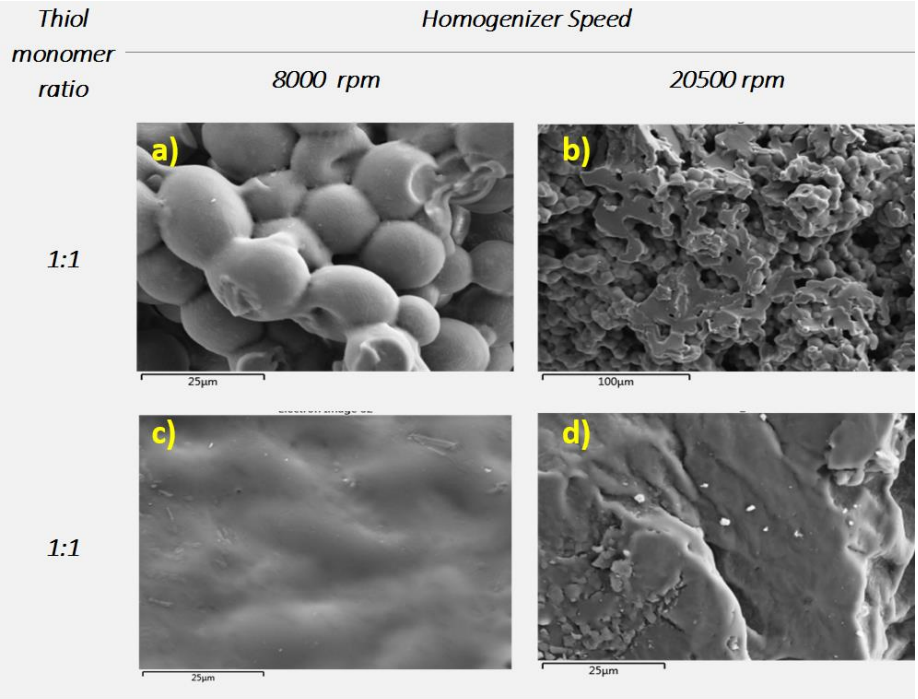

Figure 5. 8. Scanning electron microscope images of poly thiol-ally microstructure particles consisting of equal ratios of dithiol and HA. SEM images of liner thiol monomers of TEGDT (a, b) and HDT (c, d). The scale bars are 25µm (a, c) and 100 (d).

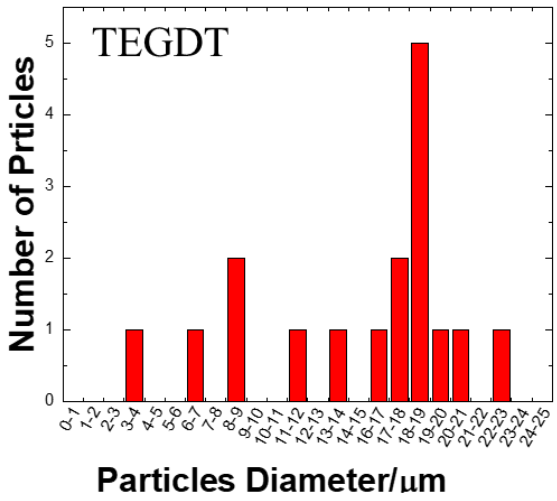

Figure 5. 9. Particle diameter distributions of TEGDT-HA (1:1); materials determined using Image J imaging software.

5.3.3 Influence of cross-linking density

Series of thiol monomers of various functionalities were determined to investigate the effect of different cross-linking densities on the morphology. SEM analysis (Figure 5.8, 5.10 and 5.11) revealed that particle shapes were found to be intensely influenced by cross-linking density. Only particles with the highest number of thiol functionality retained a spherical shape upon all tetrathiol-hexa-allyl molar ratios, varied from 1:1 to 2:1, at both 8000 rpm and 20500 rpm. However, particles of less cross-linking density were able to maintain spherical shape in the three following conditions: particles consisting of equal ratios of tri-thiol and HA were relatively uniform spheroidal particles (see Figure 5.10a and Figure 5.11b); for network based on 1.5:1 ratios of tri-thiol:HA at 8000 rpm, the particles were larger in shape (Figure 10b). Then, the morphology surface of trithiol-HA 1.5:1 at 20500 rpm, were rough surfaced, and completely coalesced into a solid, elastic mass after increasing the thiol monomer ratio to 2:1 of tri-thiol:HA at both 8000 rpm and 20500 rpm. In addition, with the

lowest number of thiol functionality, only thiol modified network of the liner thiol monomers of TEGDT-HA 1:1 at 800 rpm were in larger spherical shape (Figure 5.8a). From the previous observations, we can conclude that when the functional thiol increases, the network's ability to form particles with spherical shapes within high molar ratios of thiol monomer is increased at both the homogeneous switcher speed of 8000 rpm and 20500 rpm.

From Table 5.1 and Figures 5.2, 5.4, 5.7 and 5.9, it is evident that varying cross-linking densities affects the size and size distribution of the microsphere particles. As in the case of dithiol, TEGDT-HA 1:1 microsphere particles at 8000 rpm exhibited higher average diameters (15µm) than the microsphere particles of trithiol-HA 1:1 at 8000 rpm, with an average diameter of 2µm. In addition, particles of trithiol- HA 1:1 at 20500 rpm produced samples of similar diameter size (1 µm) to the tetrathiol-HA 1:1 particle, with an average diameter of 1 µm. These results are consistent with those of other studies and suggest that as the number of functional group increases, the microsphere diameter size decreases.[76] Bowman and co-workers (2014) refer that polymer precipitates when it reaches a critical length/size and form nuclei. Therefore, they hypothesise that nuclei react with growing polymeric chains and increase the size uniformly, thus leading to the anticipated microsphere.[66, 76] In contrast to earlier findings, however, the diameter of the particles consisting of 1:1 and 1.5:1 of tri-thiol:HA at 8000 rpm are 2 µm and 3 µm, respectively. They increased when the number of thiol functional group increased to four, which increased the diameter of 1:1 and 1.5:1 of tetrathiol:HA at 8000 rpm to 3 µm and 5 µm.

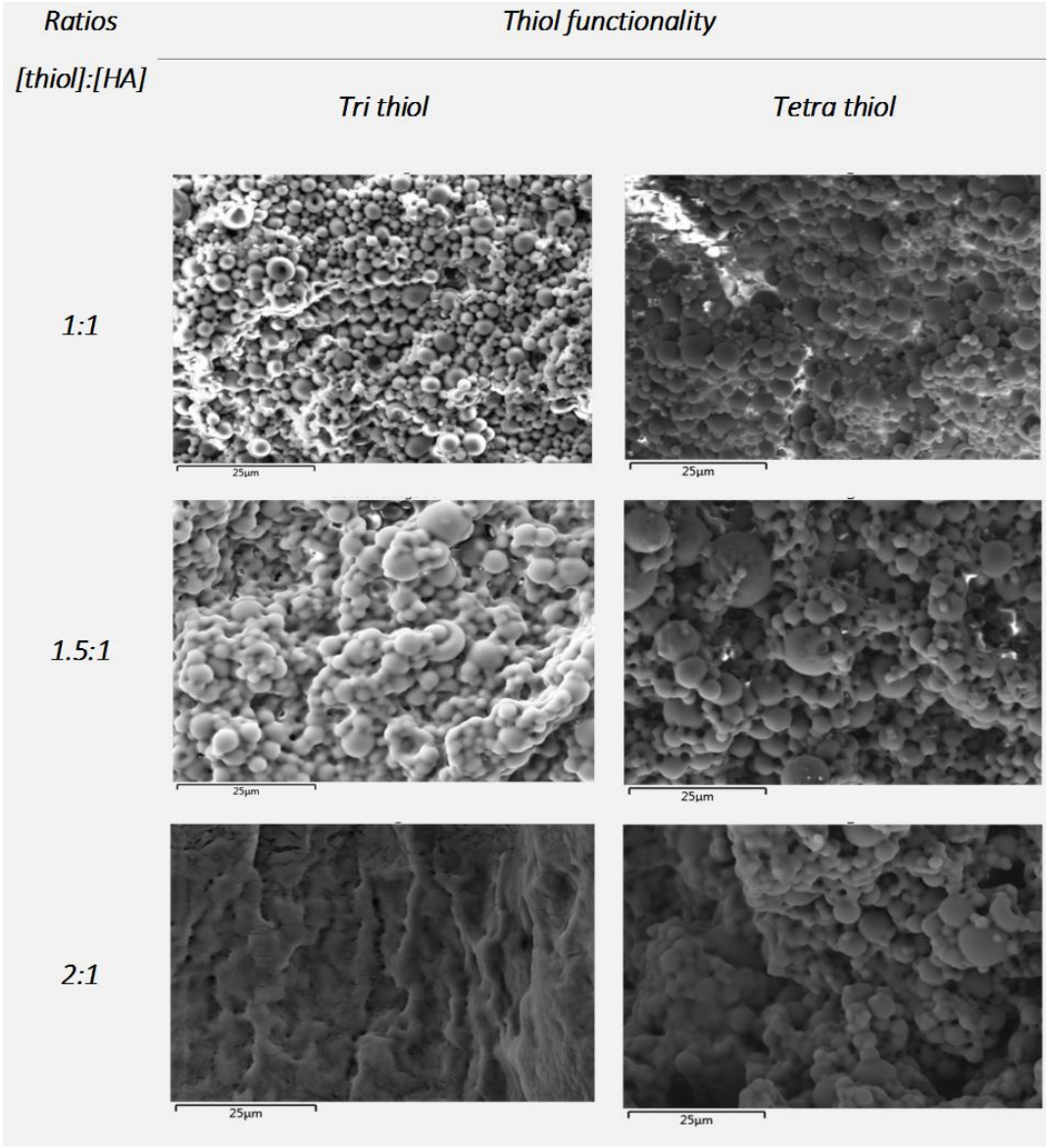

Figure 5. 10. The comparison of surface morphology between tri-thiol and tetra-thiol monomers using various thiol monomer ratios of photo-cured poly thiol-allyl microstructure particles at a homogeniser speed of 8000 rpm.

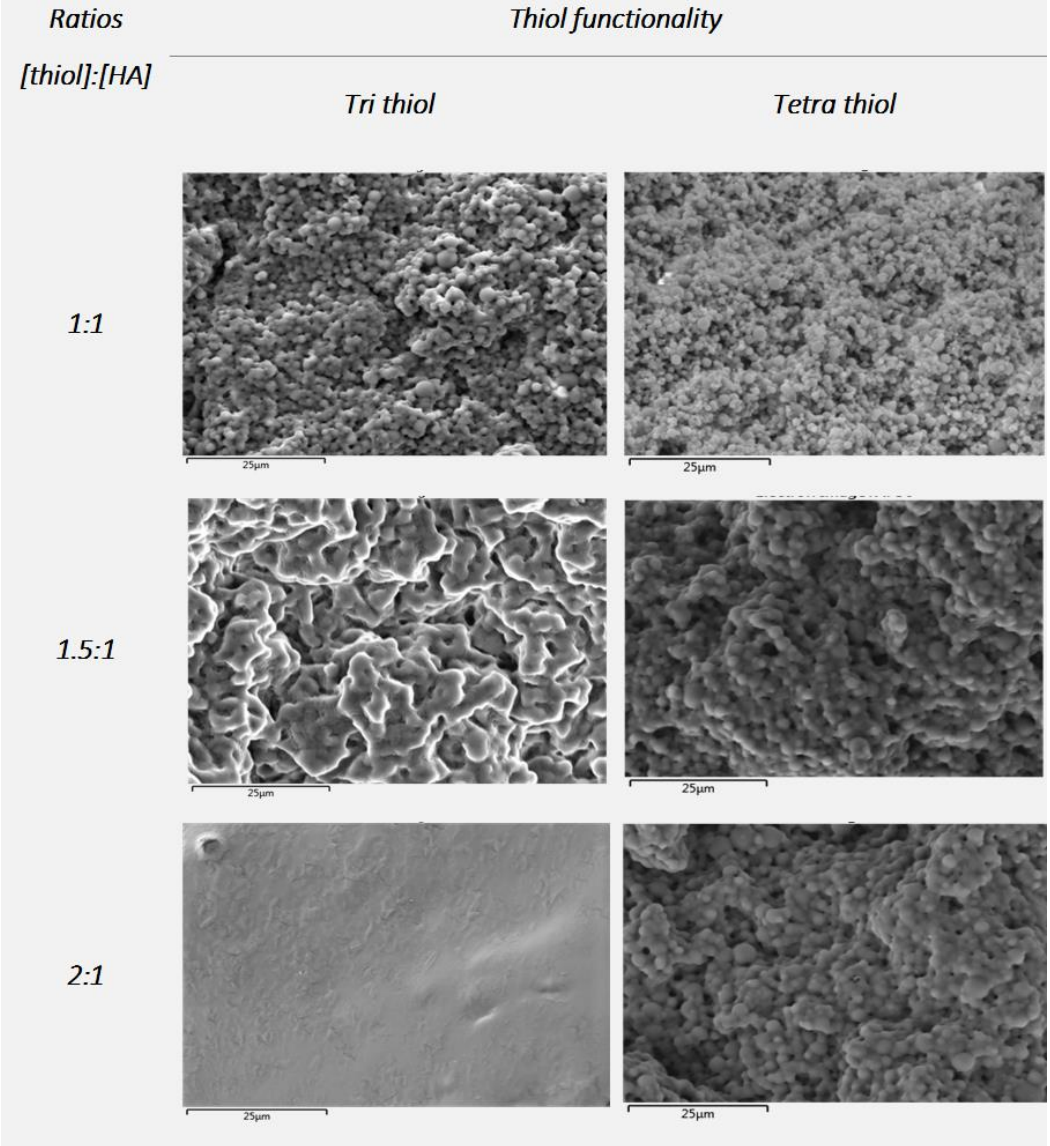

Figure 5. 11. The comparison of surface morphology between tri-thiol and tetra-thiol monomers using various thiol monomer ratios of photo-cured poly thiol-allyl microstructure particles at homogeniser speeds of 20500 rpm.

5.3.4 Influence of photo-polymerisation time

To characterise the surface morphology upon UV exposure, SEM was conducted after 1 hour and 5 hours of UV exposure at 8000 rpm and 20500 rpm (Figures 5.12 and

5.13). From Figures 12 and 13, several observations can be made. First, the most noteworthy differences in the morphology of samples that were photo-cured for 1 hour and 5 hours at both homogeniser speeds of 8000 rpm and 20500 rpm suggests that after 1 hour, photo-polymerisation adhesion between neighbouring particles were at molar ratios of 1.5:1 and 2:1 of tetrathiol:HA. While SEM images of the target particles obtained after 5 hours under UV irradiation shows that the short antiparticle distance were only at 2:1 of tetrathiol:HA.

The results of particles size distribution obtained from tetrathiol-allyl microsphere particles indicate that homogeneity of morphology (in terms of particles size distribution) during exposure to UV for 1 hour and 5 hours are comparatively high, as summarised in particle distribution size graphs at 8000 rpm and 20500 rpm in Figures 5.14 and 5.15, respectively.

To evaluate the influence of photopolymerisation time on particles' average diameter size of these surface features, Figure 5.16a and b display the average particle diameter size of tetrathiol-HA network, which consists of various molar ratios of the tetra thiol monomer at 8000 rpm (Figure 5.16a) and 20500 rpm (Figure 5.16b) upon UV exposure for 1 and 5 hours. Figure 5.16a shows that a little change in the average particle diameter size was observed after increasing the duration time under UV from 1 to 5 hours for tetrathiol-allyl microspheres particles at 8000 rpm. The increases in the average diameter size were only up to one micron for microsphere particles consisting of 1.5:1 of tetrathiol:HA; there was no change in the average particle diameter size for microsphere particles of equal ratios of tetrathiol:HA and 2:1 of tetrathiol:HA. Whereas, average particle diameters of all tetrathiol-allyl microspheres

particles at higher homogeniser speed (20500 rpm) during 5 hours under UV irradiation were larger than the corresponding particles that were consumed one hour photopolymerisation time. The gap was 1 micron between samples with equal ratios of tetra-thiol and HA and samples for particles consisting of higher molar ratios of thiol monomer to HA tetra thiol-HA 1.5:1 and tetra thiol-HA 2:1 (See Figure 5.16b). Even though the effect of photopolymerisation time was similar to the molar ratio of thiol monomer, it was less distinguished from the homogeniser power speed and cross-linking density. The relationship between shapes, the surface coalescence, size distribution and average particles size were clearly influenced by photo-curing time.[39, 134]

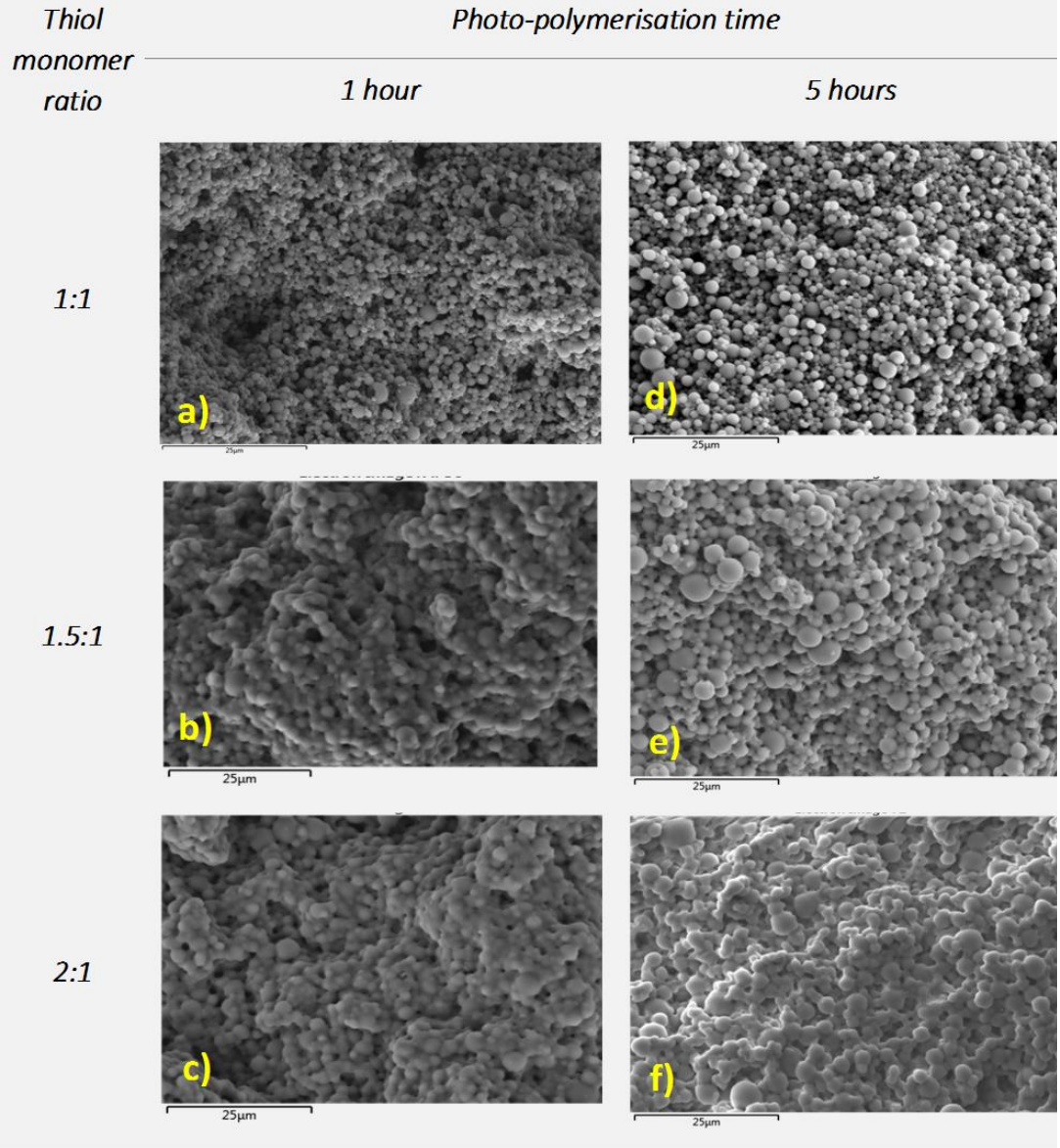

Figure 5. 12. Comparison between SEM micrographs of poly tetrathiol-allyl microsphere particles at 8000 rpm upon UV exposure for 1 hour (a, b and c) and 5 hours (d, e and f).

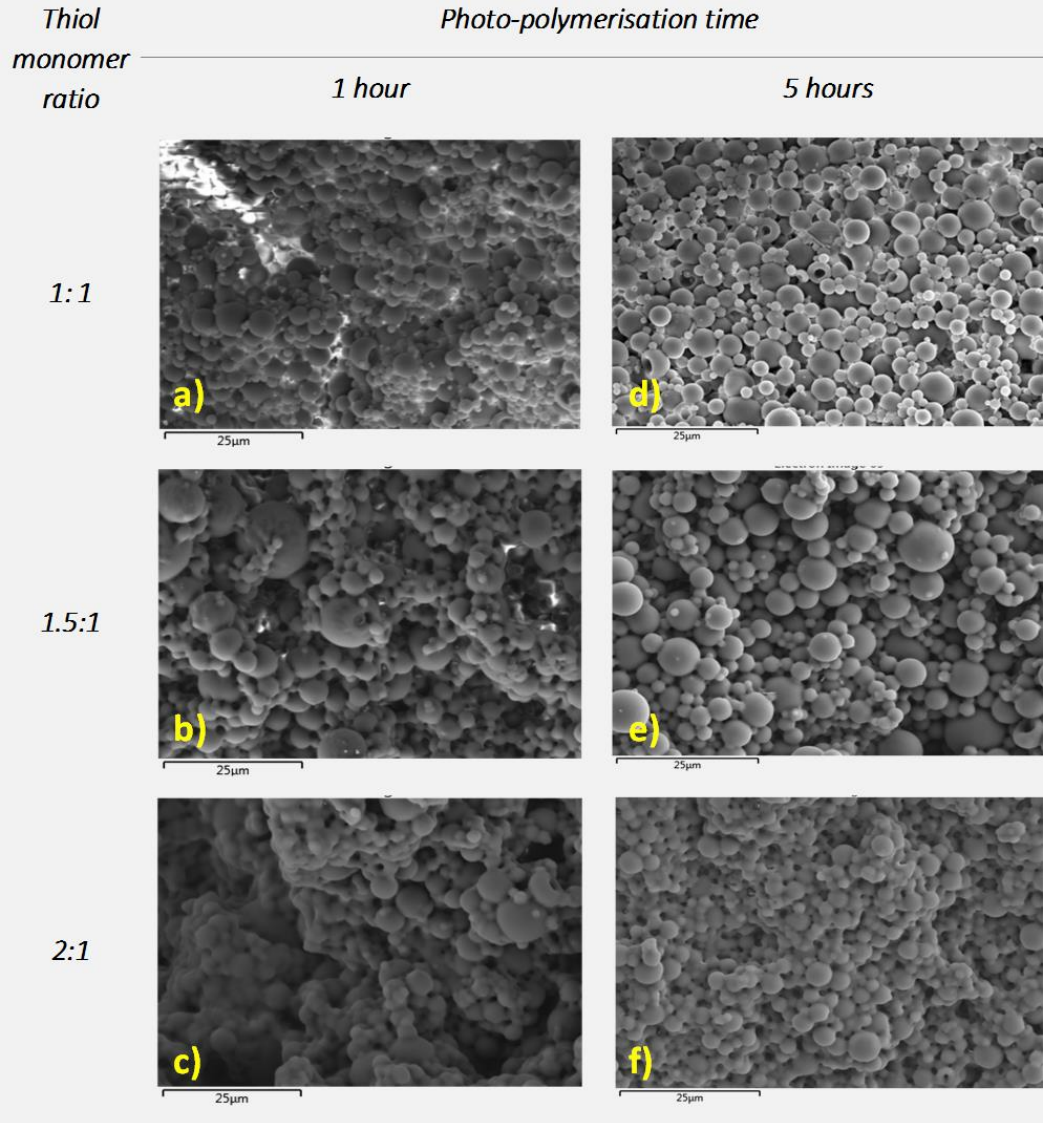

Figure 5. 13. Comparison between SEM micrographs of poly tetrathiol-allyl microstructure particles at 20500 rpm upon UV exposure for 1 hour (a, b and c) and5 hours (d, e and f). All the scale bars are 25µm.

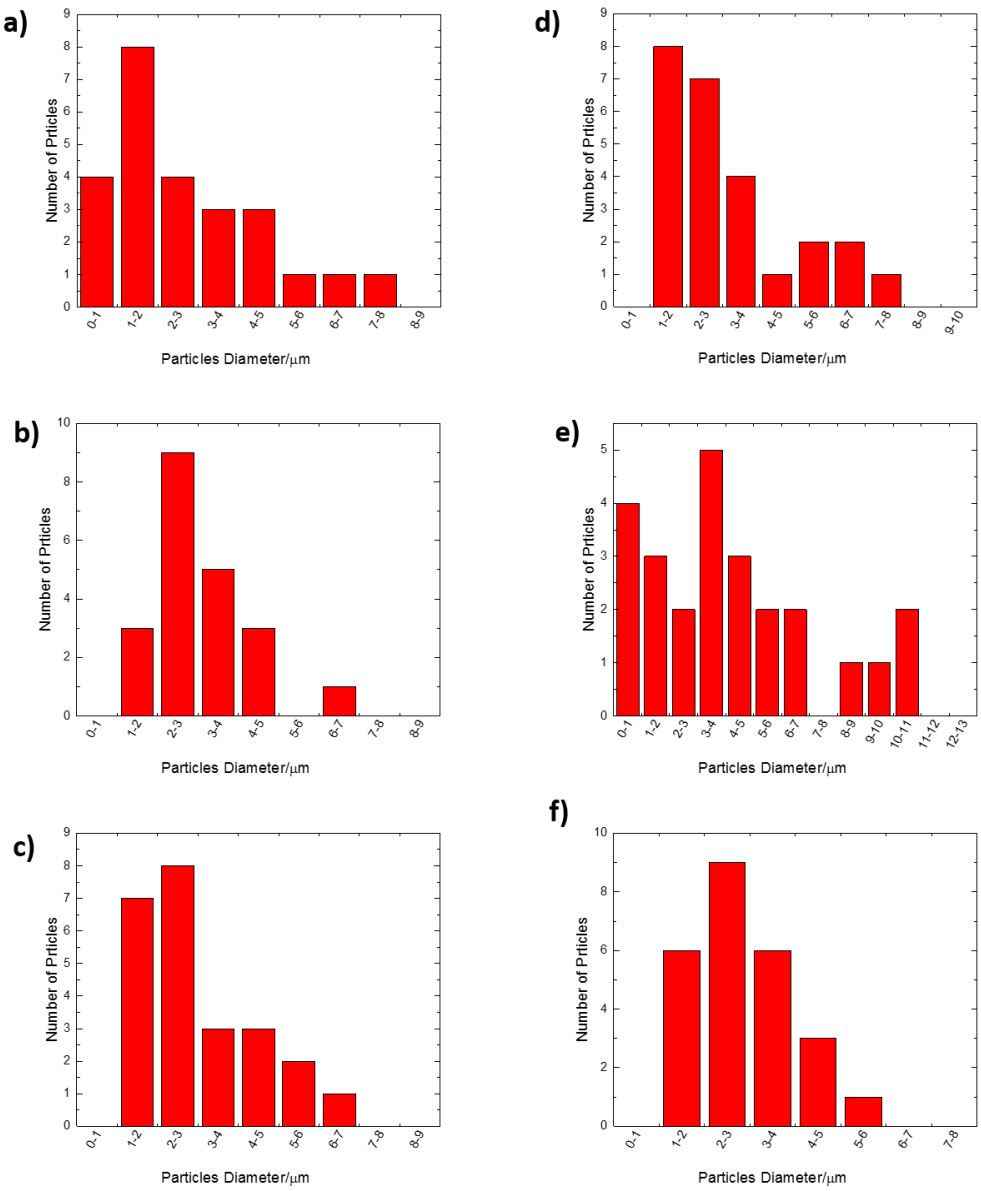

Figure 5. 14. Size-distribution analysis of poly tetrathiol-allyl microsphere particles with various thiol monomer ratios for 1 hour under UV: a (1:1), b (1.5:1) and c (2:1); and 5 hours under UV: d (1:1), e (1.5:1) and f (2:1) at 8000 rpm.

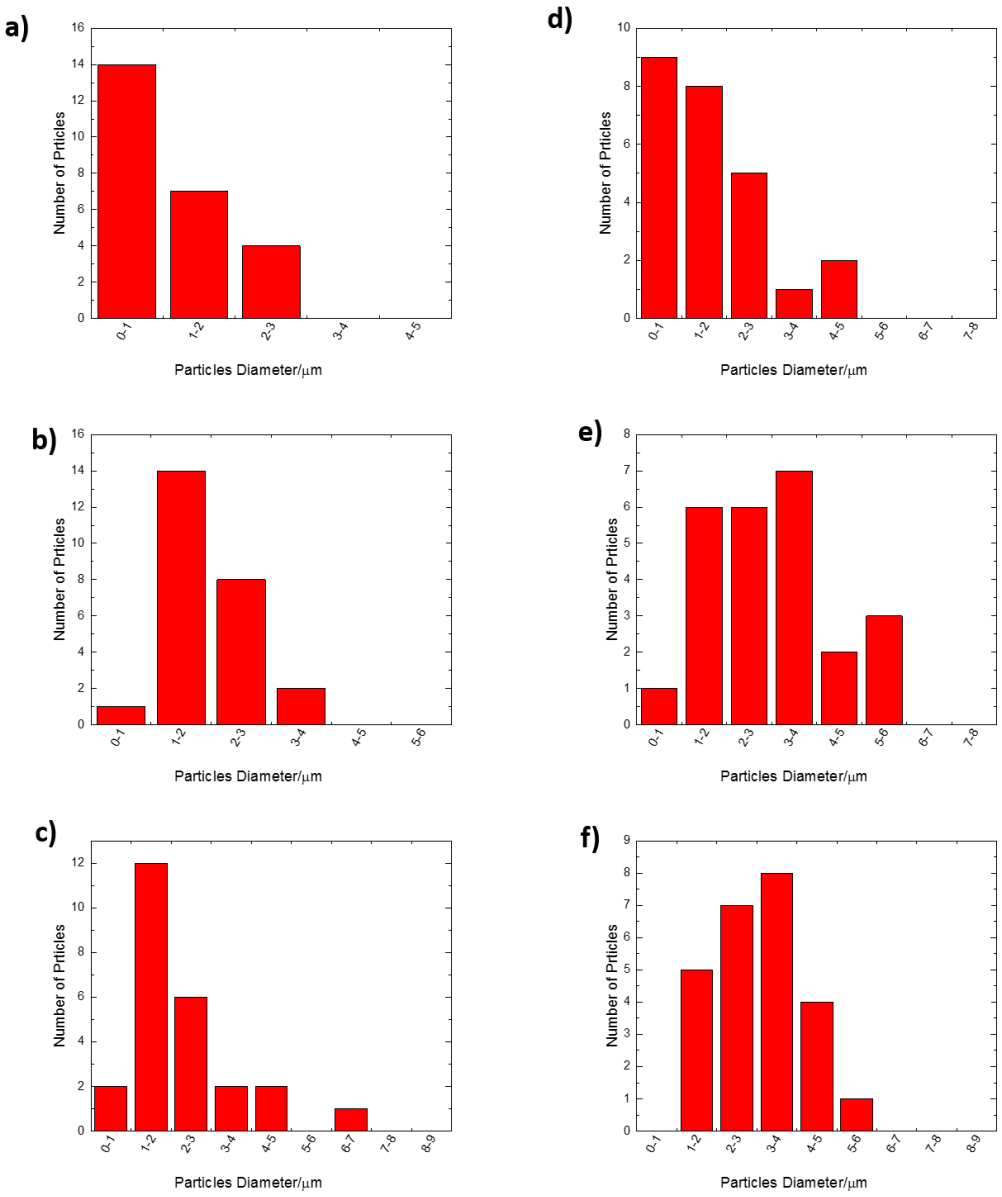

Figure 5. 15. Size-distribution analysis of poly tetrathiol-allyl microsphere particles with various thiol monomer ratios for 1 hour under UV: a (1:1), b (1.5:1) and c (2:1); and 5 hours under UV: d (1:1), e (1.5:1) and f (2:1) at 20500 rpm.

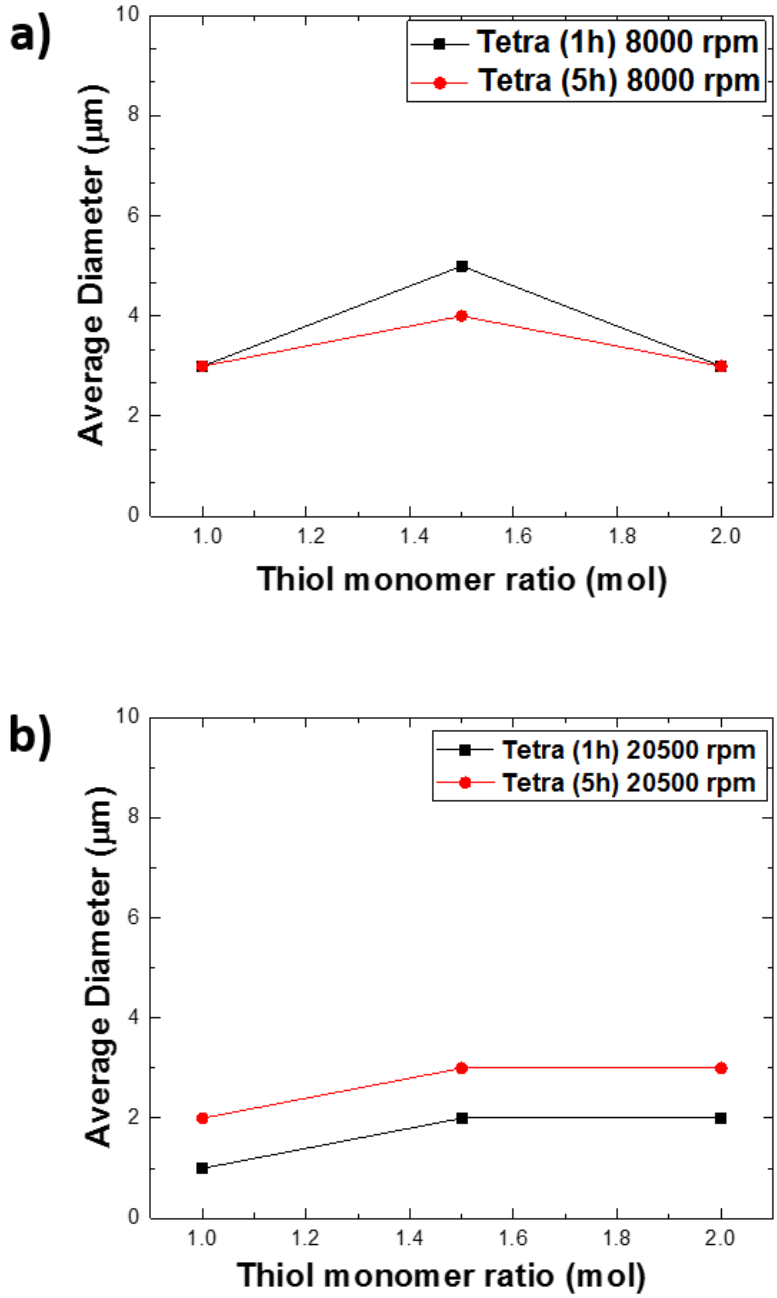

Figure 5. 16. Average particle diameter size versus thiol monomer ratio of photo initiated poly thiol-allyl microstructure particles: (a) average diameter changed slightly under 1 hour and 5 hours duration time at homogeniser speed 8000 rpm; (b) average diameter size increased due to increased photo polymerisation time from 1 hour to 5 hours at 20500 rpm.

5.3.5 Influence of thermal polymerisation method

The influence of molar ratios of thiol to allyl group on the morphology and particle size distribution of the resulting thermal polymerisation network of poly thiol-allyl microparticles at 8000 rpm was investigated using SEM (Figure 5.17) and (Figure 5.18). In the case of sample tetra thiol-HA (1:1), spherical shaped micro particles were formed (Figure 5.17a and b) An average particle diameter of 3µm was found when adding DVB cross-linker to the organic phase of the suspension mixture (Figures 5.18a and 5.19), while the average diameter of particles without DVB was 1 µm (Figures 5.19). From Figure 5.17c and d, we also observe a spherical shape particle with higher molar ratio of tetra thiol to HA at both ratios 1.5:1 and 2:1 with a size of 2 µm and 1 µm, respectively (Figure 5.19).

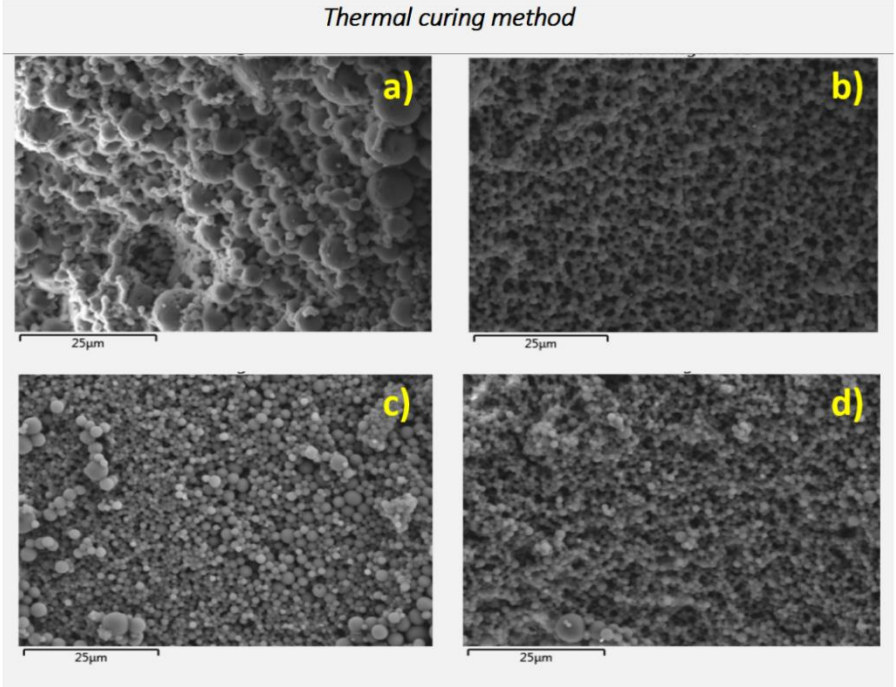

Figure 5. 17. Morphology of thermal initiated poly tetrathiol-allyl microstructure particles at 800 rpm. SEM images of equal ratios of tetrathiol and HA with (a) adding DVB and (b) without DVB; (c) SEM image of tetra thiol-HA (1.5:1) molar ratio; (d) SEM image of tetrathiol HA (2:1) molar ratio. All the scale bars are 25µm.

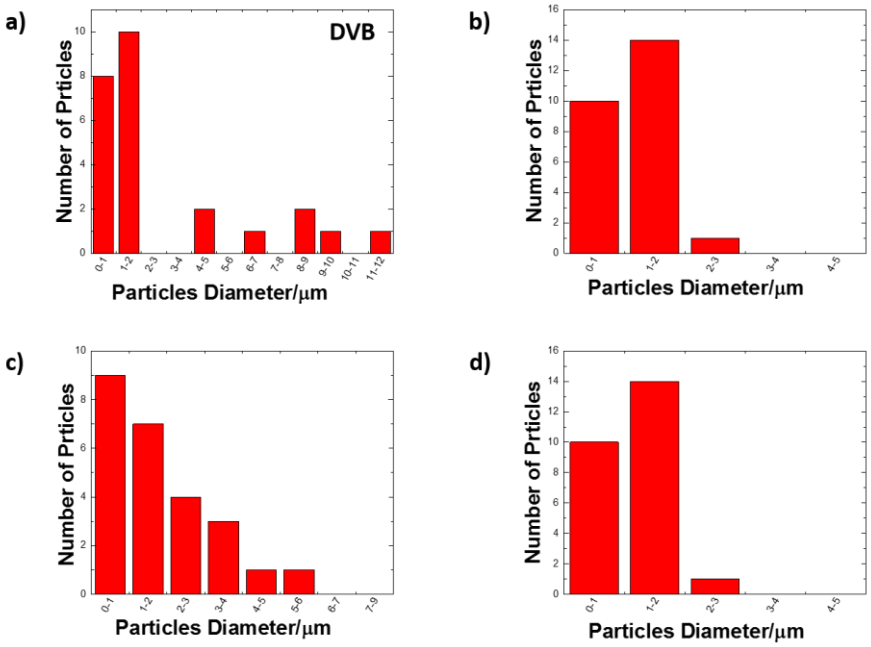

Figure 5. 18. Size distributions of thermal initiated poly tetrathiol-allyl microstructure particles at 8000 rpm (a) and (b) equal ratio of tetrathiol and HA with (a) adding DVB and (b) without DVB; (c) tetrathiol-HA (1.5:1) molar ratio; (d) tetrathiol-HA (2:1) molar ratio.

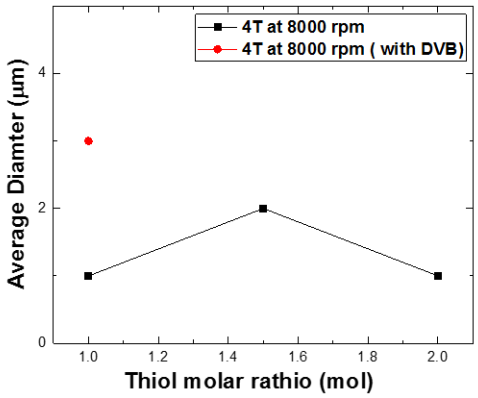

Figure 5. 19. Average particles diameter size versus thiol monomer ratio of thermal initiated poly thiol-allyl microstructure particles.

5.3.6 After post-polymerisation functionalisation

To explore the change in the microspheres' morphology obtained via suspension polymerisation, cross-sectional SEM images show the surface morphology of poly tetrathiol-allyl microsphere particles before and after post-polymerisation functionalisation (see Figures 5.20 and 5.21). SEM showed no sign of significant change in the morphology after post-polymerisation functionalisation via Michael addition reaction using acrylate monomers (HEA, MA, EGMEA and DEAEA). It is clearly seen that all samples retain spherical shape with smooth and homogeneous surfaces. The present findings seem to be consistent with other research, which found that post-polymerisation functionalisation via Michael addition has no influence on the morphology of polymeric materials of polyHIPEs.[51]

The single most striking observation to emerge from the SEM image comparison was the absence of adhesion between neighbouring functionalised particles at higher thiol monomer ratios, which is different from their corresponding particles before post-polymerisation functionalisation.

The results of particle size distribution obtained from tetratiol-allyl microsphere particles indicate that homogeneity of morphology (in terms of particles size distribution) after post-polymerisation functionalisation is relatively high, particularly in particles prepared at 20500 rpm; particle distribution size graphs at 8000 rpm and 20500 rpm are summarised in Figures 5.22 and 5.23, respectively.

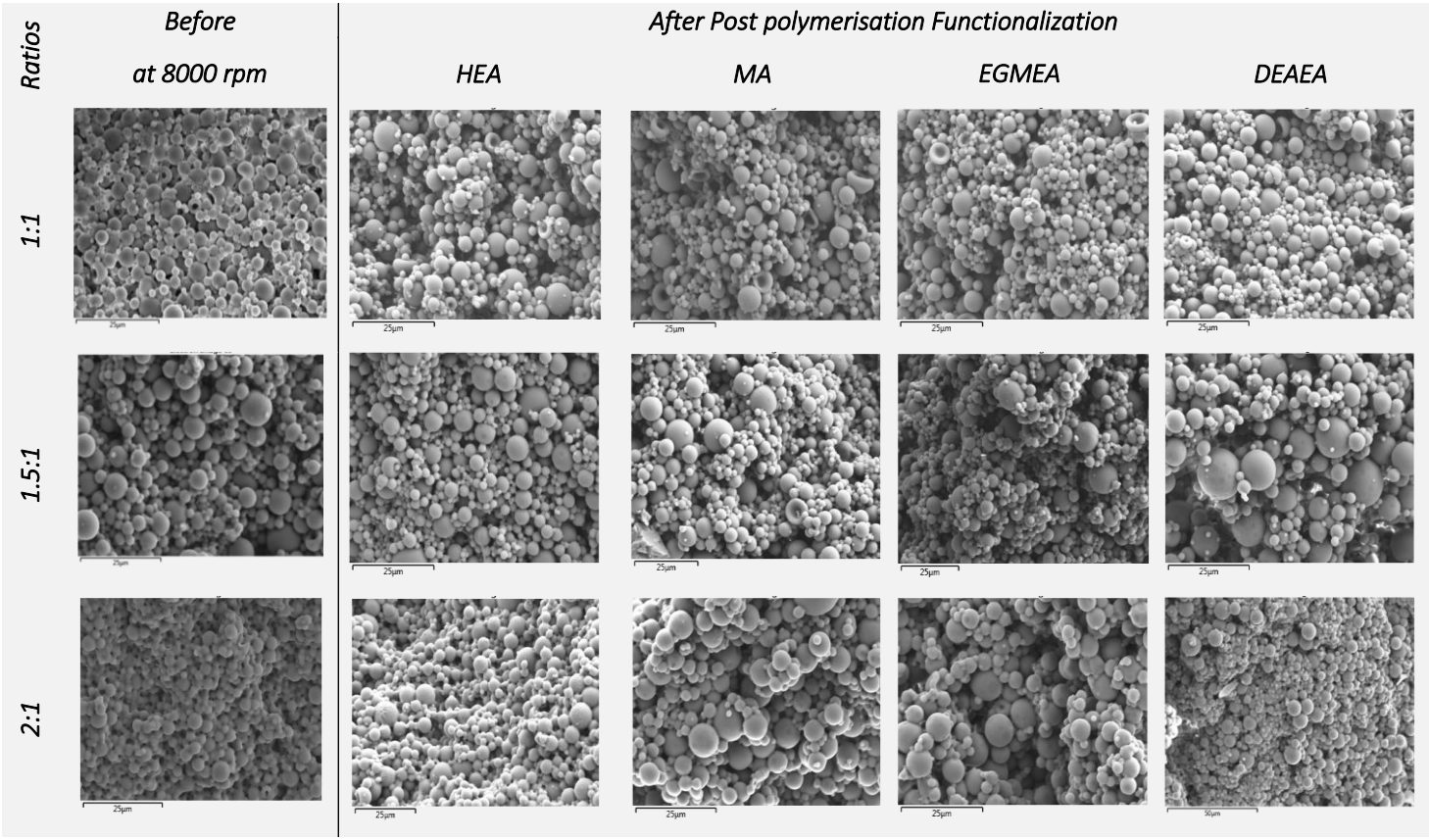

Figure 5. 20. SEM micrographs showing the morphology of poly tetra thiol-allyl particles at 8000 rpm, before (left) and after (from second to fifth column) post-polymerisation functionalisation with different types of acrylate monomer (HEA, MA, EGMEA and DEAEA). All the scale bars are 25µm.

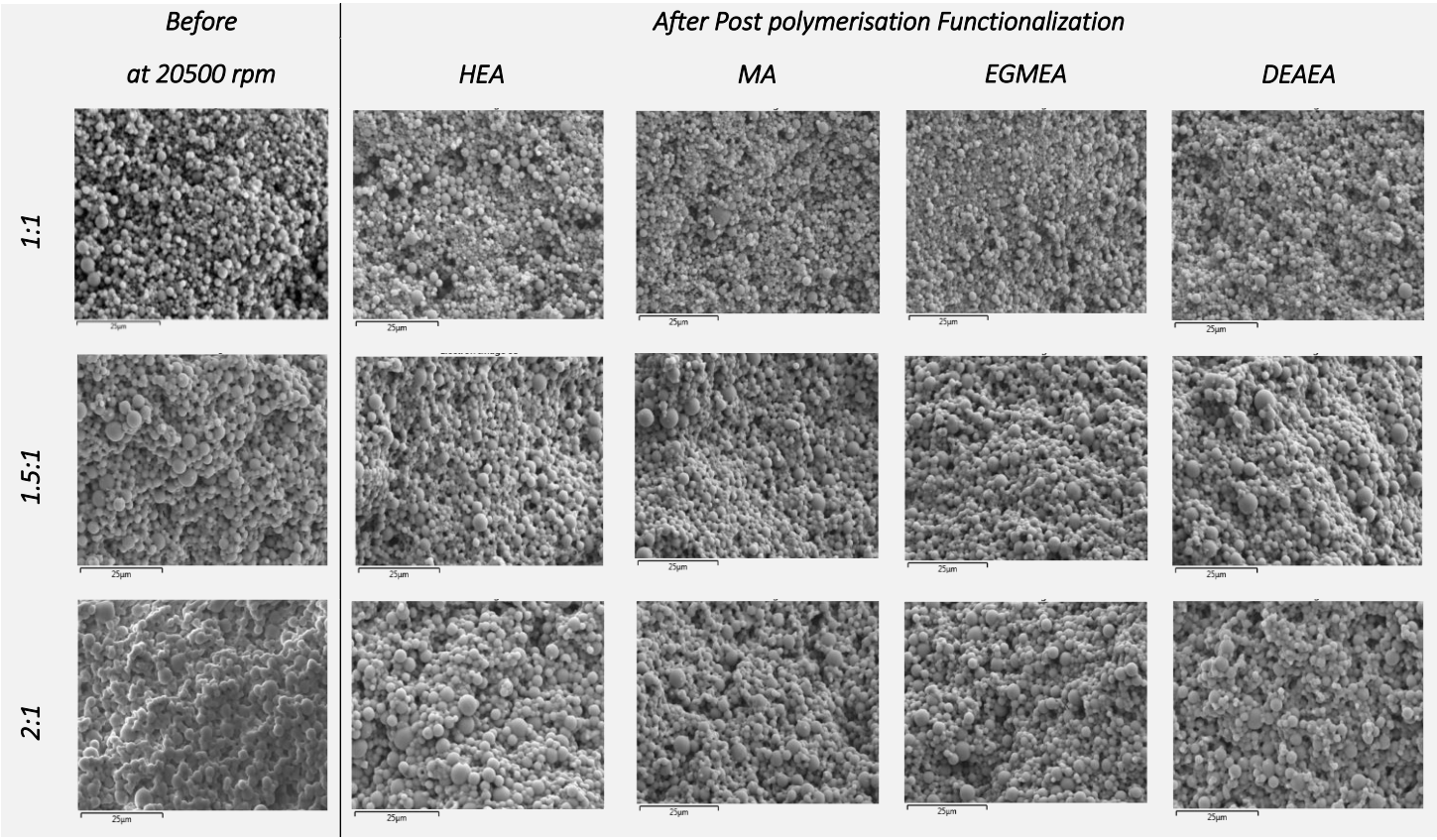

Figure 5. 21. SEM micrographs showing the morphology of poly tetra thiol-allyl particles at 20500 rpm, before (left) and after (from second to fifth column) post-polymerisation functionalisation with different types of acrylate monomer (HEA, MA, EGMEA and DEAEA). All the scale bars are 25µm.

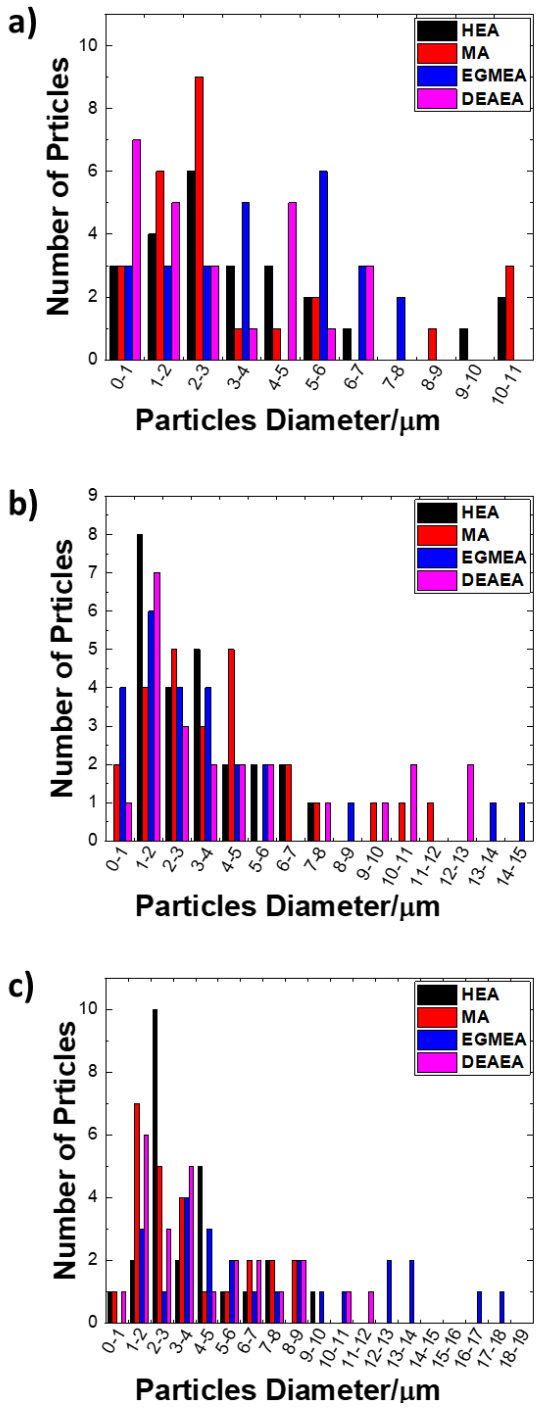

Figure 5. 22. Particle diameter of photo initiated poly tetra thiol-allyl microsphere particles at 8000 rpm obtained by image analysis of SEM after functionalisation via thiol Michael addition reaction: (a) equal ratio of tetrathiol and HA, (b) tetra thiol-HA (1.5:1) and (c) tetrathiol-HA (2:1).

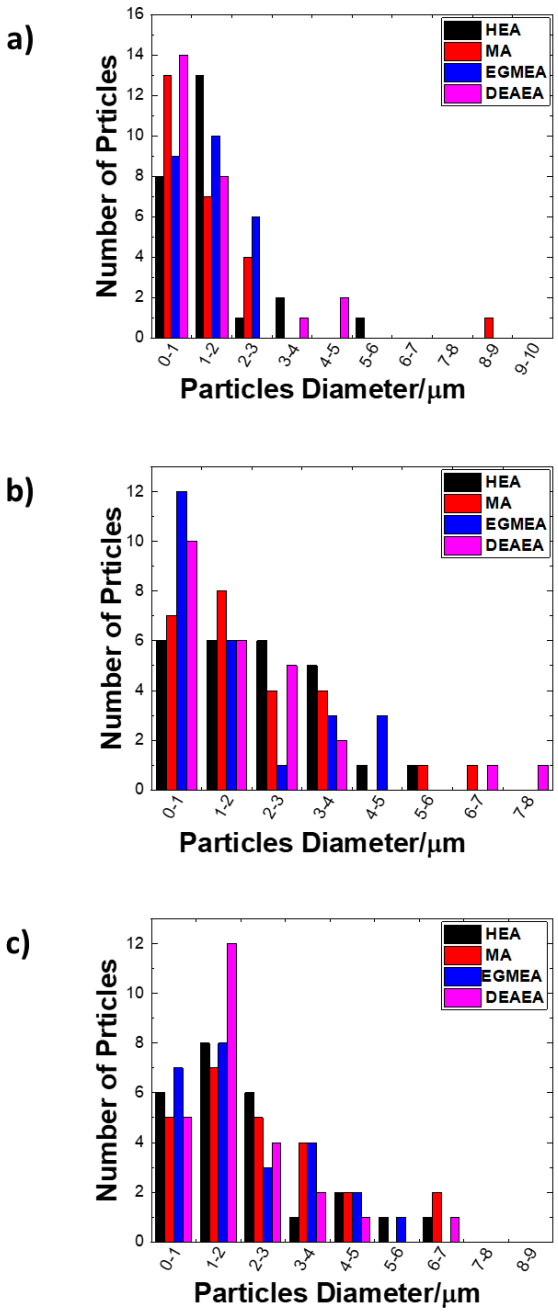

Figure 5. 23. Particle diameter of photo initiated poly tetra thiol-allyl microsphere particles at 20500 rpm obtained by image analysis of SEM after functionalisation via thiol Michael addition reaction: (a) equal ratio of tetrathiol and HA, (b) tetrathiol-HA (1.5:1) and (c) tetrathiol-HA (2:1).

Average particle diameter sizes of poly thiol-allyl microsphere particles before and after post-polymerisation functionalisation via thiol Michael addition using different types of acrylate monomer chemical structures (HEA, MA, EGMEA and DEAEA) are summarised Table 5.2. To compare directly between the average particle diameter sizes of poly thiol-allyl microsphere particles before and after post-polymerisation functionalisation, Figure 5.24 plots the dependence of average particle diameter size on the chemical structure of acrylate monomers, and presents the functionalised microsphere polymer particles consisting of tetra thiol monomer ranges of 1, 1.5 and 2 molar ratios to HA at two homogeniser speeds of 8000 rpm (Figure 5.24a) and 20500 rpm (Figure 5.24b). From Table 5.2 and Figure 5.24a, we observe that all of the functionalised poly tetrathiol-HA microsphere particles at 8000 rpm were larger or similar to their corresponding particles before post-polymerisation functionalisation, except for the following functionalised polymer particle materials, which were larger or similar to their corresponding functionalised particles. However, at higher homogeniser speed (20500 rpm), all functionalised polymer particle materials were smaller than the thiol-allyl particles before post-polymerisation functionalisation for all molar ratios of thiol monomer (see Table 5.2 and Figure 5.24b).

Average particle diameter size for given functionalised particles using HEA, MA and EGMEA either did not change or increased to 4 µm, whereas using DEAEA lead to significant increases from 3 µm to 6 µm in the average particle diameter size when increasing the thiol monomer ratio from 1 mol to 1.5 mol at 8000 rpm. After increasing the thiol monomer ratio to 2 mol, the average diameter size of particle functionalised changes was as follows: using EGMEA lead to an increase to 7 µm, whereas average particle diameter size of particles functionalised with HEA and MA did not change

and slumped to 4 μm when functionalised using DEAEA. At 20500 rpm, all average particle diameters of the resulting particles obtained from post-polymerisation functionalisation using HEA, MA EGMEA and DEAEA increased one micron when the molar ratio of thiol monomer to HA increased from 1 mol to 1.5 mol. When the thiol monomer ratio increased to 2 mol, the average particle diameter of all functionalised particles did not change: the average diameter size was still 2 μm.

Table 5. 2. Average Diameter of the Poly Tetra Thiol-Allyl Microstructure Particles after Post-Polymerisation Functionalisation Measured Using SEM

Ratios [thiol]:[HA]	***homogenizer speed***	***Average Particle Diameter (µm) Before***	***Reactant (1.5 eq)***	***Average Particle Diameter (µm) After***
1:1	8000	3 µm	HEA	4 µm
			MA	3 µm
			EGMEA	4 µm
			DEAEA	3 µm
1:1	20500	2 µm	HEA	1 µm
			MA	1 µm
			EGMEA	1 µm
			DEAEA	1 µm
1.5:1	8000	4 µm	HEA	4 µm
			MA	4 µm
			EGMEA	4 µm
			DEAEA	6 µm
1.5:1	20500	3 µm	HEA	2 µm
			MA	2 µm
			EGMEA	2 µm
			DEAEA	2 µm
2:1	8000	3 µm	HEA	4 µm
			MA	4 µm
			EGMEA	7 µm
			DEAEA	4 µm
2:1	20500	3 µm	HEA	2 µm
			MA	2 µm
			EGMEA	2 µm
			DEAEA	2 µm

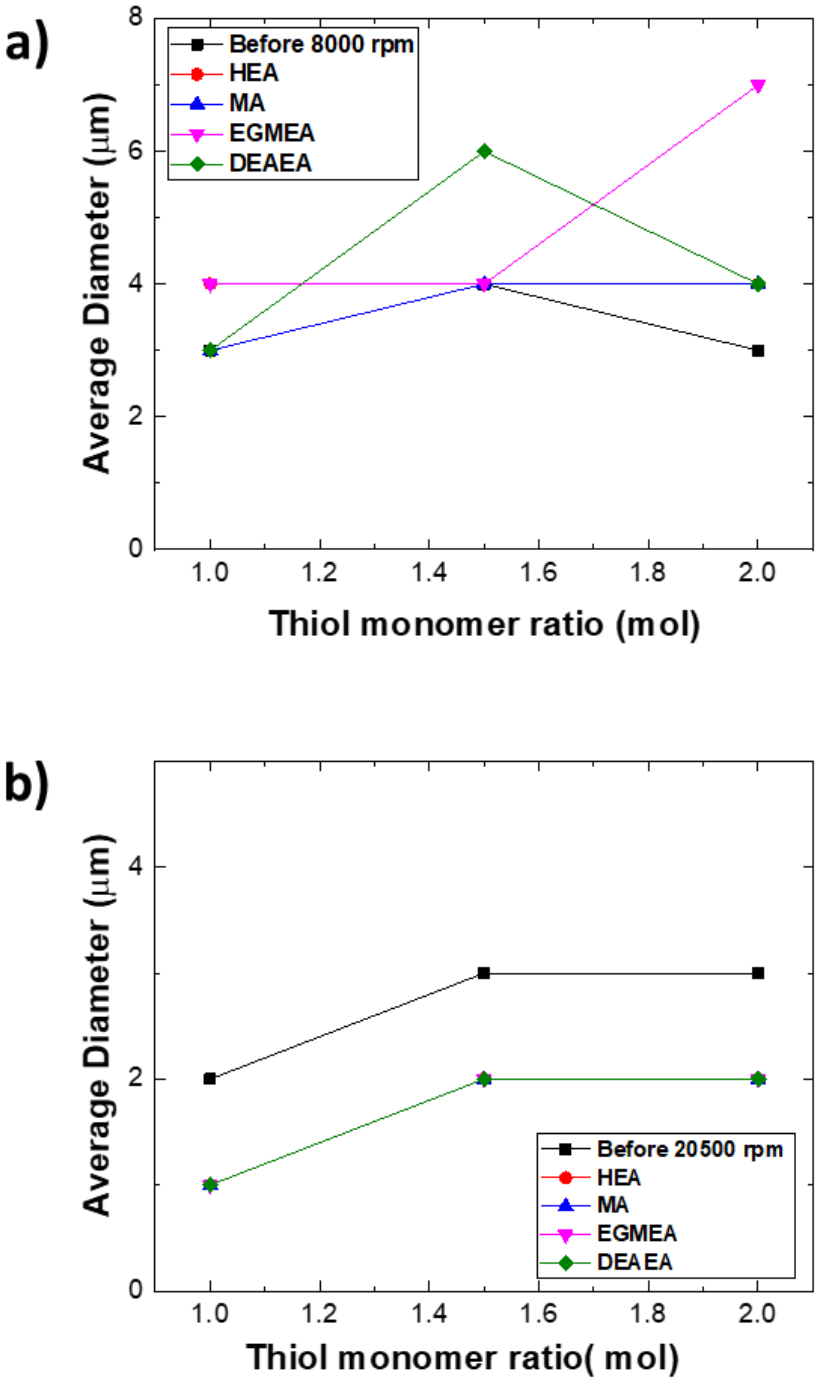

Figure 5. 24. Changes in the average particle diameter size with respect to the thiol monomer ratio before and after post-polymerisation functionalisation at homogeniser speed of (a) 8000 rpm and (b) 20500 rpm.

Table 5. 3. The Order of the Average Particle Diameter of Acrylate Monomer Correlated with Homogeniser Speed and Thiol Monomer Molar Ratio.

Thiol monomer ratio	**8000 rpm**	**20500 rpm**
1	HEA and EGMEA >MA and DEAEA	No change in the average diameter
1.5	HEA, MA and EGMEA < DEAEA	No change in the average diameter
2:1	EGMEA > HEA MA and DEAEA	No change in the average diameter

It is accepted that the average particle diameter size obtained from post-polymerisation functionalisation of acrylate monomer follows the sequence given in Table 5.3. To further evaluate the correlation between chemical structure of acrylate monomer homogeniser speed and thiol monomer ratio after post-polymerisation functionalisation, Figure 5.25 shows the influence of increasing the homogenisation speed on average particle diameter for each type of acrylate, HEA (Figure 5.25a), MA (Figure 5.25b), EGMEA (Figure 5.25c) and DEAE (Figure 5.25d), separately at several thiol monomer molar ratios. . Generally, there was substantial homogeniser speed-dependence of all functionalised poly thiol-allyl microsphere particles. The most observed change was the decline in the average particle diameter size of all functionalised particles after increasing the homogeniser speed from 8000 rpm to 20500 rpm.

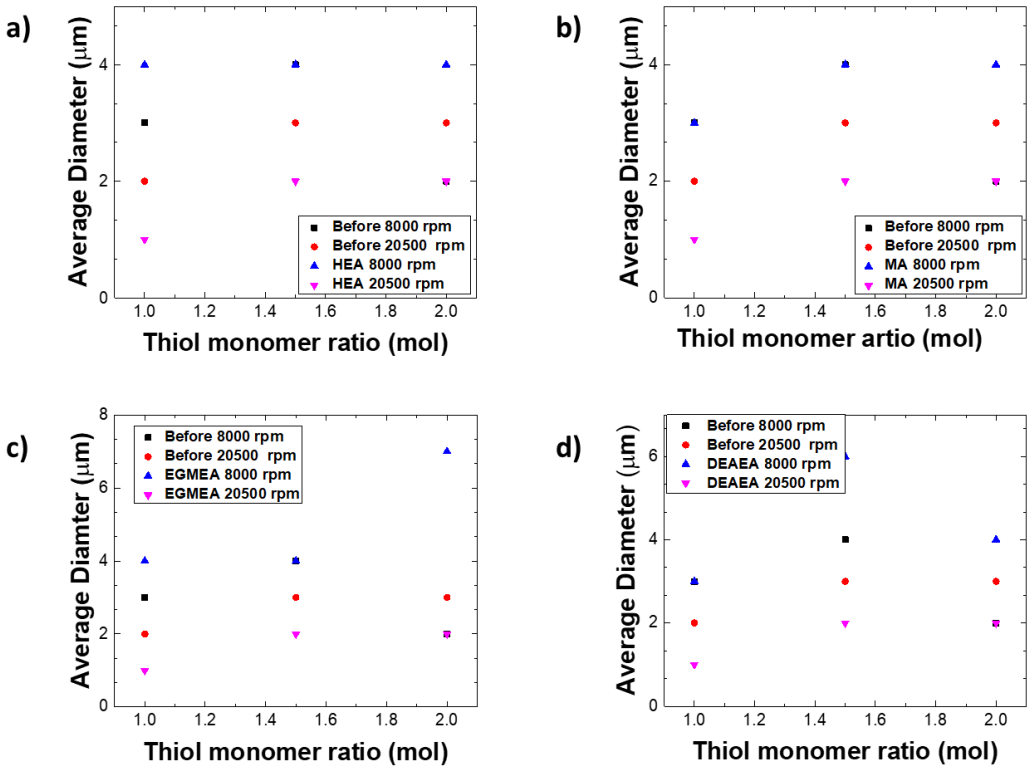

Figure 5. 25. Average particle diameter versus thiol monomer ratio of photo initiated poly tetra thiol-allyl microstructure particles before and after post-polymerisation functionalisation depending on acrylate monomer structure.

From Table 5.4 and Figure 5.26 it was found that solvent type and volume does not have significant effects on the morphological features of particle size and size distribution of poly tetrathiol-ally (1.5:1) at 8000 rpm and 1 hour under UV irradiator microsphere particles after post-polymerisation functionalisation using EGMEA with different types and volumes of solvent during functionalisation process. However, average particle diameter size was the same when the type and volume of the solvent changed.

Table 5. 4. Average Particle Diameter Size of the Poly Tetra Thiol-Allyl Microsphere Particles after Post-Polymerisation Functionalisation Using EGMEA with Different Solvent Type and Volume Measured Using SEM Images.

Ratios [tetra-thiol]:[HA]	***homogenizer speed for 1 hour***	***Average Particle Diameter (µm)***	***Reactant (1.5 eq)***	***Solvent***	***Solvent volume***	***Average Particle Diameter (µm)***
1.5:1	8000	5 µm	EGMEA	DMSO		4 µm
				Ethanol		4 µm
				DMF	5mL	4 µm
					1 mL	4 µm

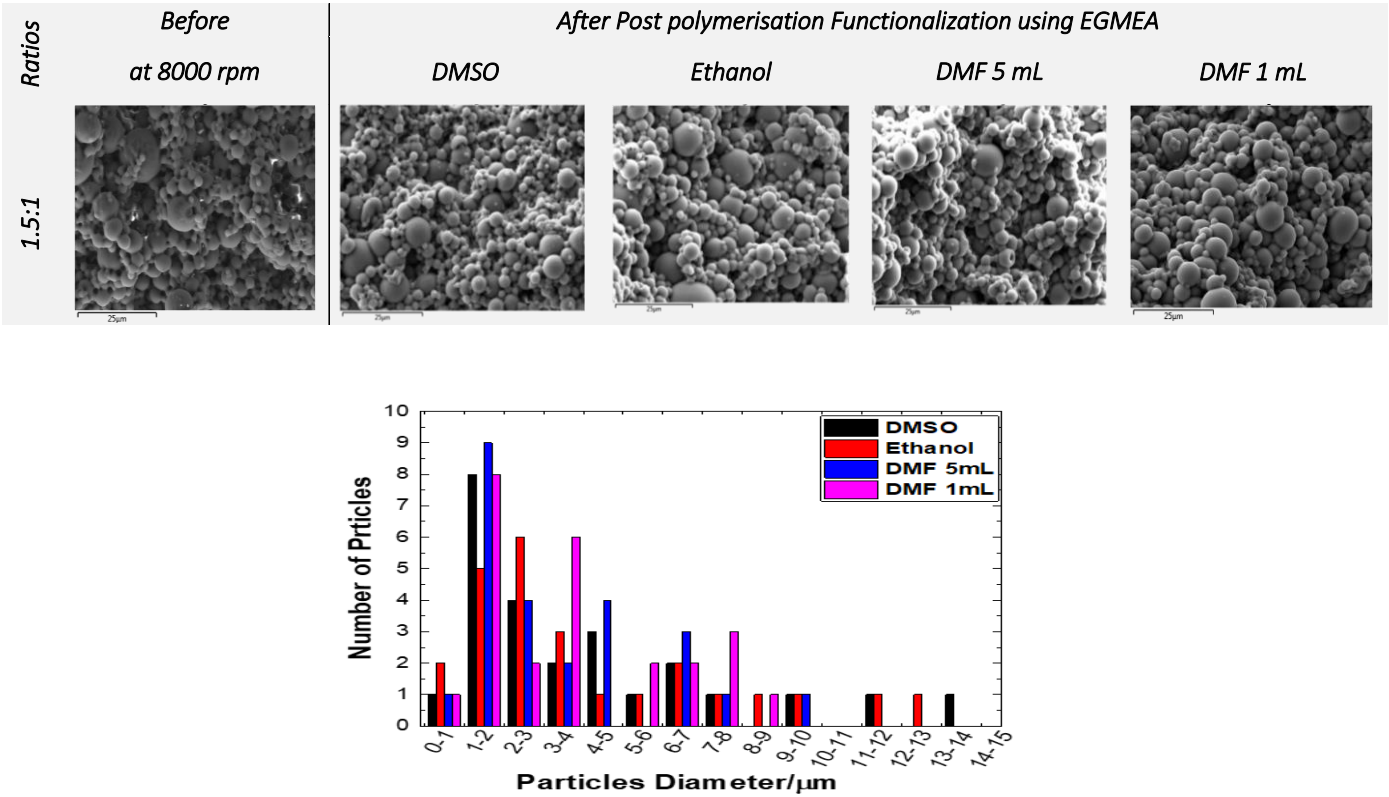

Figure 5. 26. The top is SEM images of photo initiated poly tetrathiol-allyl microstructure particles after post-polymerisation functionalisation using EGMEA with different types and volume of solvents. The bottom is their corresponding particles distributions. All the scale bars are 25µm.

5.3.7 Comparison of glass transition temperature and morphology – a study of the poly thiol-allyl microparticles by DSC and SEM

The model of this chapter was to study the morphology of polymeric colloid microstructure particles obtained from thiol-allyl suspension polymerisation. In this section, we outline the correlation between T_g value (chapter 4) and particle size (this chapter), which have been discussed previously in detail. The resulting average particle diameter size and T_g value obtained for the same system are summarised in Figure 5.27. Starting with an observation on increasing the molar ratio of thiol monomer to HA, there is a general increase in the average particle diameter size and a reduction in T_g. As the molar ratio of thiol monomer to HA increases from 1 mol to 1.5 mol, the average particle diameter size shifts to a larger size. This is in contrast to the evaluation of the average particle diameter size determined by SEM: above 1 mol, there is a clear decrease in the T_g value (see Figure 5.27b). The efficiency of the influence of thiol monomer ratio in the composition majority was les at double the ratio of thiol monomer to HA, as both T_g value and average particles diameter size changed slightly.

We note that low T_g values were observed within rough surface morphology such as poly trithiol-allyl microstructure particles with ratios of 1.5:1 of tetrathiol:HA. The T_g were -5.49 ˚C and -2.74 ˚C at 8000 rpm and 20500 rpm, respectively. Furthermore, network based at molar ratio 2:1 of trithiol:HA exhibited T_g of -2.18 ˚C and -3.94 ˚C after increasing the speed from 8000 rpm to 20500 rpm. Dithiol composites consisting of equal ratios of TEGDT/HDT with HA exhibited extremely rough surface after increasing the homogeniser speed from 8000 rpm to 20500 rpm. Their T_g values were also very low: both TEGDT and HDT increased from -18.23 ˚C and -17.49 ˚C to -

16.18 ˚C and -14.40 ˚C as previously described in chapter 4. The lowest T_g values (-18.23°C) within the largest average particle diameter size (15 μm) were observed at TEGDT (8000 rpm). Particle diameter distribution results of TEGDT-HA (1:1) Thermal initiated follow the same trend of observed opposite behaviour between particle size and the T_g (as shown in Figure 5.28). We conclude that average particle diameter size and T_g value can be predicted based on the measurement of one of them (size and T_g) or on the type of condition parameters that have been applied.

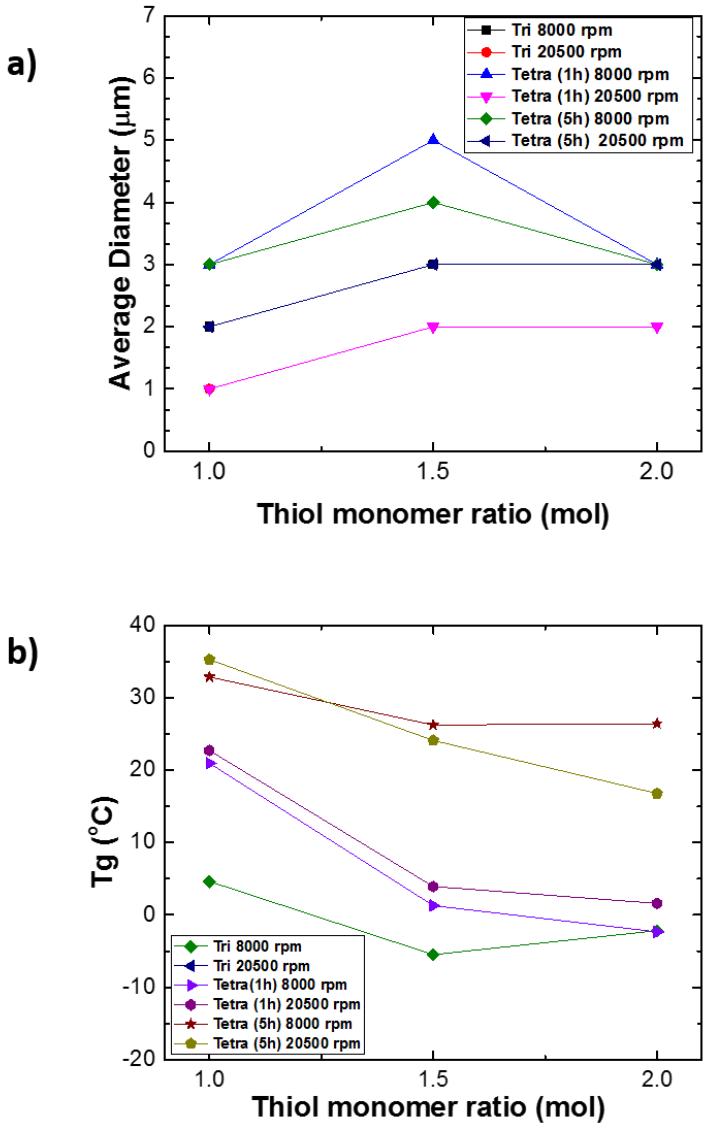

Figure 5. 27. Changes in the average particle diameter size (a) and T_g (b) with respect to the thiol monomer ratio for photo initiated poly thiol microstructure particles.

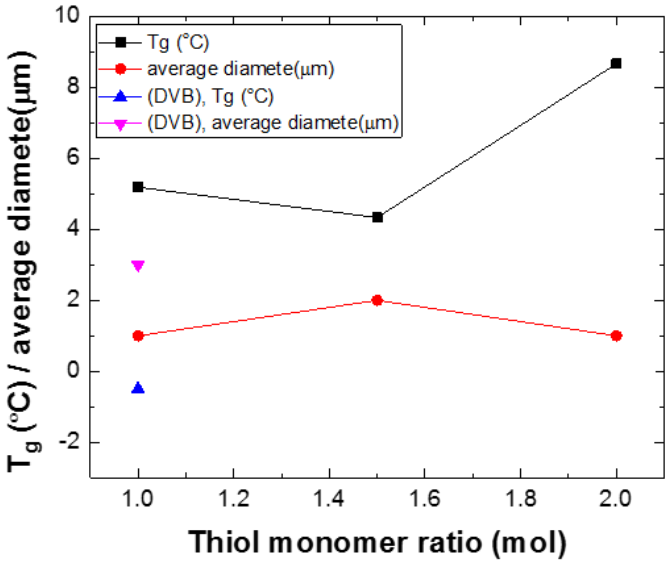

Figure 5. 28. Changes in the average particle diameter size and T_g with respect to the thiol monomer ratio for thermal initiated poly thiol microstructure particles.

As expected, both homogeniser speed and photo polymerisation time oppositely affected the average particle diameter and T_g. While photo polymerisation time has a strong influence on the T_g, it shows weak effect on the average particle diameter size (See Figure 5.29a and b). Contrary to the above observation, as we can see from Figure 5.29a and b, there is a similar level of influence of homogeniser speed on both average particle diameter and T_g; it changes after increasing the homogeniser speed from 8000 rpm to 20500 rpm. However, one exception has been identified: when T_g value of particles tetra thiol-allay (2:1) were under UV for 5 hours, they reduced dramatically and there was no change in the average particle diameter size after increasing the homogeniser speed from 8000 rpm to 20500 rpm (see Figure 5.29c and d).

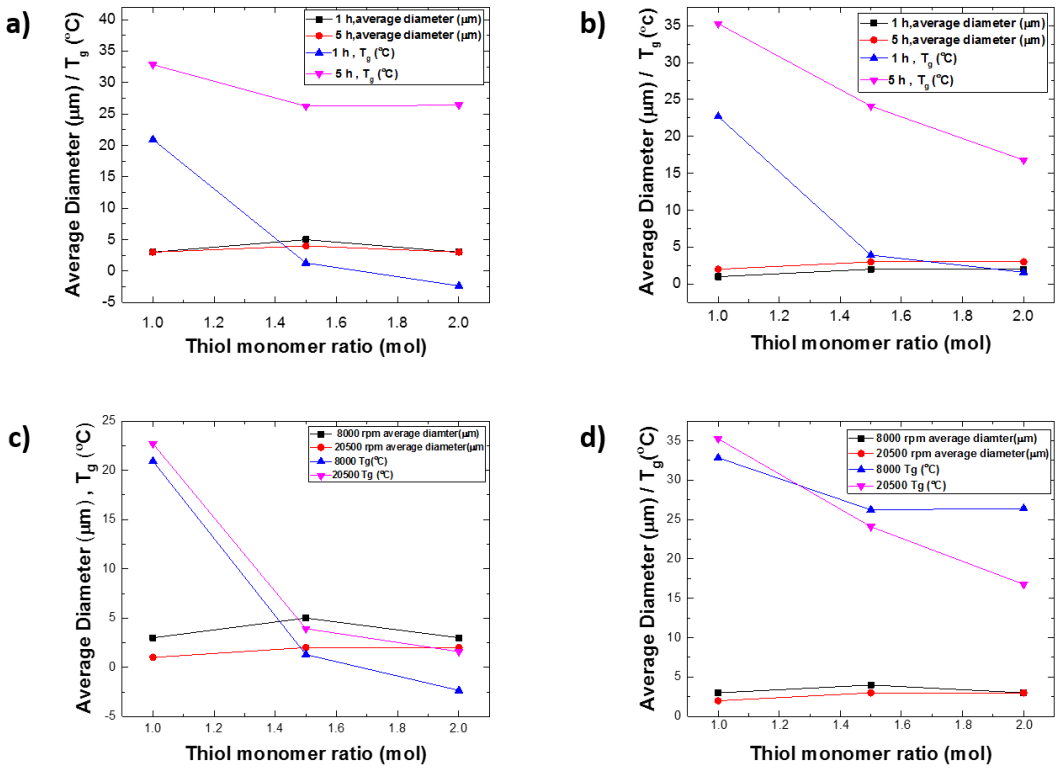

Figure 5. 29. Changes in the average particles diameter size and T_g with respect to the thiol monomer ratio for thermal initiated poly thiol microstructure particles. The top is influence of photo polymerisation time on the T_g and average diameter (a) at 8000 rpm and (b) at 20500 rpm. The bottom shows the influence of homogenizer speed on the T_g and and average diameter (c) 1hour duration time (b) 5 hours duration.

5.4 Conclusions

In summary, this chapter has dealt in detail with the changes in the morphology of thiol-allyl microstructure particles before and after post-polymerisation functionalisation using SEM. We have demonstrated that by carefully controlling the

following factors: thiol monomer ratio, homogeniser speed, cross-linking density, photo-polymerisation time, thermal curing method, acrylate monomer structure and solvent type and volume during functionalisation processes, it is possible to fine-tune the particle shape and size of poly thiol-allyl microstructure colloid particles before and after post-polymerisation functionalisation.

From this performed study, it is evident that all average particle diameters increase on increasing the **molar ratio of thiol monomer**. However, there were no significant changes in the average particle diameter size after increasing the molar ratio of thiol monomer to HA from 1.5:1 to 2:1. Furthermore, increasing the thiol monomer ratio generated particles with different surface morphologies. For example, poly trithiol-allyl particles' shape changed from spherical to complete coalescence for the particles after increasing the ratio of tri-thiol monomer to HA from equal to double. In the case of tetra-thiol, adhesion between neighbouring particles of tetrathiol-HA at both ratios of 1.5 mole and 2 mole were observed after increasing the molar ratio of tetra thiol monomer to HA.

Apart from poly thiol-allyl microsphere particles consisting of 2:1 of tetrathiol:HA under UV for 5 hours, increasing the **homogeniser speed** from 8000 rpm to 20500 rpm exhibited a decrease in the average particle diameter size. As well as, leading to adhesion between neighbouring particles of tetrathiol-HA at ratios of both 1.5 and 2 mole and extremely rough surface morphology and complete coalescence for particles of equal ratio of dithiol with HA and particles of network based on higher molar ratios (1.5 and 2) of tri thiol monomer. In addition, the change in the **cross-link density** revealed that particles with the highest number of thiol functionality retained spherical

shape for all tetrathiol-hexa-allyl molar ratio, varied from 1:1 to 2:1, at both speeds of 8000 rpm and 20500 rpm. However, particles of less cross-linking density were able to remain spherical during particles synthesis using system of dithiol-HA (1:1) at 8000 rpm; trithiol-HA (1:1) at 8000 rpm; trithiol- HA (1:1) at 20500 rpm; and trithiol-HA (1.5:1) at 8000 rpm. Particle size is likely to decrease when the number of the thiol functional group increases from 2 to 3 at 8000 rpm; however, particle size is likely to increase when the number of thiol functional group increases from 3 to 4 at 8000 rpm; it did not change at 20500 rpm. Although a great influence of the above mentioned factors on the particles' shape and size has already been observed, **photo-polymerisation time** demonstrated weak effect on the particles' shape and size**. Thermal initiated** microstructure polymer particles show the same behaviour of photo-initiated tetra thiol-allyl particles at 8000 rpm.

Some of the most important aspects of the particles' shape **after post-polymerisation functionalisation using several acrylate monomer structures (HEA, MA, EGMEA and DEAEA**) is the absence of adhesion between neighbouring functionalised particles at higher thiol monomer ratios, which is different from their corresponding particles before post-polymerisation functionalisation. Indeed, all samples retained spherical shape with smooth and homogeneous surfaces. Generally, most functionalised particles' sizes were similar or smaller than the micro spherical particles before post-polymerisation functionalisation; the exception was the functionalised microsphere particles at 8000 rpm of tetrathiol-HA (1.5:1) using DEAEA, and tetrathiol-HA (2:1) using EGMEA, which are larger than their corresponding particles before post-polymerisation functionalisation. There was no

significant change in the particles' morphology when using different types and **volume of solvent** during functionalisation process.

Opposite behaviour was observed from the comparison between the performance of average particle diameter size and T_g (from chapter 4). Research in this area is still in its infancy, and with questions remaining, it is anticipated that it is wide open to future research.

6 Preparation of Porous Polymeric Scaffolds via Emulsion Templating

6.1 Introduction

Poly high internal phase emulsions (PolyHIPEs) is an approach that has been applied to produce porous polymers.[140] The maximum volume fraction of the internal phase (the dispersed phase) for uniform spherical droplets is 74%. Above this point, the droplets distort to form polyhedra, where a thin film of the continuous phase (external phase) surrounds the dispersed phase.[140] This unique structure is called high internal phase emulsions (HIPEs).[140-143] The key to stabilising HIPEs is to select an appropriate surfactant, usually a non-ionic surfactant.[141] Polymerising the continuous phase, which contains monomer such as styrene and cross-linkers will form the porous polymer, after removal of the internal phase. Free radical polymerisation is the most common method used for synthesis of polyHIPEs, in addition to ATRP, thiol-ene/yne click chemistry, ROMP and Polycondensation.[141, 144]

Over the past two decades, rapid progress in the tissue engineering field, and a growing demand for regenerative medicine, have made researchers hopeful of complete successful in the near future.[145] Regardless of the fact that diminishing improvements have been made in the field of biomaterials, even new and multifunctional biomaterials have been investigated. However, there are still some drawbacks associated with biomaterials, scaffold fabricating techniques and cells which are challenging the success of tissue engineering[145]

At present, scaffold-based tissue engineering design is growing to involve cells, bioactive molecules and structural matrices. Each of these components is combined into a structure that supports the repair and regeneration of damaged or diseased tissue.

It is not yet possible to determine a so-called ‘ideal scaffold’, as scaffold-based tissue-engineering approaches are still experimental.[146]

Furthermore, the main purpose is to regenerate diseased or damaged tissues and introduce appropriate methods to control key features of cell behaviour such as adhesion, migration, proliferation and differentiation. In the last few years, with regard to biophysical issues for example, certain forces have been demonstrated to be potent enough to influence the biological response of cells in culture, even during the absence of biochemical factors. Therefore, growing attention is being paid to the development of biomaterials that mimic mechanical aspects of cell interaction with its native environment, such as the structural role of the extracellular matrix (ECM) in modulating cell behaviour.[147]

In recent times, the use of thiol-ene and thiol-yne reactions has been successfully reported for the preparation of polyHIPEs polymers.[32, 47, 51, 60, 135, 148-151]
Thiol-ene polymerisation offers opportunities for synthesising degradable polyHIPEs, as both thiols and alkenes with ester functionalities in the chain exist. Biodegradability is more difficult to achieve with other step growth mechanisms due to the higher temperature required for polymerisation and for generating side products. Thiol-ene polymerisation, in combination with high internal phase emulsion templating, provides perspective possibility for a wide range of functional macromolecular materials .[149, 152] This method of polymer formation has well-defined morphologies, and their mechanical properties are dependent on the porosity and the type of network formed by either thiol-ene or thiol-yne reactions.[150] Cameron et al. demonstrated that the thiol-ene/yne photo polymerisation yield well-defined poly-HIPE materials with

mechanical properties dependent on the extent of crosslinking, by employed commercially-available multifunctional thiols with either multifunctional acrylates or alkynes.[47]

PolyHIPEs are often known for their unique open cell structure, with two kinds of porous characteristics: droplet-templated porous, called voids, and interconnecting porous, called windows (see Figure 6.1).[140-142] The creation of interconnecting voids is not yet completely understood. Some researchers refer to the volume contraction that occurs on the conversion of a monomer to a polymer. Others assign it to mechanical splits in the thin polymer films between adjacent droplets during the post-polymerisation processes of Soxhlet extraction and vacuum drying. Because of their unique porous structure, particularly the cell open porosity, PolyHIPEs are used in a range of potential applications such as scaffolds for tissue engineering, separation, support for synthesis, sensors and catalysts.[141]

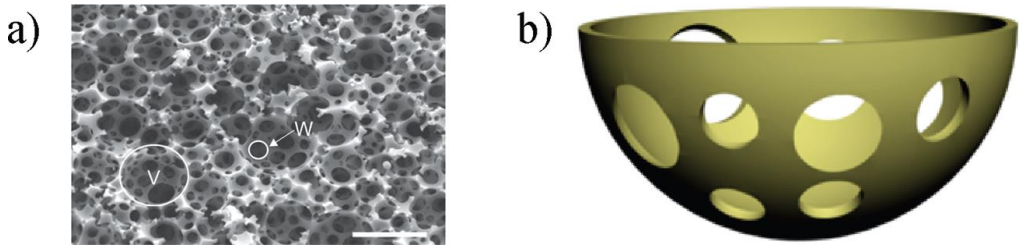

Figure 6. 1. SEM image of a typical polyHIPE material. 3V and W indicate void and window, respectively; (b) a cross-section model of an open cell structure unit in a typical polyHIPE.

In fact, there are several methods by which the average void and interconnect diameter of PolyHIPE materials can be tailored to produce PolyHIPE materials with wide range of void and interconnect sizes. [153] For example, the addition of electrolytes to the water

phase prior to HIPE preparation has been known to affect emulsion stability, and therefore the final structure of the resulting porous product. Also, Cameron et al. reported that increasing the aqueous phase temperature prior to emulsification, and the presence of additives and co-solvents in the aqueous phase, can lead to materials with larger void and interconnect sizes.[153]

Mert and Krajnc investigated the effect of the presence of comonomer in the polymer matrix on the morphological features, mechanical strength and thermal stability of polyHIPEs. They found that by incorporating norbornene into the polymer matrix poly (dicylopentadiene), the polyHIPEs exhibited enhanced the thermal properties without compromising the morphological features of the resulting poly (dicylopentadine-co-norbornene). In addition, the addition of 50 mol% of norbornene into the polymer matrix increases the compression modulus and the compressive strength.[123]

In general, the formation of the emulsions is a very complex process. Oil phase, aqueous phase, emulsifier and energy are required for this process. As yet, most researchers have focused on the effects of surfactant concentration, interactions between particles and aqueous/oil phase ratios on the physicochemical properties of the resulting emulsions, including the emulsion types, stability, droplet size and its distribution, and so on. Certainly, the emulsification techniques also affect the microstructure and, consequently, the properties of the resulting emulsions. Several processes occur during emulsification; for example, droplet breakup, adsorption of colloidal particles and droplets collision, which highly depend on the emulsification techniques. Emulsions with different microstructure and properties will be formed since these processes are changed relative to each other. Unfortunately, knowledge about the influence of the emulsification method is far from fully understood up to now. Understanding this correlation will have important implications for explaining

the mechanism of emulsion formation and the technological utility of these formed emulsions.[154]

The range of emulsification equipment is very wide: mechanical stirring systems, colloidal mills, high-pressure homogenizers, porous membranes, ultrasound homogenizers. The type of mixing system employed strongly affects the droplet size of the dispersed phase, particularly in the case of polyHIPEs.[155] However, only a limited number of studies has so far been devoted to the study of the effect of emulsification conditions on the morphology of polyHIPEs materials.[155 155] Lépine et al. investigated the influence of motor speed and emulsification time on the porous structure characteristics of polyHIPEs. They proved that the use of a laboratory scale homogenizer for the preparation HIPEs allows easy control of the morphology of the resulting polyHIPE materials,[155] and within this study we have emphasized this. We report the effect of homogenisation equipment on the morphology of polyHIPE using three methods: stirring with an overhead stirrer (300 rpm), using a vortex mixer (30 Hertz), and using a homogenizer (up to 8000 rpm), were all used to prepare the emulsion. A porous polymeric foam with an interconnected pore structure was produced by polymerisation of the continuous phase of the HIPEs. It was characterised using an SEM (scanning electron microscopy)

6.3 Results and Discussion

6.3.1 Preparation of thiol-acrylate polyHIPEs

The preparation of thiol-ene polyHIPEs from trimethylolpropane tris(3-mercaptopropionate) (trithiol) and DPEHA has been described previously.[47] The mechanism of the thiol-ene click reaction between the comonomers is shown in Figure 6.2 This describes the homopolymerisation of the acrylate monomer.

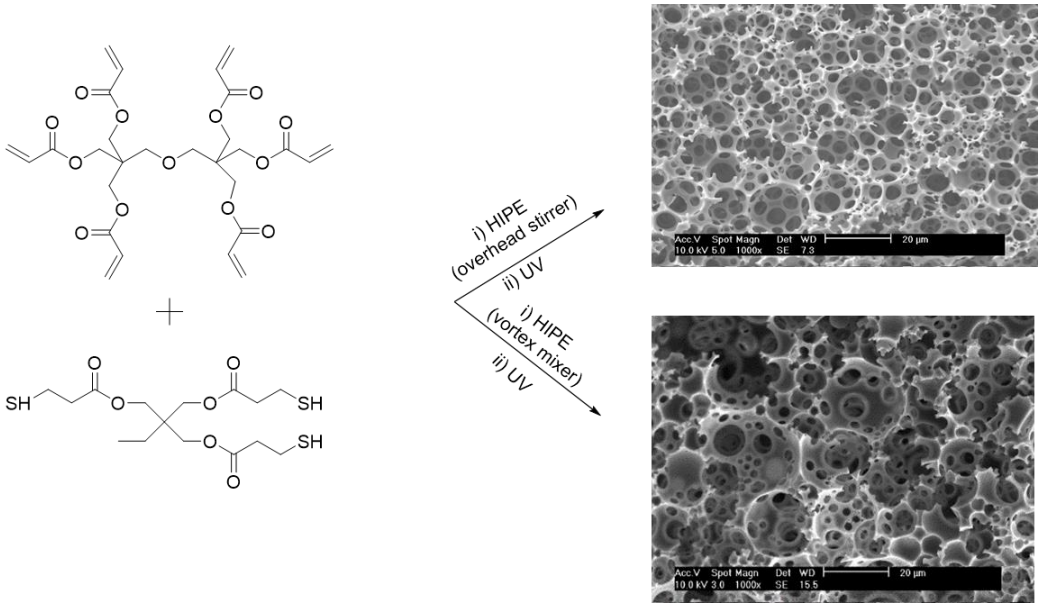

Figure 6. 2. Synthesis of thiol-acrylate polyHIPEs from trithiol DPEHA by overhead stirrer and vortex mixer. Scale bar = 20µm.

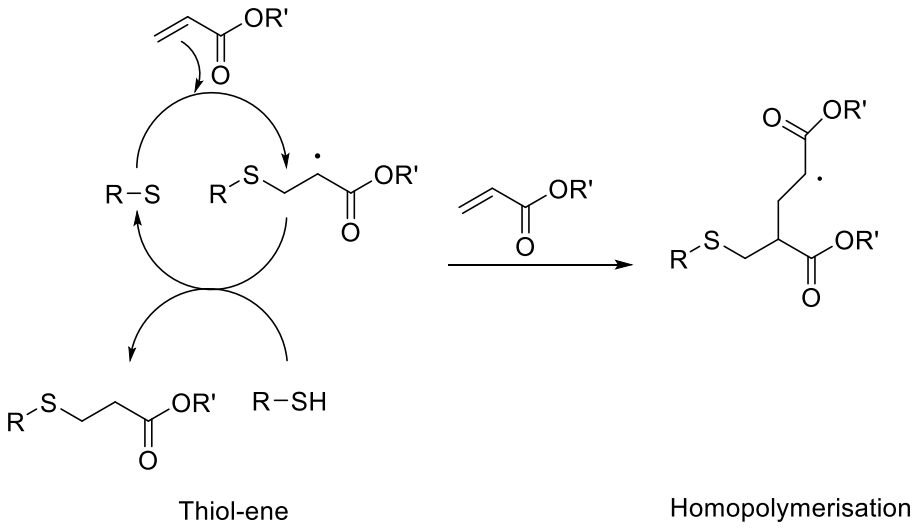

Scheme 6. 1. Two reactions accruing during network formation thiols (left) and acrylate (right).

The mechanism (Scheme6.1) describes the step growth reaction, which is usually a major rate reaction in the form of a thiol-ene reaction. This is a representative reaction rather than an ene homopolymerisation reaction.

In this study, a comparison of the influence of the homogenising (stirring) equipment on the quality of porous polymer foam is shown in Figure 6.3 and Figure 6.4 The use of different methods to prepare polyHIPEs raises the question of the comparability of the results. The results below compare the materials produced via the three methods: overhead stirrer, vortex mixer and homogeniser.

The water was added dropwise to an oil phase consisting of trithiol, DPEHA, DCE, surfactant and a photoinitiator. The emulsion was formed by mixing the oil phase and the water phase using an overhead stirrer, a vortex mixer and a homogeniser. It was then poured into a mould and cured by passing under UV radiation. The solid

polyHIPE was then washed in acetone to remove the aqueous droplet phase, and dried via a vacuum oven (see Figure 6.3). This shows that the porous polymer materials were successfully prepared when using the overhead stirrer and the vortex mixer, whereas not in the case of using the homogeniser (up to 8000 rpm), even when we reduced the amount of the internal phase by up to 0.5 volume of the fraction of water (see Figure 6.4). This shows that the emulsion at 0.8 (Figure 6.4d) volume of the fraction of water was very unstable against sedimentation just one minute after emulsification. The comparison of the emulsions produced with the homogeniser indicates the influence of the type of mixing of the oil phase with the water phase. Nevertheless, both overhead stirrer and vortex mixer can produce porous polymer foam (void).

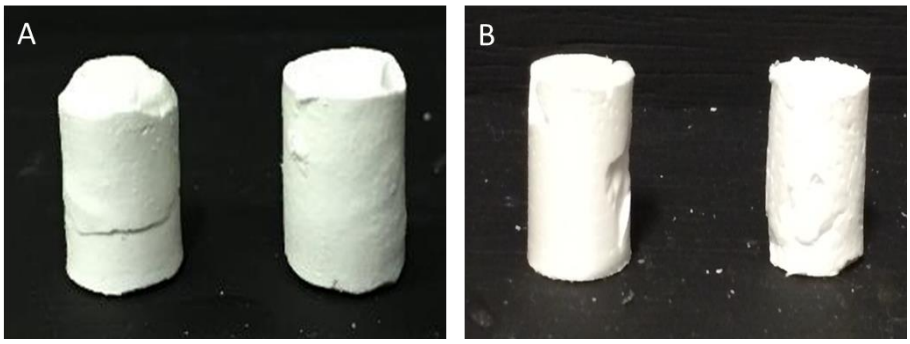

Figure 6. 3. Images of porous polymeric materials obtained after polymerisation of HIPEs of thiol-ene: a) using an overhead stirrer and b) using a vortex mixer. All materials were purified by Soxhlet extraction.

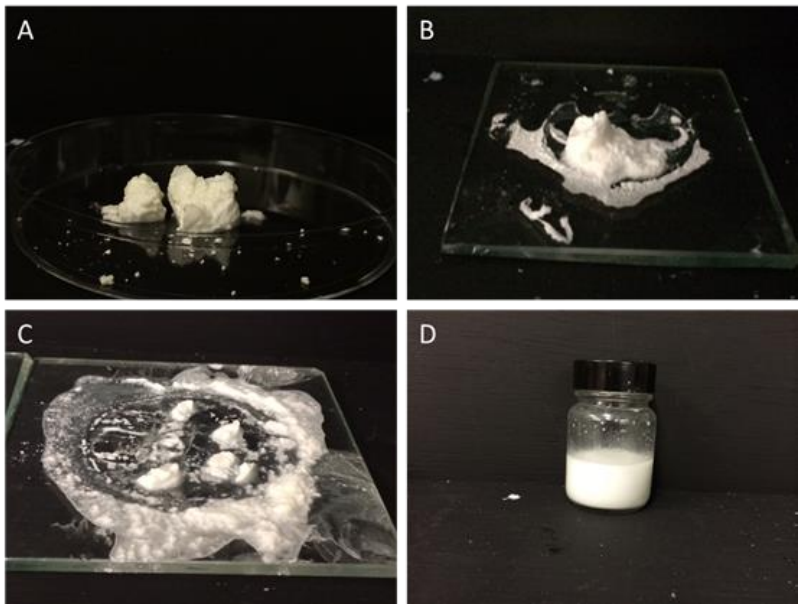

Figure 6. 4. Image of the white, very fragile polymeric material at varying volume fractions of water: 0.5 (A), 0.6 (B), 0.7 (C) and 0.8 (D).

6.3.2 Influence of the emulsification equipment on the morphology of polyHIPEs

The morphology of the polyHIPEs obtained was investigated using SEM. SEM images with different scale bars have been taken from different locations of the porous materials prepared by the overhead stirrer and the vortex mixer. PolyHIPE samples were found to be highly porous, and a fully interconnected, open cell morphology was observed as shown in Figure 6.5 and Figure 6.6. It can be seen that the windows' size decreased when using the vortex mixer. Based on these preliminary results, it was hypothesised that using the vortex mixer in combination would increase the film thickness.

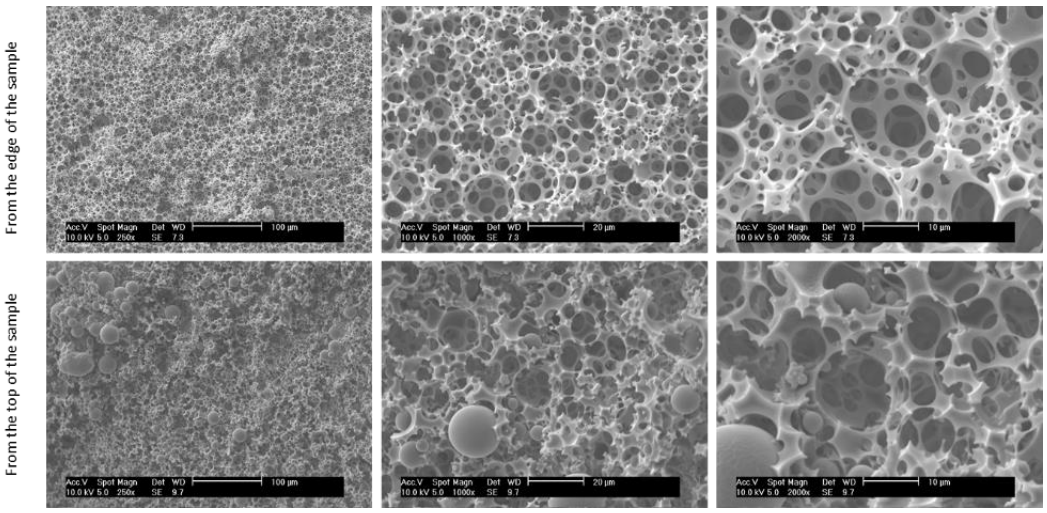

Figure 6. 5. Scanning electron micrographs of thiol-ene polyHIPEs by overhead stirrer.

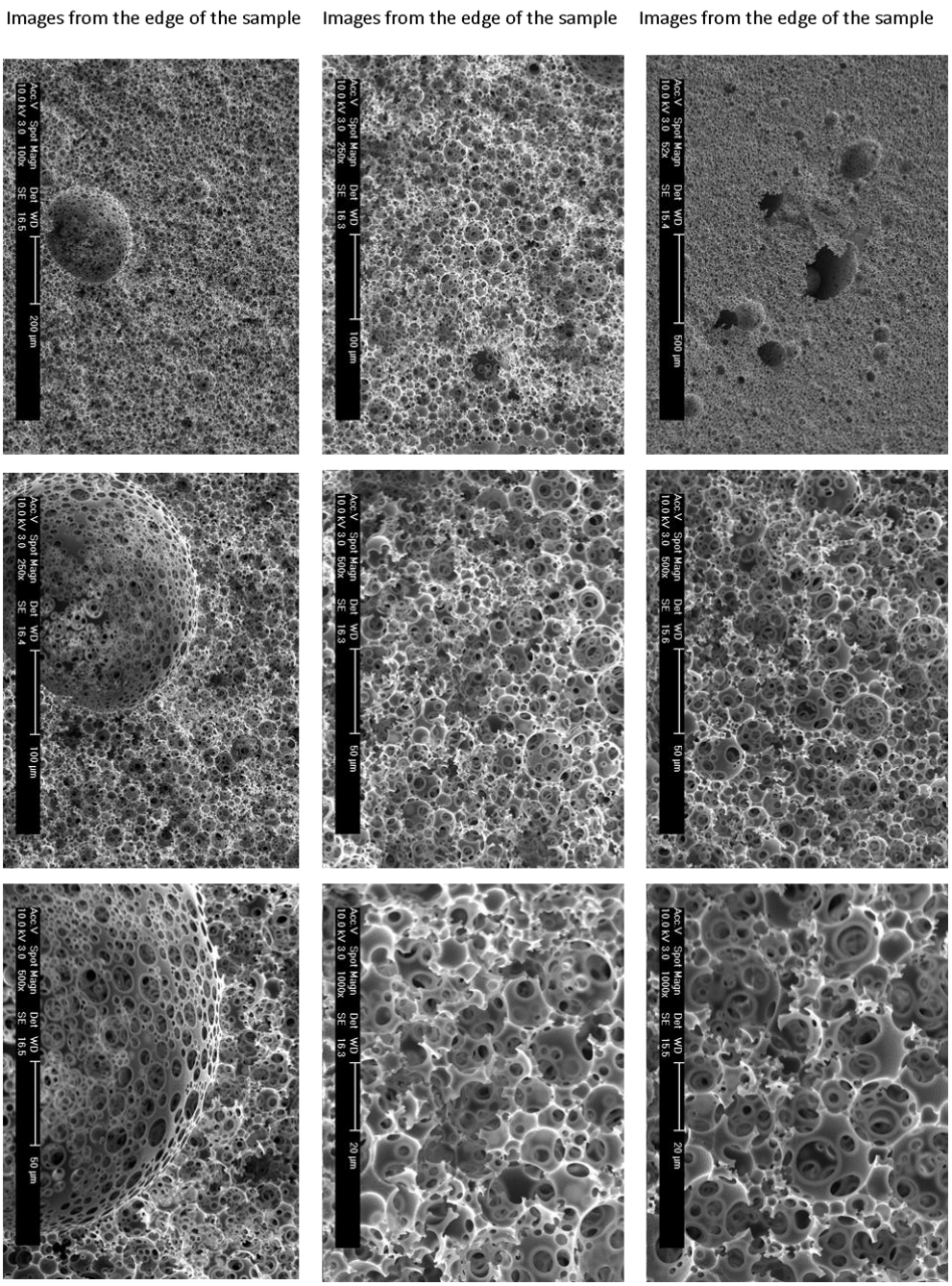

Figure 6. 6. Scanning electron micrographs of thiol-ene polyHIPEs by vortex mixer.

It is useful to compare voids to verify whether or not the change of mixing equipment resulted in an increase in void diameter. Qualitatively, it is evident that using a vortex mixer instead of an overhead stirrer caused the void size to increase. Evidence for this can be seen in Figure 6.7, which summarises the results regarding the average void

size diameter and allows for a comparison among all solid foams produced by using a vortex mixer and an overhead stirrer. **(**Image J[24] was used to calculate the average void size using a random sample of 100 voids from each SEM image). A statistical correction factor was employed to provide accurate values. Additionally, a significant difference in void size measurements is apparent. Although the voids produced using a vortex mixer are in the same size range as those produced using an overhead stirrer, they are of a slightly larger distribution. In the case of solid foams prepared by a vortex mixer, the number of voids at 25 μm and 30 μm was 41 and 16, respectively. However, they were 18 and 3 voids in the case of using an overhead stirrer. All materials gave void size distributions, with the majority of voids between 10 and 30 μm. The distribution of void diameters was wide in all cases, but within the range that has previously been used for cell culture. Interestingly, the pore size distribution and interconnectivity of emulsion-template foams can be modified by using different types of equipment for mixing the oil phase with the water phase, whether using an overhead stirrer or a vortex mixer.

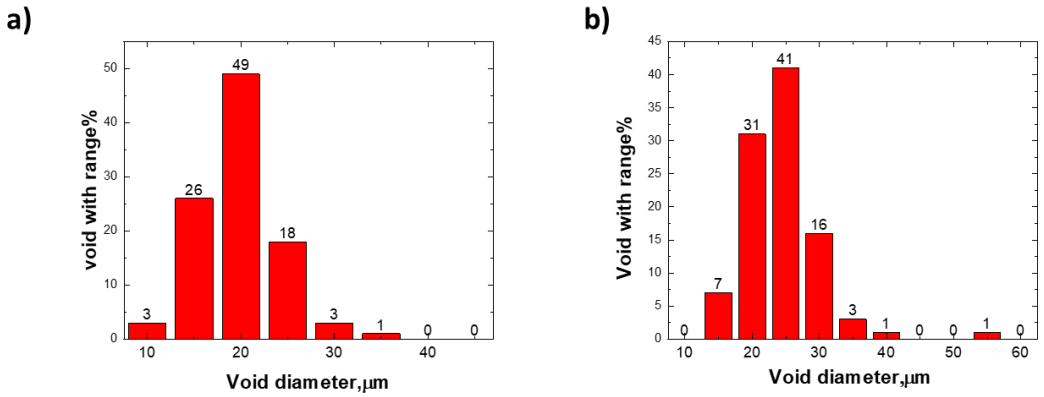

Figure 6. 7. Void diameter distribution by analysis of SEM of thiol-ene polyHIPEs (a) by overhead stirrer (b) by vortex mixer.

6.4 Conclusions

Highly Porous polythiolacrylte were successfully synthesised via HIPEs using step-growth polymerisation reaction. The reaction of polyHIPES were homogenised using three different devices: high speed homogeniser, vortex mixer and overhead stirrer. It has been found out using homogenizer speed for mixing of the oil phase with the water phase (up to 8000 rpm), with amount an internal phase at 0.5, 0.6 and 0.8, made the resulting emulsion unstable against sedimentation. Whereas, the porous polymer materials were successfully prepared when using the overhead stirrer and the vortex mixer. There was a notable effect of changing the emulsification equipment (overhead stirrer or vortex mixer) on the morphology of polymerised porous materials.

7 Conclusions

The basic conclusion and main findings of this project investigating the behaviour of poly thiol-allyl micro-composite particles can be summarised as follows:

We developed a novel multifunctional crosslinker (HA) and reported the first study of the use of this reagent in the case of thiol-ene suspension click polymerisation. HA was successfully synthesised by combining epoxy ring opening reactions/reagents with the Michael Addition reaction reagent. This method yielded cross-linked composite micro-particles in the form of poly thiol-allyl particles. To further broaden the applicability of these approaches, the thiol acrylate Michael Addition reaction was exploited for facile surface functionalization of the poly thiol-allyl composite microparticles with the attachment of different acrylate monomers (HEA, MA, EGMEA and DEAEA). EDX mapping confirmed that C, N, O and S are uniformly spread over particles before and after post-polymerisation functionalisation. It was observed that the absence of an intensity peak of thiol in the FTIR and Raman spectra after post-polymerisation functionalisation indicates that the sulphur in the EDX data is present as a thiolate.

This work demonstrates that an understanding of phenomena such as the thiol monomer ratio to HA, the homogenizer speed, the crosslinking density, the photopolymerisation time and the thermal curing method allows us to devise strategies to control T_g and the morphology of poly thiol-allyl particles before and after post polymerisation. The opposite behaviour was observed from the comparison between the performance of average diameter size particles and T_g.

The reaction of polyHIPEs were homogenised using three different devices: a high speed homogeniser, a vortex mixer and an overhead stirrer. It has been found that using a homogenizer for mixing the oil with the water (at up to 8000 rpm) does not enable to polymerize the resulting emulsion. On the other hand, the porous polymer

materials were successfully prepared when using the overhead stirrer and the vortex mixer. There was a notable effect of changing the emulsification equipment (the overhead stirrer or the vortex mixer) on the morphology of the polymerised porous materials.

Future work and remaining questions

Further investigations are required regarding the changes in the average chemical composition in the elemental mapping for the prepared poly thiol-allyl microstructure particles. Further studies should also be carried out to investigate and explore the effect of increasing the molar ratio of HA to thiol monomer. Then study the chemical structure, T_g and the morphology of poly thiol-allyl microstructure particles before and after post-polymerisation functionalization.

8 References

1. F. W. Harris, *Journal of Chemical Education*, 1981, **58**, 837.
2. J. F. Coelho, P. C. Ferreira, P. Alves, R. Cordeiro, A. C. Fonseca, J. R. Góis and M. H. Gil, *EPMA journal*, 2010, **1**, 164-209.
3. J. W. Nicholson, in *The Chemistry of Polymers (3)*, The Royal Society of Chemistry, 2006, DOI: 10.1039/9781847552655-00001, pp. 1-22.
4. M. T. Gokmen and F. E. Du Prez, *Progress in Polymer Science*, 2012, **37**, 365-405.
5. R. Arshady, *Colloid and polymer science*, 1992, **270**, 717-732.
6. E. Vivaldo-Lima, P. E. Wood, A. E. Hamielec and A. Penlidis, *Industrial & engineering chemistry research*, 1997, **36**, 939-965.
7. M. T. H. Nutan and I. K. Reddy, in *Pharmaceutical Suspensions: From Formulation Development to Manufacturing*, eds. A. K. Kulshreshtha, O. N. Singh and G. M. Wall, Springer New York, New York, NY, 2010, DOI: 10.1007/978-1-4419-1087-5_2, pp. 39-65.
8. A. I. Cooper, W. P. Hems and A. B. Holmes, *Macromolecules*, 1999, **32**, 2156-2166.
9. O. Z. Durham and D. A. Shipp, *Colloid and Polymer Science*, 2015, **293**, 2385-2394.
10. V. N. Pavlyuchenko and S. S. Ivanchev, *Russian Chemical Reviews*, 1981, **50**, 380.
11. J. H. Kim, T. Y. Jeon, T. M. Choi, T. S. Shim, S.-H. Kim and S.-M. Yang, *Langmuir*, 2013, **30**, 1473-1488.
12. H. Kawaguchi, *Progress in polymer Science*, 2000, **25**, 1171-1210.
13. Y. Wang and Y. Xia, *Nano letters*, 2004, **4**, 2047-2050.
14. A. Štorha, E. A. Mun and V. V. Khutoryanskiy, *Rsc Advances*, 2013, **3**, 12275-12279.
15. X. Yang, L.-W. Zhu, L.-S. Wan, J. Zhang and Z.-K. Xu, *Journal of Materials Research*, 2013, **28**, 642-650.
16. S. Hashim and B. W. Brooks, *Chemical engineering science*, 2002, **57**, 3703-3714.

17. M. Alvarez-Paino, A. Munoz-Bonilla, G. Marcelo, J. Rodriguez-Hernandez and M. Fernandez-Garcia, *Polymer Chemistry*, 2012, **3**, 3282-3288.
18. H. C. Kolb, M. G. Finn and K. B. Sharpless, *Angewandte Chemie International Edition*, 2001, **40**, 2004-2021.
19. J.-F. Lutz and H. G. Börner, *Progress in Polymer Science*, 2008, **33**, 1-39.
20. S. Parker, R. Reit, H. Abitz, G. Ellson, K. Yang, B. Lund and W. E. Voit, *Macromolecular rapid communications*, 2016, **37**, 1027-1032.
21. C. E. Hoyle and C. N. Bowman, *Angewandte Chemie International Edition*, 2010, **49**, 1540-1573.
22. B. Yao, J. Sun, A. Qin and B. Z. Tang, *Chinese Science Bulletin*, 2013, **58**, 2711-2718.
23. B. H. Northrop and R. N. Coffey, *Journal of the American Chemical Society*, 2012, **134**, 13804-13817.
24. B. D. Fairbanks, D. M. Love and C. N. Bowman, *Macromolecular Chemistry and Physics*, 2017, **218**, 1700073.
25. S. Hafeez, L. Barner and L. Nebhani, *Macromolecular rapid communications*, 2018, **39**, 1800169.
26. M. Claudino, M. Jonsson and M. Johansson, *RSC Advances*, 2014, **4**, 10317-10329.
27. N. B. Cramer and C. N. Bowman, *Journal of Polymer Science Part A: Polymer Chemistry*, 2001, **39**, 3311-3319.
28. A. Dondoni and A. Marra, *Chemical Society Reviews*, 2012, **41**, 573-586.
29. A. B. Lowe, *Polymer Chemistry*, 2010, **1**, 17-36.
30. M. B. Marakalala, E. M. Mmutlane and H. H. Kinfe, *Beilstein Journal of Organic Chemistry*, 2018, **14**, 1668-1692.
31. S. V. Bhosale and S. V. Bhosale, *Mini-Reviews in Organic Chemistry*, 2007, **4**, 231-242.
32. E. Lovelady, S. D. Kimmins, J. Wu and N. R. Cameron, *Polymer Chemistry*, 2011, **2**, 559-562.
33. C. E. Hoyle, T. Y. Lee and T. Roper, *Journal of Polymer Science Part A: Polymer Chemistry*, 2004, **42**, 5301-5338.
34. J. W. Chan, H. Zhou, C. E. Hoyle and A. B. Lowe, *Chemistry of Materials*, 2009, **21**, 1579-1585.

35. N. B. Cramer, T. Davies, A. K. O'Brien and C. N. Bowman, *Macromolecules*, 2003, **36**, 4631-4636.
36. N. B. Cramer and C. N. Bowman, *Journal of Polymer Science Part A: Polymer Chemistry*, 2001, **39**, 3311-3319.
37. B. Colak, J. C. S. Da Silva, T. A. Soares and J. E. Gautrot, *Bioconjugate Chemistry*, 2016, **27**, 2111-2123.
38. A. E. Rydholm, C. N. Bowman and K. S. Anseth, *Biomaterials*, 2005, **26**, 4495-4506.
39. J. Tan, C. Li, J. Zhou, C. Yin, B. Zhang, J. Gu and Q. Zhang, *Rsc Advances*, 2014, **4**, 13334-13339.
40. O. Z. Durham, H. R. Norton and D. A. Shipp, *RSC Advances*, 2015, **5**, 66757-66766.
41. K. L. Poetz, O. Z. Durham and D. A. Shipp, *Polymer Chemistry*, 2015, **6**, 5464-5469.
42. O. Z. Durham, S. Krishnan and D. A. Shipp, *ACS Macro Letters*, 2012, **1**, 1134-1137.
43. O. Z. Durham, D. V. Chapman, S. Krishnan and D. A. Shipp, *Macromolecules*, 2017, **50**, 775-783.
44. F. Alimohammadi, C. Wang, O. Z. Durham, H. R. Norton, C. N. Bowman and D. A. Shipp, *Polymer*, 2016, **105**, 180-186.
45. O. Z. Durham and D. A. Shipp, *Polymer*, 2014, **55**, 1674-1680.
46. D. V. Amato, D. N. Amato, A. S. Flynt and D. L. Patton, *Polymer Chemistry*, 2015, **6**, 5625-5632.
47. S. Caldwell, D. W. Johnson, M. P. Didsbury, B. A. Murray, J. J. Wu, S. A. Przyborski and N. R. Cameron, *Soft Matter*, 2012, **8**, 10344-10351.
48. D. P. Nair, M. Podgorski, S. Chatani, T. Gong, W. Xi, C. R. Fenoli and C. N. Bowman, *Chemistry of Materials*, 2013, **26**, 724-744.
49. G.-Z. Li, R. K. Randev, A. H. Soeriyadi, G. Rees, C. Boyer, Z. Tong, T. P. Davis, C. R. Becer and D. M. Haddleton, *Polymer Chemistry*, 2010, **1**, 1196-1204.
50. R. K. Iha, K. L. Wooley, A. M. Nystrom, D. J. Burke, M. J. Kade and C. J. Hawker, *Chemical reviews*, 2009, **109**, 5620-5686.
51. C. R. Langford, D. W. Johnson and N. R. Cameron, *Polymer Chemistry*, 2014, **5**, 6200-6206.

52. T. C. Rhoades, J. C. Wistrom, R. D. Johnson and K. M. Miller, *Polymer*, 2016, **100**, 1-9.
53. A.-S. Glaive, T. Modjinou, D.-L. Versace, S. Abbad-Andaloussi, P. Dubot, V. r. Langlois and E. Renard, *ACS Sustainable Chemistry & Engineering*, 2017, **5**, 2320-2329.
54. K. T. Wacker, A. C. Weems, S.-M. Lim, S. Khan, S. E. Felder, A. P. Dove and K. L. Wooley, *Biomacromolecules*, 2018, **20**, 109-117.
55. J.-T. Miao, L. Yuan, Q. Guan, G. Liang and A. Gu, *ACS Sustainable Chemistry & Engineering*, 2018, **6**, 7902-7909.
56. A. Sudo, Y. Shirakawa and T. Sakue, *Journal of Polymer Science Part A: Polymer Chemistry*, 2017, **55**, 1524-1529.
57. J. Dai, S. Ma, L. Zhu, S. Wang, L. Yang, Z. Song, X. Liu and J. Zhu, *Polymer*, 2017, **108**, 215-222.
58. M. Fiore, A. Marra and A. Dondoni, *The Journal of organic chemistry*, 2009, **74**, 4422-4425.
59. F. Le Dévédec, C. J. Allen, D. M. Stevens, D. J. Rager-Aguiar, T. T. Ruckh and C. E. Elmquist, *Journal*, 2017.
60. B. Sergent, M. Birot and H. Deleuze, *Reactive and Functional Polymers*, 2012, **72**, 962-966.
61. D. A. Tomalia, D. R. Swanson, B. Huang, V. R. Pulgam, J. R. Heinzelmann, S. Svenson, L. A. Reyna, M. A. Zhuravel, A. S. Chauhan and C. R. DeMattei, *Journal*, 2011.
62. D. A. Shipp, S. Krishnan and O. Z. Durham, *Journal*, 2013.
63. S. E. Paramonov, E. M. Bachelder, T. T. Beaudette, S. M. Standley, C. C. Lee, J. Dashe and J. M. J. Fréchet, *Bioconjugate Chemistry*, 2008, **19**, 911-919.
64. W. Gu, G. Chen and M. H. Stenzel, *Journal of Polymer Science Part A: Polymer Chemistry*, 2009, **47**, 5550-5556.
65. Y. J. Kwon, E. James, N. Shastri and J. M. J. Fréchet, *Proceedings of the National Academy of Sciences*, 2005, **102**, 18264-18268.
66. J. S. Downey, R. S. Frank, W.-H. Li and H. D. H. Stöver, *Macromolecules*, 1999, **32**, 2838-2844.
67. S. L. Goh, N. Murthy, M. Xu and J. M. J. Fréchet, *Bioconjugate chemistry*, 2004, **15**, 467-474.

68. M. T. Gokmen, J. Brassinne, R. A. Prasath and F. E. Du Prez, *Chemical Communications*, 2011, **47**, 4652-4654.
69. T. T. Truong, S. H. Thai, H. T. Nguyen, T. H. Nguyen and L.-T. T. Nguyen, *Journal of materials science*, 2018, **53**, 2236-2252.
70. Y. Fang, H. Ha, K. Shanmuganathan and C. J. Ellison, *ACS applied materials & interfaces*, 2016, **8**, 11050-11059.
71. M. Jawerth, M. Johansson, S. Lundmark, C. Gioia and M. Lawoko, *Acs Sustainable Chemistry & Engineering*, 2017, **5**, 10918-10925.
72. M. Shibata and Y. Hashimoto, *European Polymer Journal*, 2017, **93**, 561-571.
73. E. M. Barker and J. P. Buchanan, *Polymer*, 2016, **92**, 66-73.
74. F. Jasinski, A. s. Rannée, J. Schweitzer, D. Fischer, E. Lobry, C. l. Croutxé-Barghorn, M. Schmutz, D. Le Nouen, A. Criqui and A. Chemtob, *Macromolecules*, 2016, **49**, 1143-1153.
75. R. A. Prasath, M. T. Gokmen, P. Espeel and F. E. Du Prez, *Polymer Chemistry*, 2010, **1**, 685-692.
76. C. Wang, M. Podgórski and C. N. Bowman, *Materials Horizons*, 2014, **1**, 535-539.
77. Y.-H. Chen, H.-P. Liu, H.-Y. Chen, F.-J. Tsai, C.-H. Chang, Y.-J. Lee, W.-Y. Lin and W.-C. Chen, *Kidney international*, 2011, **80**, 369-377.
78. T. Zhao, L. Li, R. Chen, H. Wu, X. Zhang, S. Chen, M. Xie, F. Wu, J. Lu and K. Amine, *Nano Energy*, 2015, **15**, 164-176.
79. K. Zangeneh Kamali, P. Alagarsamy, N. M. Huang, B. H. Ong and H. N. Lim, *The Scientific World Journal*, 2014, **2014**.
80. S. Rades, V.-D. Hodoroaba, T. Salge, T. Wirth, M. P. Lobera, R. H. Labrador, K. Natte, T. Behnke, T. Gross and W. E. S. Unger, *Rsc Advances*, 2014, **4**, 49577-49587.
81. Z. Chen, D. Chao, J. Liu, M. Copley, J. Lin, Z. Shen, G.-T. Kim and S. Passerini, *Journal of Materials Chemistry A*, 2017, **5**, 15669-15675.
82. G. Coquil, J. Fullenwarth, G. Grinbom, M. T. Sougrati, L. Stievano, D. Zitoun and L. Monconduit, *Journal of Power Sources*, 2017, **372**, 196-203.
83. Y. Wang, W. Chen, X. Chen, H. Feng, D. Shen, B. Huang, Y. Jia, Y. Zhou and Y. Liang, *Journal of Environmental Sciences*, 2018, **65**, 347-355.

84. S.-C. Shi, J.-Y. Wu, T.-F. Huang and Y.-Q. Peng, *Surface and Coatings Technology*, 2016, **303**, 250-255.
85. M. Asif, Y. Tan, L. Pan, M. Rashad, J. Li, X. Fu and R. Cui, *Physical Chemistry Chemical Physics*, 2016, **18**, 26854-26864.
86. S.-C. Shi, *Materials*, 2016, **9**, 856.
87. G. C. da Silva, M. R. Fernandes and E. A. Ticianelli, *ACS Catalysis*, 2018, **8**, 2081-2092.
88. K. Bramhaiah and N. S. John, *RSC Advances*, 2013, **3**, 7765-7773.
89. H. N. Tran, S.-J. You and H.-P. Chao, *Journal of Environmental Chemical Engineering*, 2016, **4**, 2671-2682.
90. S. Li, S. Mo, J. Li, H. Liu and Y. Chen, *Rsc Advances*, 2016, **6**, 56874-56884.
91. V. T. P. Vinod, S. Wacławek, C. Senan, J. Kupčík, K. Pešková, M. Černík and H. M. Somashekarappa, *RSC Advances*, 2017, **7**, 13997-14009.
92. E. D. H. Mansfield, V. R. de la Rosa, R. M. Kowalczyk, I. Grillo, R. Hoogenboom, K. Sillence, P. Hole, A. C. Williams and V. V. Khutoryanskiy, *Biomaterials Science*, 2016, **4**, 1318-1327.
93. S. M. Rogers, N. Dimitratos, W. Jones, M. Bowker, A. G. Kanaras, P. P. Wells, C. R. A. Catlow and S. F. Parker, *Physical Chemistry Chemical Physics*, 2016, **18**, 17265-17271.
94. P. K. Gallagher, M. E. Brown and R. B. Kemp, *Journal*, 1998.
95. D. Guzmán, X. Ramis, X. Fernández-Francos and A. Serra, *Polymers*, 2015, **7**, 680-694.
96. S. Ebnesajjad, in *Chemical Resistance of Commodity Thermoplastics*, eds. E. Baur, K. Ruhrberg and W. Woishnis, William Andrew Publishing, 2016, DOI: https://doi.org/10.1016/B978-0-323-47358-3.00017-X, pp. xiii-xxv.
97. C. L. Klix, G. Maret and P. Keim, *Physical Review X*, 2015, **5**, 041033.
98. D. Christie, C. Zhang, J. Fu, B. Koel and R. D. Priestley, *Journal of Polymer Science Part B: Polymer Physics*, 2016, **54**, 1776-1783.
99. I. M. Kalogeras, *Encyclopedia of Polymer Blends, Volume 3: Structure*, 2016, **3**.
100. S. Mutlur, *Adv. Top. Charact. Compos*, 2004, 11-33.
101. A. Hale, in *Handbook of Thermal Analysis and Calorimetry*, ed. S. Z. D. Cheng, Elsevier Science B.V., 2002, vol. 3, pp. 295-354.

102. X. Zhang, X. Peng and S. W. Zhang, in *Science and Principles of Biodegradable and Bioresorbable Medical Polymers*, Elsevier, 2017, pp. 1-33.
103. V. I. Roldughin, O. A. Serenko, E. V. Getmanova, N. A. Novozhilova, G. G. Nikifirova, M. I. Buzin, S. N. Chvalun, A. N. Ozerin and A. M. Muzafarov, *Polymer Composites*, 2016, **37**, 1978-1990.
104. B. J. Ash, R. W. Siegel and L. S. Schadler, *Journal of Polymer Science Part B: Polymer Physics*, 2004, **42**, 4371-4383.
105. M. G. A. Vieira, M. A. da Silva, L. O. dos Santos and M. M. Beppu, *European Polymer Journal*, 2011, **47**, 254-263.
106. P. Menčík, R. Přikryl, I. Stehnová, V. Melčová, S. Kontárová, S. Figalla, P. Alexy and J. Bočkaj, *Materials (Basel)*, 2018, **11**, 1893.
107. *Journal of Polymer Science: Polymer Chemistry Edition*, 1981, **19**, 1767-1779.
108. H. Wang, T. Chang, X. Li, W. Zhang, Z. Hu and A. M. Jonas, *Nanoscale*, 2016, **8**, 14950-14955.
109. C. Zhang, V. M. Boucher, D. Cangialosi and R. D. Priestley, *Polymer*, 2013, **54**, 230-235.
110. C. Zhang, Y. Guo and R. D. Priestley, *Macromolecules*, 2011, **44**, 4001-4006.
111. N. Teramoto, M. Saitoh, J. Kuroiwa, M. Shibata and R. Yosomiya, *Journal of applied polymer science*, 2001, **82**, 2273-2280.
112. Y. Cang, A. N. Reuss, J. Lee, J. Yan, J. Zhang, E. Alonso-Redondo, R. Sainidou, P. Rembert, K. Matyjaszewski and M. R. Bockstaller, *Macromolecules*, 2017, **50**, 8658-8669.
113. H. Xu, B. Yang, J. Wang, S. Guang and C. Li, *Journal of Polymer Science Part A: Polymer Chemistry*, 2007, **45**, 5308-5317.
114. J. Ding, G. Xue, Q. Dai and R. Cheng, *Polymer*, 1993, **34**, 3325-3327.
115. C. L. Rodrigues, E. Miguez and M. I. B. Tavares, *Materials Sciences and Applications*, 2016, **7**, 575.
116. M. R. Vengatesan and V. Mittal, *Surface modification of nanoparticle and natural fiber fillers*, 2015, 1-28.

117. J. Zhang, R. Deubler, M. Hartlieb, L. Martin, J. Tanaka, E. Patyukova, P. D. Topham, F. H. Schacher and S. Perrier, *Macromolecules*, 2017, **50**, 7380-7387.
118. J. E. G. Lipson and S. T. Milner, *Journal of Polymer Science Part B: Polymer Physics*, 2006, **44**, 3528-3545.
119. T. Y. Lee, J. Carioscia, Z. Smith and C. N. Bowman, *Macromolecules*, 2007, **40**, 1473-1479.
120. C. Wang, S. Chatani, M. Podgórski and C. N. Bowman, *Polymer Chemistry*, 2015, **6**, 3758-3763.
121. M. Podgórski, E. Becka, S. Chatani, M. Claudino and C. N. Bowman, *Polymer chemistry*, 2015, **6**, 2234-2240.
122. S. Mane, S. Ponrathnam and N. Chavan, *Can. Chem. Trans*, 2015, **3**, 473-485.
123. E. H. Mert, C. Slugovc and P. Krajnc, *eXPRESS polymer letters*, 2015, **9**.
124. L. Kwisnek, S. Heinz, J. S. Wiggins and S. Nazarenko, *Journal of membrane science*, 2011, **369**, 429-436.
125. B. R. Donovan, J. S. Cobb, E. F. T. Hoff and D. L. Patton, *RSC Advances*, 2014, **4**, 61927-61935.
126. Y. Uemura, T. Shimasaki, N. Teramoto and M. Shibata, *Journal of Polymer Research*, 2016, **23**, 216.
127. A. B. Lowe, *Polymer*, 2014, **55**, 5517-5549.
128. Q. Li, H. Zhou and C. E. Hoyle, *Polymer*, 2009, **50**, 2237-2245.
129. B. G. Rutherglen and D. A. Shipp, in *Fine Particles in Medicine and Pharmacy*, ed. E. Matijević, Springer US, Boston, MA, 2012, DOI: 10.1007/978-1-4614-0379-1_6, pp. 175-194.
130. C. Manoharan, A. Basarkar and J. Singh, in *Pharmaceutical Suspensions: From Formulation Development to Manufacturing*, eds. A. K. Kulshreshtha, O. N. Singh and G. M. Wall, Springer New York, New York, NY, 2010, DOI: 10.1007/978-1-4419-1087-5_1, pp. 1-37.
131. J. Yang, T.-J. Wang, H. He, F. Wei and Y. Jin, *Industrial & engineering chemistry research*, 2003, **42**, 5568-5575.
132. A. L. Nogueira, M. B. Quadri, P. H. H. Araújo and R. A. F. Machado, *Procedia Engineering*, 2012, **42**, 1045-1052.
133. V. Chaudhary and S. Sharma, *Journal of Polymer Research*, 2019, **26**, 102.

134. A. J. Guenthner, D. M. Hess and J. J. Cash, *Polymer*, 2008, **49**, 5533-5540.
135. M. Sušec, R. Liska, G. Russmüller, J. Kotek and P. Krajnc, *Macromolecular bioscience*, 2015, **15**, 253-261.
136. V. Privman, in *Fine Particles in Medicine and Pharmacy*, ed. E. Matijević, Springer US, Boston, MA, 2012, DOI: 10.1007/978-1-4614-0379-1_1, pp. 1-24.
137. S.-C. Park, J.-D. Cho and J.-W. Hong, *Open Journal of Organic Polymer Materials*, 2013, **3**, 92.
138. I. D. Tevis, L. B. Newcomb and M. Thuo, *Langmuir*, 2014, **30**, 14308-14313.
139. T. G. Mason and J. Bibette, *Langmuir*, 1997, **13**, 4600-4613.
140. N. R. Cameron, *Polymer*, 2005, **46**, 1439-1449.
141. D. Wu, F. Xu, B. Sun, R. Fu, H. He and K. Matyjaszewski, *Chemical reviews*, 2012, **112**, 3959-4015.
142. S. D. Kimmins and N. R. Cameron, *Advanced Functional Materials*, 2011, **21**, 211-225.
143. H. Zhang and A. I. Cooper, *Soft Matter*, 2005, **1**, 107-113.
144. S. Kovačič, P. Krajnc and C. Slugovc, *Chemical communications*, 2010, **46**, 7504-7506.
145. F. T. Zohora and A. Y. M. A. Azim, *European Scientific Journal*, 2014, **10**.
146. D. W. Hutmacher, M. Sittinger and M. V. Risbud, *TRENDS in Biotechnology*, 2004, **22**, 354-362.
147. M. T. Raimondi, S. M. Eaton, M. M. Nava, M. Laganà, G. Cerullo and R. Osellame, *Journal of applied biomaterials & functional materials*, 2012, **10**, 56-66.
148. D. W. Johnson, C. R. Langford, M. P. Didsbury, B. Lipp, S. A. Przyborski and N. R. Cameron, *Polymer Chemistry*, 2015, **6**, 7256-7263.
149. I. Pulko and P. Krajnc, *Macromolecular rapid communications*, 2012, **33**, 1731-1746.
150. L. Kircher, P. Theato and N. R. Cameron, *Polymer*, 2013, **54**, 1755-1761.
151. C. R. Langford, D. W. Johnson and N. R. Cameron, *Macromolecular rapid communications*, 2015, **36**, 834-839.
152. M. Turnšek and P. Krajnc, *Macromolecular Chemistry and Physics*, 2013, **214**, 2528-2533.

153. R. J. Carnachan, M. Bokhari, S. A. Przyborski and N. R. Cameron, *Soft Matter*, 2006, **2**, 608-616.
154. N. Zhang, L. Zhang and D. Sun, *Langmuir*, 2015, **31**, 4619-4626.
155. O. Lépine, M. Birot and H. Deleuze, *Colloid and Polymer Science*, 2008, **286**, 1273-1280.

9 Appendix

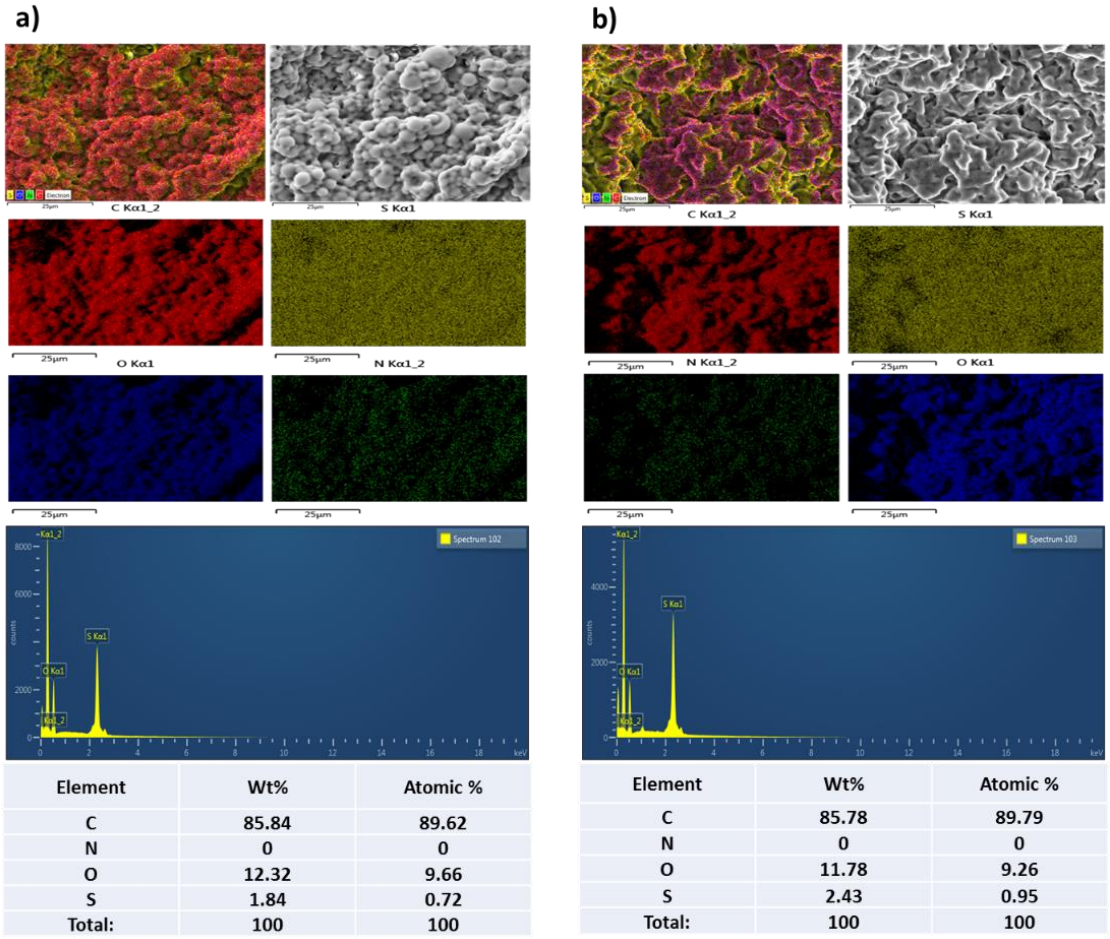

Element	Wt%	Atomic %
C	85.84	89.62
N	0	0
O	12.32	9.66
S	1.84	0.72
Total:	100	100

Element	Wt%	Atomic %
C	85.78	89.79
N	0	0
O	11.78	9.26
S	2.43	0.95
Total:	100	100

SEM image, element distribution and EDX data for TMTMP-HA (1.5:1) microsphere polymer particles at (a) 8000 rpm and (b) 20500 rpm.

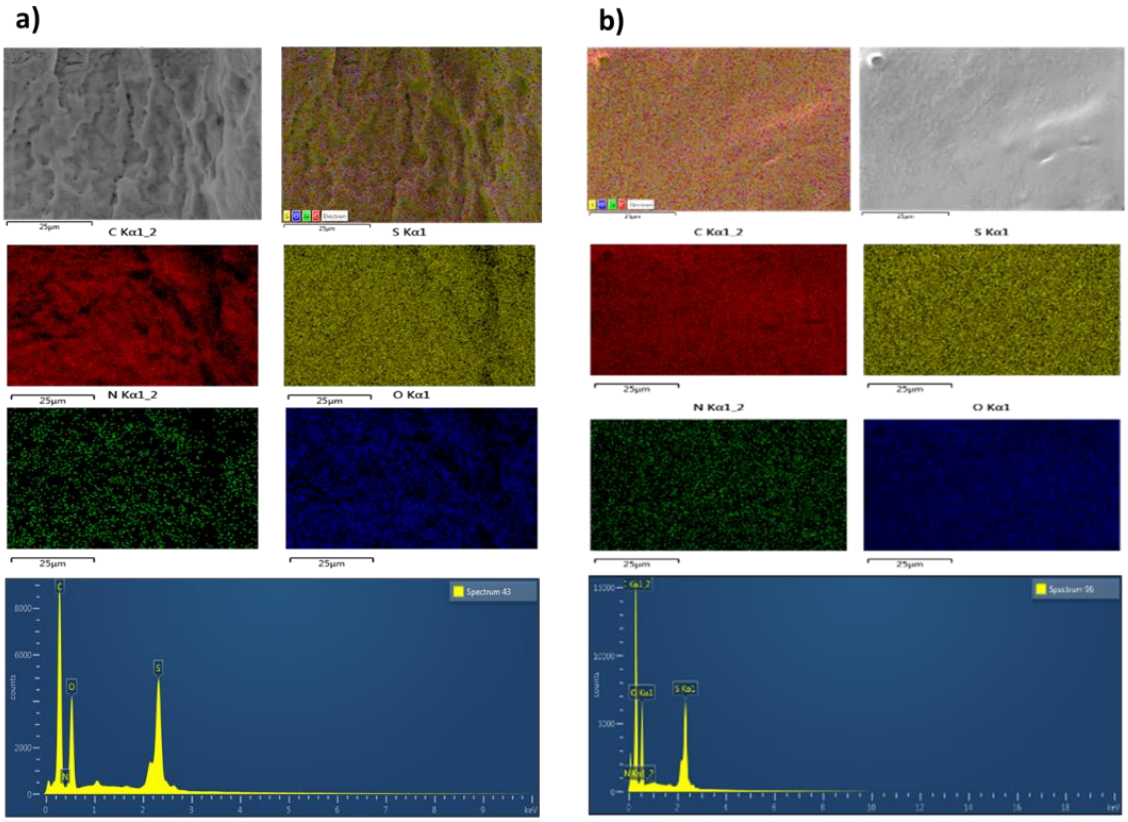

Element	Wt%	Atomic %
C	93.46	96.06
N	-0.41	-0.36
O	4.21	3.25
S	2.73	1.05
Total:	100	100

Element	Wt%	Atomic %
C	81.41	85.94
N	0	0
O	16.89	13.39
S	1.69	0.67
Total:	100	100

SEM image, element distribution and EDX data for TMTMP-HA (2:1) microsphere polymer particles at (a) 8000 rpm and (b) 20500 rpm.

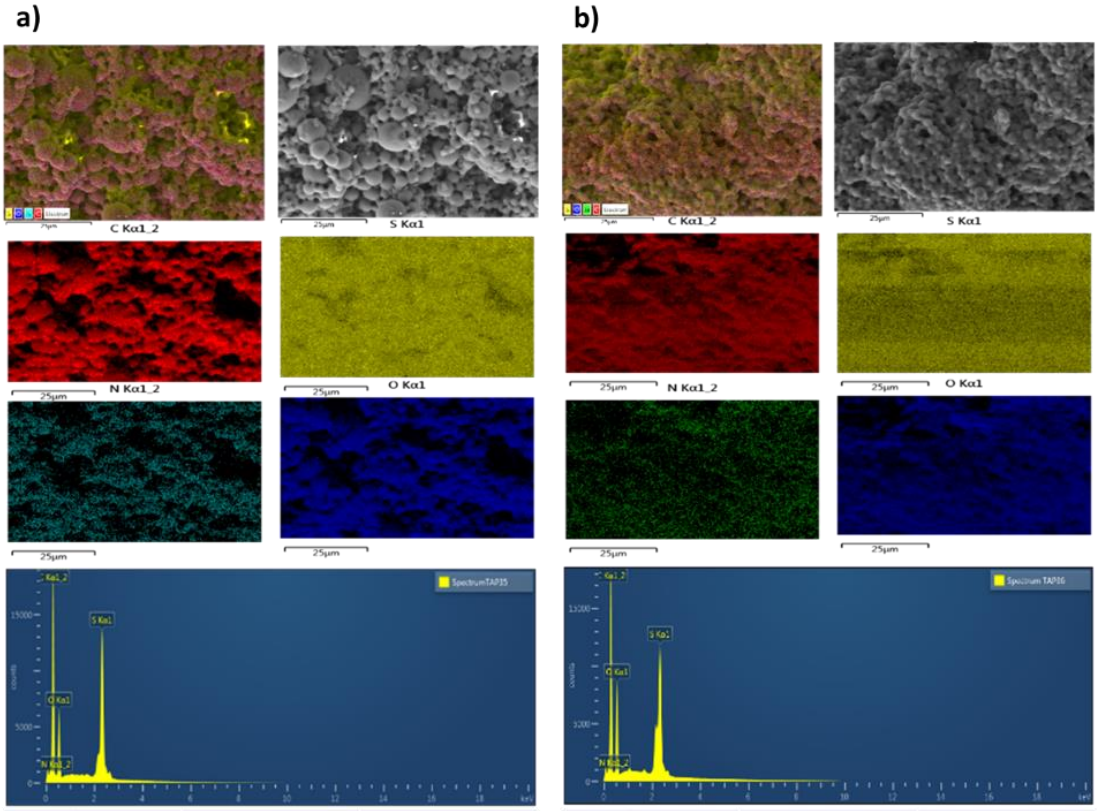

Element	Wt%	Atomic %
C	83.04	87.63
N	0.34	0.31
O	13.82	10.95
S	2.8	1.11
Total:	100	100

Element	Wt%	Atomic %
C	79.81	84.85
N	0	0
O	17.79	14.2
S	2.39	0.95
Total:	100	100

SEM image, element distribution and EDX data for PETMP-HA (1.5:1) microsphere polymer particles. Synthesised under UV for one hour at (a) 8000 rpm and (b) 20500 rpm.

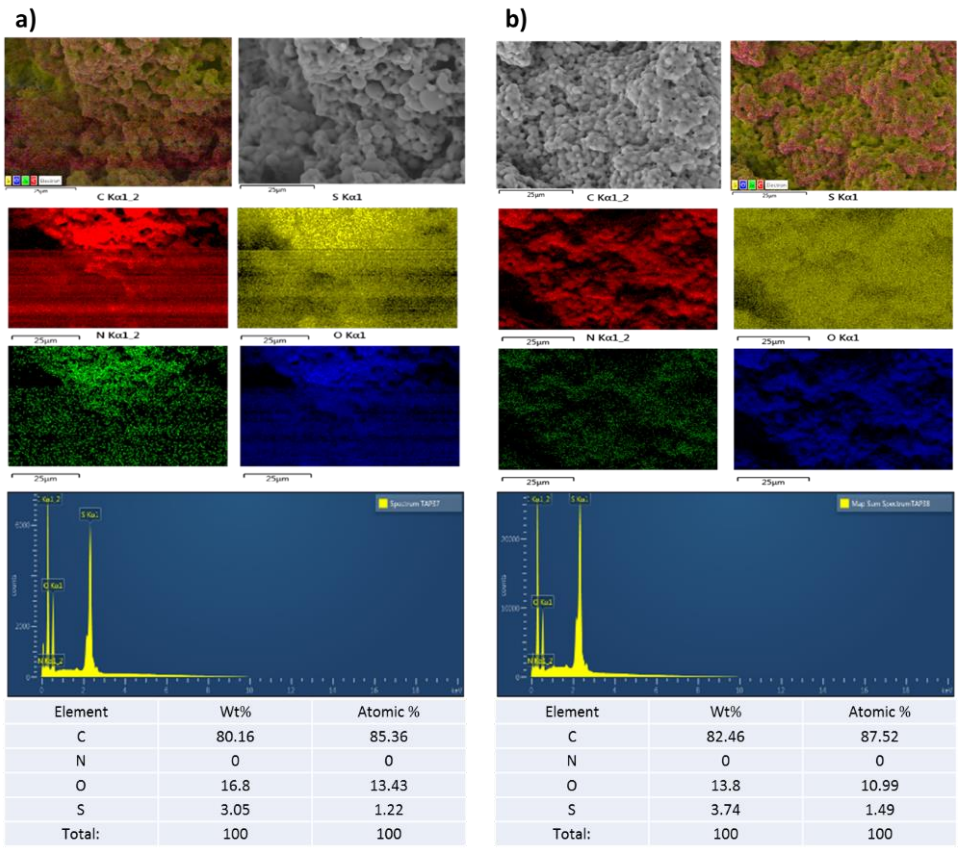

Element	Wt%	Atomic %
C	80.16	85.36
N	0	0
O	16.8	13.43
S	3.05	1.22
Total:	100	100

Element	Wt%	Atomic %
C	82.46	87.52
N	0	0
O	13.8	10.99
S	3.74	1.49
Total:	100	100

SEM image, element distribution and EDX data for PETMP-HA (2:1) microsphere polymer particles. Synthesised under UV for one hour at (a) 8000 rpm and (b) 20500 rpm.

a)

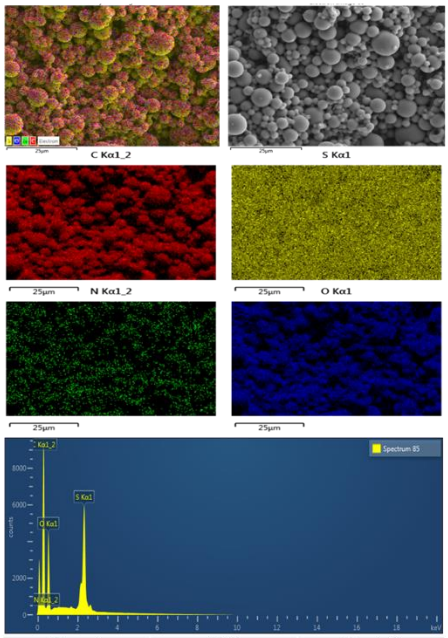

Element	Wt%	Atomic %
C	79.73	84.73
N	0	0
O	18.01	14.37
S	2.26	0.9
Total:	100	100

b)

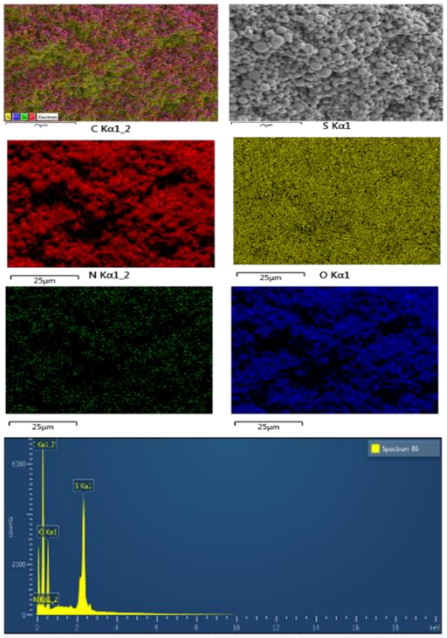

Element	Wt%	Atomic %
C	81.01	85.89
N	0	0
O	16.46	13.1
S	2.53	1
Total:	100	100

SEM image, element distribution and EDX data for PETMP-HA (1.5 :1) microsphere polymer particles. Synthesised under UV for five hours at (a) 8000 rpm and (b) 20500 rpm.

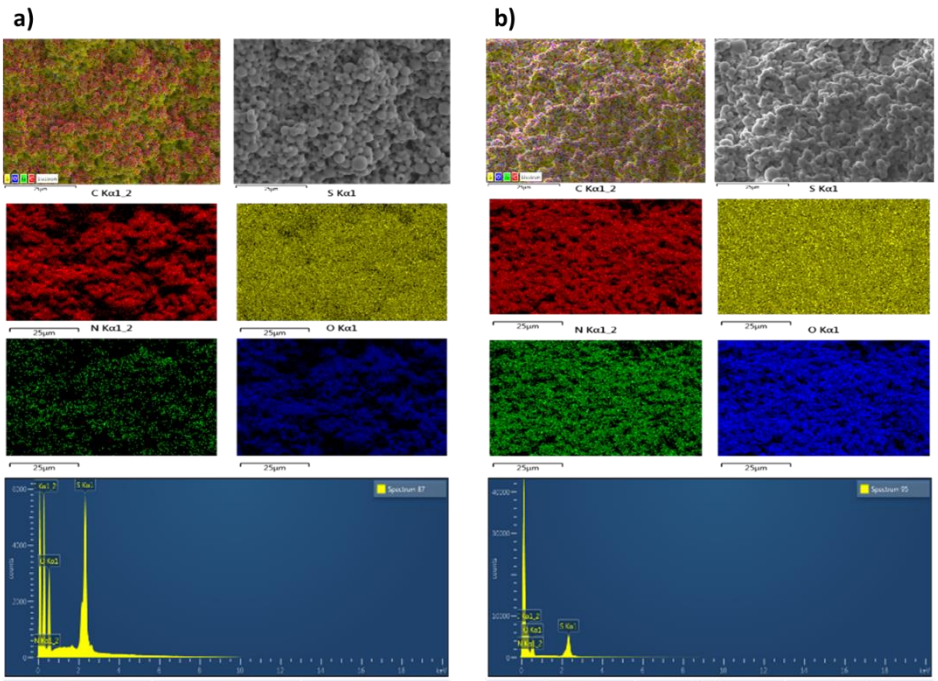

Element	Wt%	Atomic %
C	78.48	83.99
N	0	0
O	18.34	14.74
S	3.18	1.28
Total:	100	100

Element	Wt%	Atomic %
C	53.01	57.71
N	35.85	33.47
O	10.45	8.54
S	0.69	0.28
Total:	100	100

SEM image, element distribution and EDX data for PETMP-HA (2:1) microsphere polymer particles. Synthesised under UV for five hours at (a) 8000 rpm and (b) 20500 rpm.

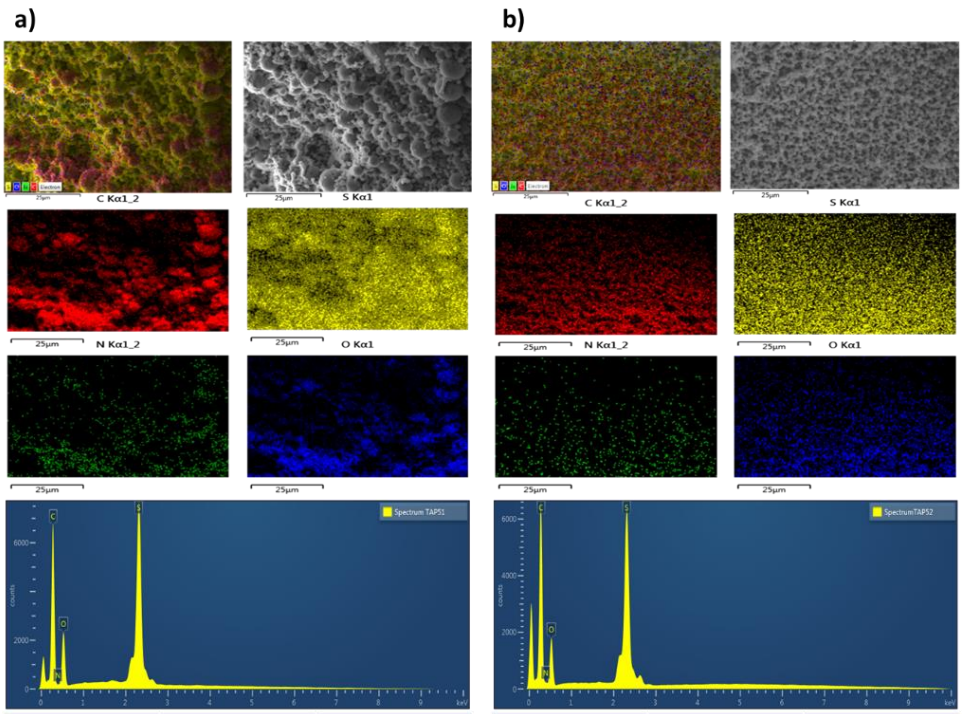

Element	Wt%	Atomic %
C	97.04	98.52
N	-0.12	-0.11
O	1.08	0.82
S	2	0.76
Total:	100	100

Element	Wt%	Atomic %
C	98.9	99.44
N	0.01	0.01
O	0.38	0.28
S	0.72	0.27
Total:	100	100

SEM image, element distribution and EDX data for PETMP-HA (1:1) microsphere polymer particles. Synthesised using thermal initiator at 8000 rpm (a) with DVB and (b) without DVB

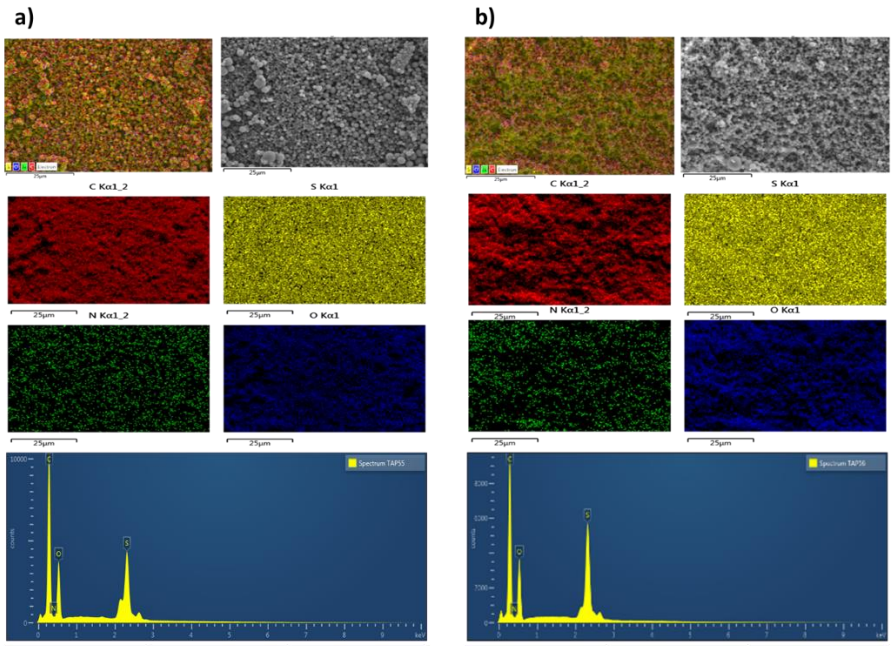

Element	Wt%	Atomic %
C	93.56	96.01
N	-0.06	-0.05
O	4	3.08
S	2.5	0.96
Total:	100	100

Element	Wt%	Atomic %
C	94.23	96.6
N	0.01	0
O	3.06	2.36
S	2.71	1.04
Total:	100	100

SEM image, element distribution and EDX data for PETMP-HA (a) 1:1 and 2:1 (b) microsphere polymer particles. Synthesised using thermal initiator at 8000.

SEM image, element distribution and EDX data after post-polymerisation functionalisation via thiol acrylate Michael addition reaction using different acrylate monomers: (a) HEA, (b) MA, (c) EGMEA and(d) DEAEA for PETMP-HA (1:1) microsphere polymer particles, synthesised under UV for 5 hours at 20500 rpm.

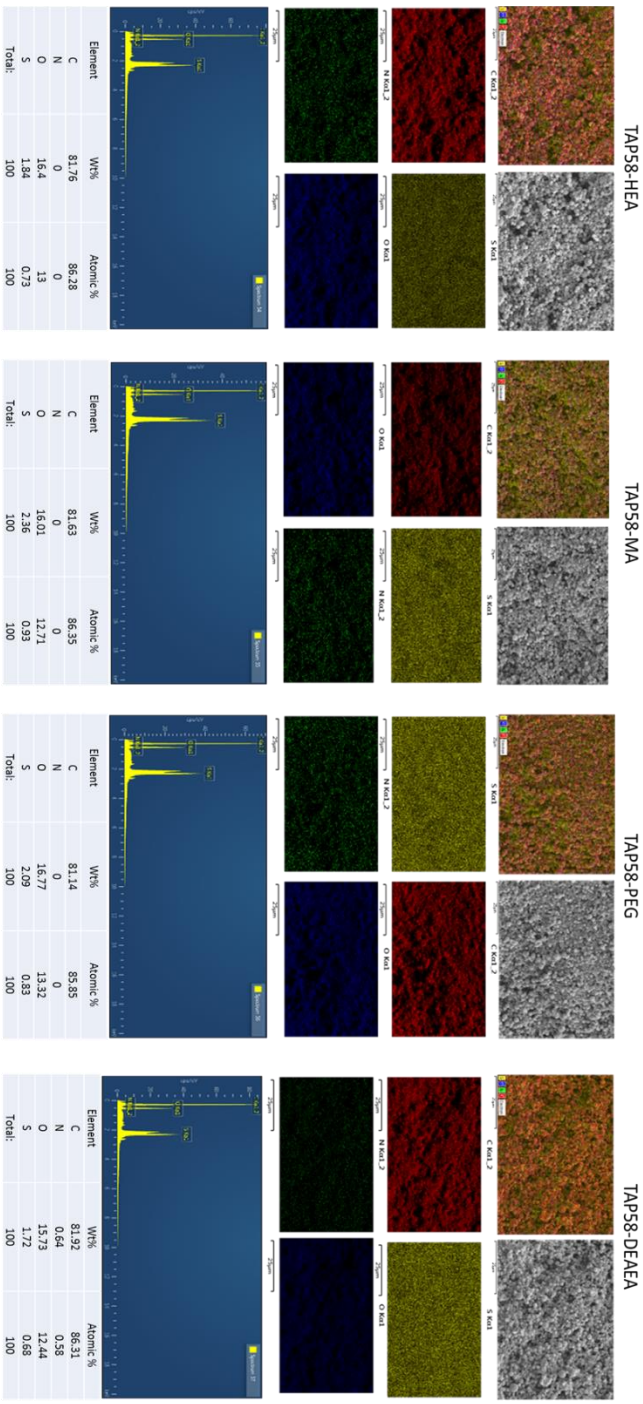

SEM image, element distribution and EDX data after post-polymerisation functionalisation via thiol acrylate Michael addition reaction using different acrylate monomers: (a) HEA, (b) MA, (c) EGMEA and(d) DEAEA for PETMP-HA (1.5:1) microsphere polymer particles, synthesised under UV for 5 hours at 8000 rpm.

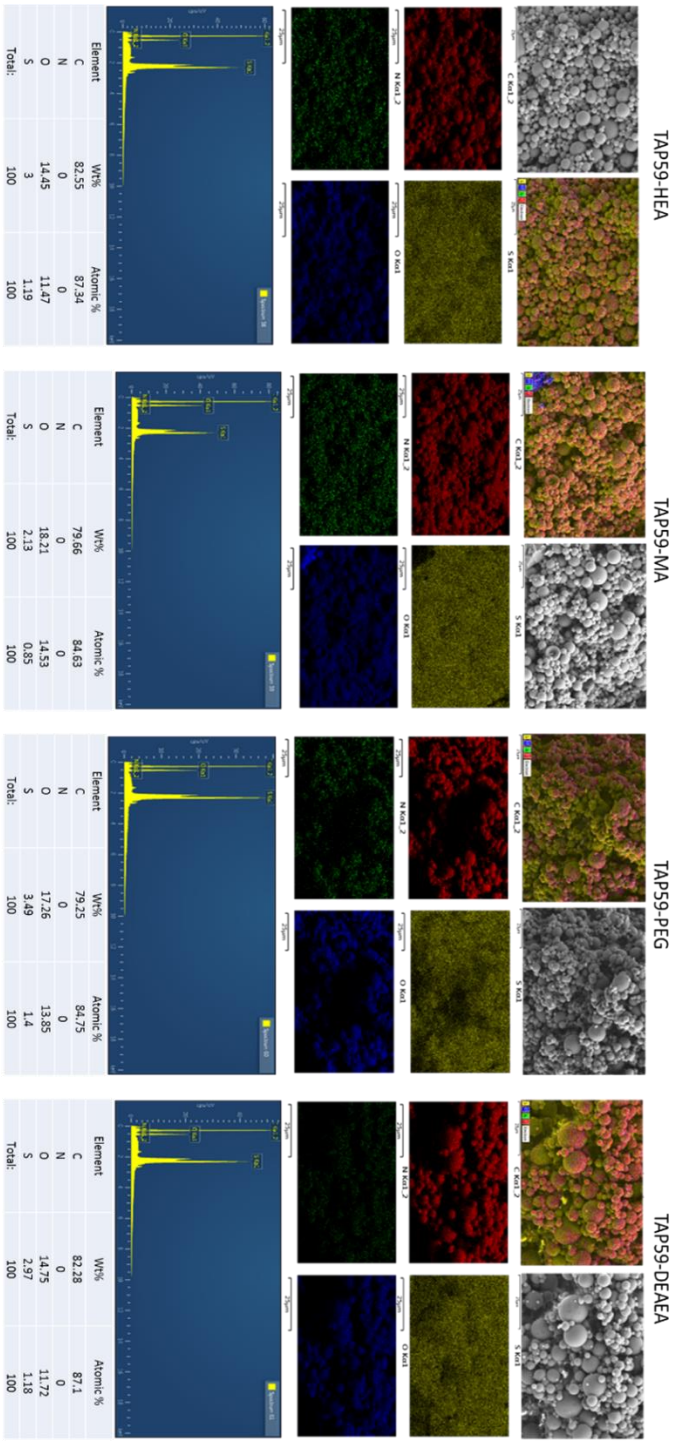

SEM image, element distribution and EDX data after post-polymerisation functionalisation via thiol acrylate Michael addition reaction using different acrylate monomers: (a) HEA, (b) MA, (c) EGMEA and(d) DEAEA for PETMP-HA (1.5:1) microsphere polymer particles, synthesised under UV for 5 hours at 20500rpm.

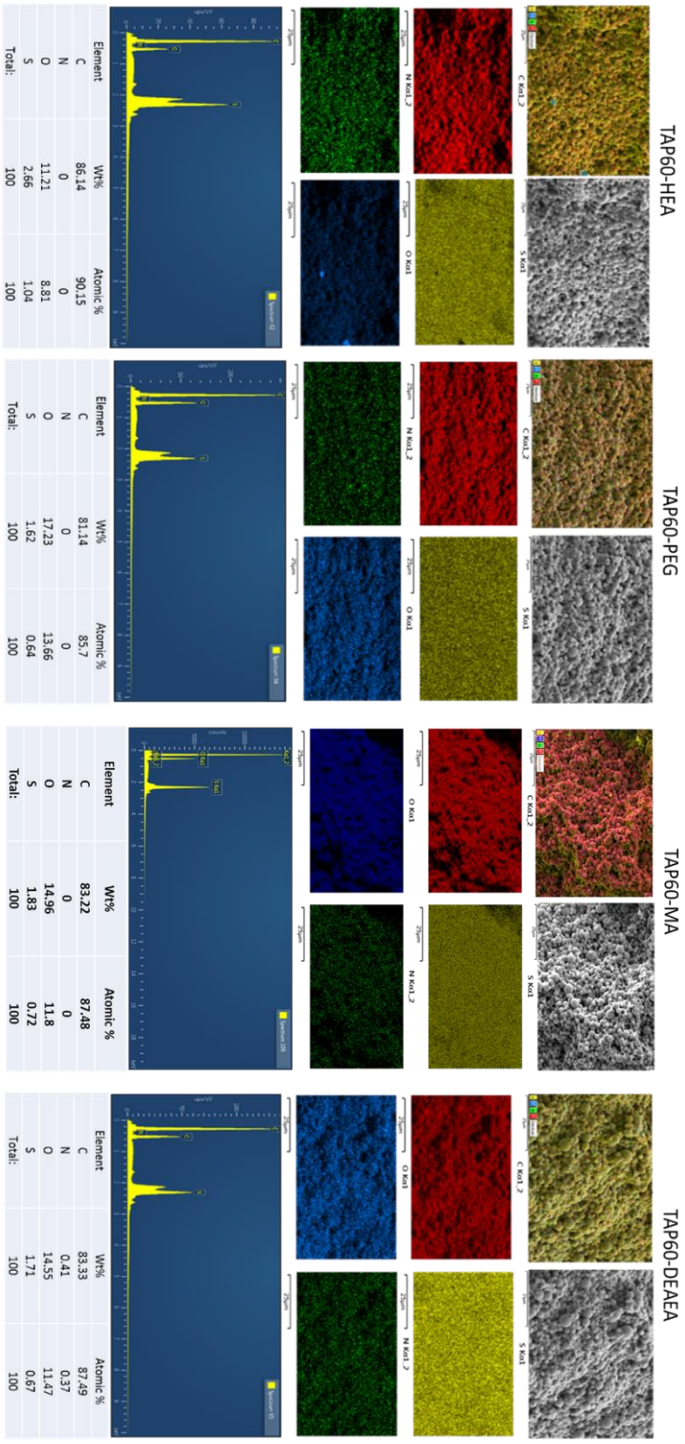

SEM image, element distribution and EDX data after post-polymerisation functionalisation via thiol acrylate Michael addition reaction using different acrylate monomers: (a) HEA, (b) MA, (c) EGMEA and(d) DEAEA for PETMP-HA (2:1) microsphere polymer particles, synthesised under UV for 5 hours at 8000rpm.

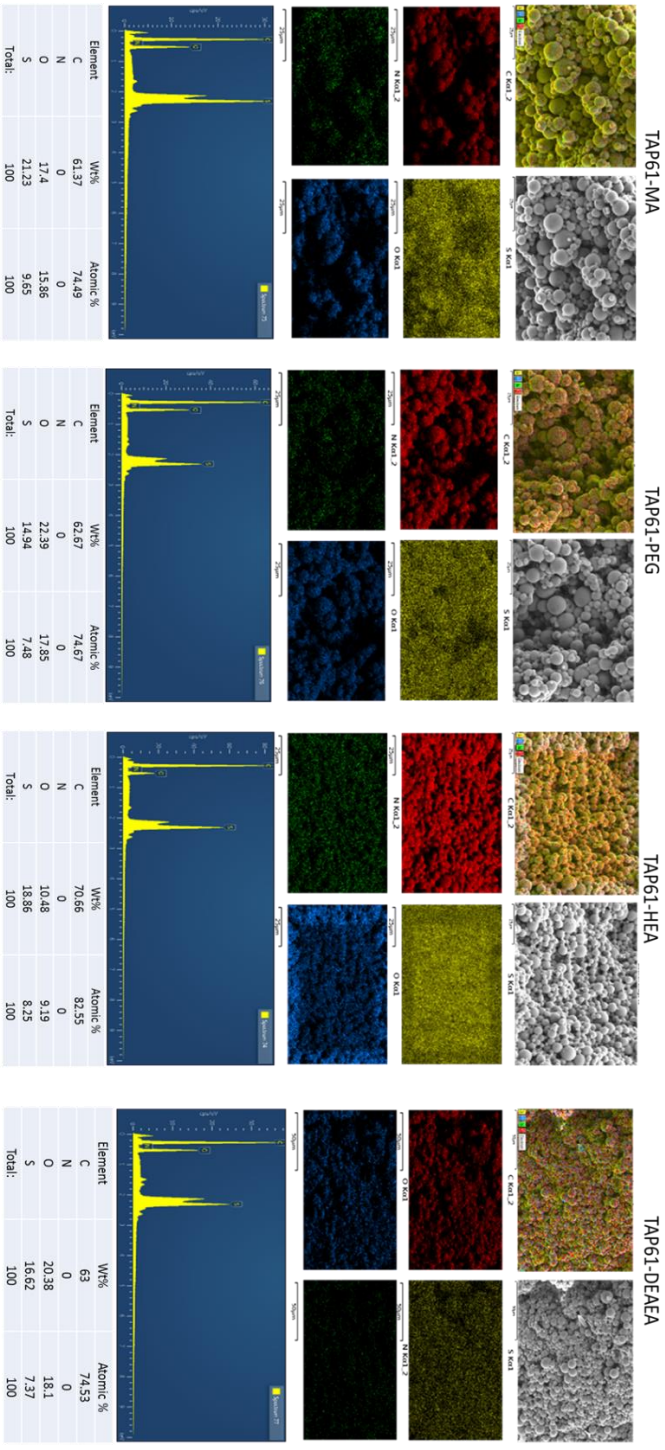

SEM image, element distribution and EDX data after post-polymerisation functionalisation via thiol acrylate Michael addition reaction using different acrylate monomers: (a) HEA, (b) MA, (c) EGMEA and(d) DEAEA for PETMP-HA (2:1) microsphere polymer particles, synthesised under UV for 5 hours at 20500rpm.